Ultrasound transmission tomography : a low-cost realization

Document Version:
Publisher's PDF, also known as Version of Record (includes final page, issue and volume numbers)

Please check the document version of this publication:

• A submitted manuscript is the version of the article upon submission and before peer-review. There can be important differences between the submitted version and the official published version of record. People interested in the research are advised to contact the author for the final version of the publication, or visit the DOI to the publisher's website.
• The final author version and the galley proof are versions of the publication after peer review.
• The final published version features the final layout of the paper including the volume, issue and page numbers.

Link to publication

Download date: 16. Nov. 2023

ULTRASOUND TRANSMISSION TOMOGRAPHY

a low-cost realization

G. Sollie

ULTRASOUND TRANSMISSION TOMOGRAPHY

a low-cost realization

door

Gerrit Sollie

geboren op 22 september 1958 te Kampen

Dit proefschrift is goedgekeurd door de promotoren

prof.dr.ir. J.E.W. Beneken
en
prof.dr.ir. N. Bom

Aan Marlene

Voorwoord

Het verschijnen van dit proefschrift en het uitvoeren van het beschreven onderzoek zouden niet mogelijk geweest zijn zonder de inbreng die vele mensen op verscheidene vlakken gehad hebben. Ik wil dan ook iedereen die een bijdrage aan dit werk heeft geleverd van harte bedanken.

Mijn bijzondere dank gaat uit naar mijn beide promotoren, prof.dr.ir J.E.W. Beneken van de Technische Universiteit Eindhoven en prof.dr.ir. N. Bom van de Erasmus Universiteit in Rotterdam, voor de tijd en de energie die zij gestoken hebben in het tot stand komen van dit proefschrift.

Drs. Thijs Stapper wil ik heel hartelijk bedanken voor de onschatbare bijdrage die hij aan dit werk heeft geleverd, zowel in de dagelijkse begeleiding van het onderzoek als bij het schrijven van het proefschrift.

Mijn dank gaat verder uit naar prof.dr.ir. W.G.M. van Bokhoven en prof.dr.ing. H.J. Butterweck voor de leerzame gesprekken en hun nuttige commentaar.

Voor de technische ondersteuning van het onderzoek ben ik veel dank verschuldigd aan Henny van der Zanden en Geert van den Boomen, waarbij ik Geert in het bijzonder wil bedanken voor al het werk wat hij besteed heeft aan de figuren in dit proefschrift.

Voor de bijdragen die zij in de vorm van hun afstudeerwerk aan het onderzoek geleverd hebben wil ik Willy Baas, Peter Wardenier, Piet Muijtens, Jos Janssen, Roland Mathijssen, Leon Bemelmans, Kees van den Keijbus, Rudy Pijfers, Marco Heddes, Albert Baars, Sjef van den Buys en Lex van Gijssel hartelijk bedanken.

Verder wil ik ir. J.C. Somer en dhr. J.M.Q. van der Voort van de Rijks Universiteit Limburg bedanken voor hun adviezen en medewerking op het gebied van de PVDF transducer, en de fotografische dienst van de Technische Universiteit Eindhoven voor het snelle en goede fotografeerwerk.

I owe many thanks to Kate and Chris for all the time they spent on correcting my English.

De leden van de vakgroep Medische Elektrotechniek worden heel hartelijk bedankt voor de goede sfeer en de collegialiteit die ik de afgelopen jaren heb ervaren.

Mijn familie, schoonfamilie en vrienden wil ik bedanken voor hun steun en de, soms zo broodnodige, afleiding die ze mij gaven.

In het bijzonder wil ik mijn ouders bedanken. Hun niet aflatende morele en materiële steun heeft de opleiding mogelijk gemaakt die ten grondslag heeft gelegen aan dit proefschrift.

Ten slotte wil ik, hoewel woorden hier te kort schieten, Marlene bedanken voor haar geduld als ik weer eens geen tijd had, haar grenzeloze vertrouwen in mijn kunnen, de onmisbare steun op moeilijke momenten, de zovele in stilte geserveerde natjes en droogjes en, wat voor mij het belangrijkste is, haar liefde.

Gert Sollie
juli 1988

Contents:

CHAPTER 1:

Introduction

Man has always been trying to develop his capabilities beyond the limitations of the human body. This resulted in various kinds of technical developments like cars, airplanes, submarines, wired and wireless telecommunication etcetera, etcetera.......

In the field of extending human sight various developments can be mentioned that make it possible to see objects at tremendous distances or to see things that are so small that man hasn't even been aware of their existence. An extra challenge is to look inside non-transparent objects without the need to open them. This latter extension of the eye is obviously very useful in medicine, where it can be necessary to look inside a patient to make a diagnosis without the need of an operation. A well-known technique for investigating and imaging the interior of living beings is X-ray photography. More recently ultrasound also proved to be very useful in medical imaging, and one of the most recent developments in medical imaging is Magnetic Resonance Imaging (MRI). One of the reasons why ultrasound became so popular is the fact that the radiation is much less harmful than X-rays.

This thesis describes a new technical realization of an imaging technique using both ultrasound and computed tomography. First, a short look will be taken at some highlights in the history of ultrasonic imaging and at some ultrasound techniques which are being used in medical imaging at the moment.

1.1 History

One of the very few, if not the only positive effect of a war is the stimulation of technical developments. As in many other techniques presently in use for peaceful purposes this has also been the case in the development of ultrasound techniques. The idea of transmitting an underwater "sound beam" and receiving the echoes from submerged

obstacles was born in connection with the Titanic disaster in 1912. It was during World War I (1917) that Paul Langevin succeeded in developing a pulse-echo system for the detection of submarines which was in fact the first sonar (SOund Navigation And Ranging) system. Although ultrasound had already been in use for therapeutic purposes for some years (Pohlman, 1939) it took until 1947 before the first attempts to use ultrasound in diagnostic applications were published (Dussik et al., 1947). In those first applications ultrasound was used in a way, similar to the use of X-rays, to produce some kind of "shadow" images of the head (Hueter and Bolt, 1951). These images were used to determine deviations in the geometry of the ventricles of the brain in order to detect brain tumors. Although the first results seemed to be very promising, the shadow imaging turned out to be disappointing because the images proved to be merely transmission patterns of the skull and contained hardly any, or no information at all about the brain (Ballantine et al., 1954). This caused a severe set-back in the development of ultrasound transmission techniques.

During World War II higher frequencies became available in ultrasound, and pulse-echo systems were developed for non-destructive material testing. As soon as the war was over the results were published and shortly after that these techniques found their application in medical imaging. Around 1950 several pulse-echo scanners were produced simultaneously by independent investigators (Ludwig and Struthers, 1950, French et al., 1950, Howry and Bliss, 1952). During the first decade the development of the pulse-echo techniques was rather slow, but after 1960 these techniques developed rapidly into a very widespread and commonly used imaging technique in clinical practice. A not often recognized, but important reason for this acceleration in the development of the pulse-echo techniques was the discovery of piezoelectric ceramics as new transducer materials. In Section 1.2 a short description of several pulse-echo techniques will be given.

In spite of the fact that the development of the transmission techniques had suffered the previously mentioned set-back, a few investigators kept working on these techniques and some of them achieved quite an improvement (see Section 1.3). Nevertheless transmission techniques did not become of any clinical significance. Around 1974 the interest in transmission techniques revived a little as a result of the introduction of computed tomography. This was originally

Introduced in the field of X-ray imaging but it also proved to be applicable in ultrasound imaging. More detailed information about transmission techniques will be given in Section 1.3.

Another application of ultrasound in medicine is the use of the Doppler effect to study movement within the body. The first applications of this technique were in the late fifties and it developed quite rapidly into a frequently used diagnostic tool. The Doppler imaging techniques will not be discussed here, as this subject is beyond the scope of this study. Interested readers are referred to Reid (1978), Baker et al. (1978), Hoeks (1982) and Reneman and Hoeks (1982).

1.2 Pulse-echo techniques

In this paragraph a brief description will be given of the ultrasound pulse-echo techniques that are commonly used in clinical diagnosis at the moment. Most of the modern diagnostic pulse-echo systems have sound frequencies ranging from about 1 to 10 MHz. In a pulse-echo system a short ultrasound pulse is transmitted into the body by a transducer. Parts of the acoustic energy of this pulse reflect on various boundaries and scatterers within the body and travel back towards the transducer. The time between the generation of a pulse and the reception of an echo indicates the depth of the structure on which the pulse was reflected. In pulse-echo systems the sound propagation velocity within the body is assumed to be known and constant.

In the following paragraphs brief descriptions will be given of several possibilities to represent the echoes on a screen, mostly of a cathode ray tube. More detailed descriptions of these pulse-echo techniques are given by Kossoff (1976), Wells (1978), Somer (1978) and Macovski (1983a).

* The A-mode (amplitude-mode).
In this mode the envelope of the received echo-signals is shown as a vertical deflection of the trace on the screen. This gives an image as in Figure 1.1a.

* The B-mode (brightness-mode).
In this mode the envelope is shown as the brightness of the trace instead of the vertical deflection as shown in Figure 1.1b.

SKIN SURFACE

TRANSDUCER ————————SOUND BEAM

ⓐ ——→ TIME

ⓑ
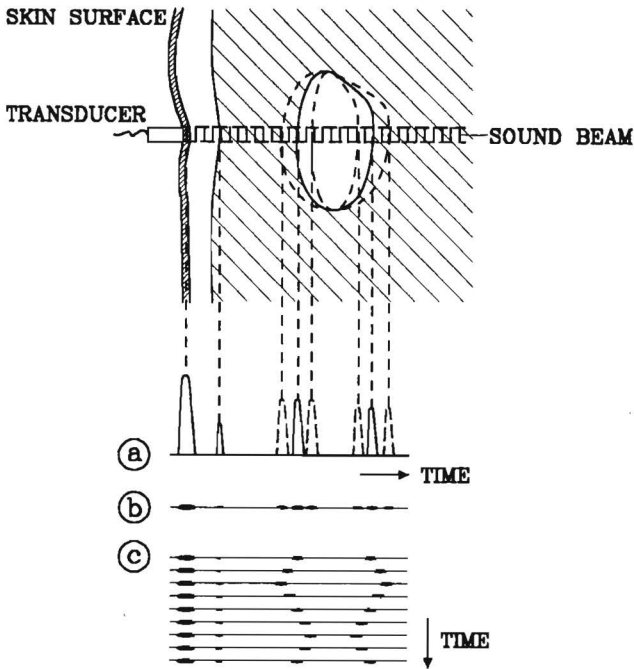
ⓒ ↓ TIME

Fig.1.1) Modes for representing reflections within a single sound beam.
a) A-mode, b) B-mode, c) M- or TM-mode.

   * The M- or TM-mode (time-motion-mode).
This mode is used to document the movement of structures. In this mode
ultrasound pulses are generated repeatedly at a constant time-interval
and the B-mode lines from these pulses are written as adjacent lines on
a display. In this way recordings are obtained which correspond to the
position of the reflecting structures as a function of time. Figure 1.1c is
an example of an M-mode recording in the case that the surface of the
structure moves between the dashed lines.
   * The linear scan.
The linear scan is performed as follows. The transducer is moved along a
straight line perpendicular to the direction of the sound beam. The
B-mode lines recorded with this transducer are written as vertical lines
on the screen and the horizontal position of the lines on the screen is
related to the position of the transducer. In this way a sort of cross-
sectional image can be produced as shown in Figure 1.2a. An important

4

development in linear scanning was the introduction of the linear array transducer (Bom, 1971). This kind of transducer offers the possibility of electronically moving the ultrasound beam combined with the possibility to focus the beam at a variable depth (dynamic focussing). Technical developments have made it possible to obtain up to 50 scans per second which enables real-time imaging. This is a very useful feature in various applications, for example in cardiology and obstetrics.

    * The sector scan.

With this kind of scanning it is not the position of the transducer that varies but the direction of the sound beam. Because the direction of the B-mode lines on the display is the same as the direction of the ultrasound beam, this technique produces cross-sectional images too. Whereas the linear scan produces rectangular images the sector scan produces sector shaped images (Figure 1.2b). The sector-scan is particularly useful when there is only a small area through which the object of interest can be investigated (for example in imaging the heart between two ribs). Sector scanning also offers the possibility of real-time imaging. This can be achieved by using a rotating or "wobbling" transducer driven by a motor or by using a phased array transducer. With the latter it is possible to sweep the ultrasound beam without mechanical movements (Somer, 1968).
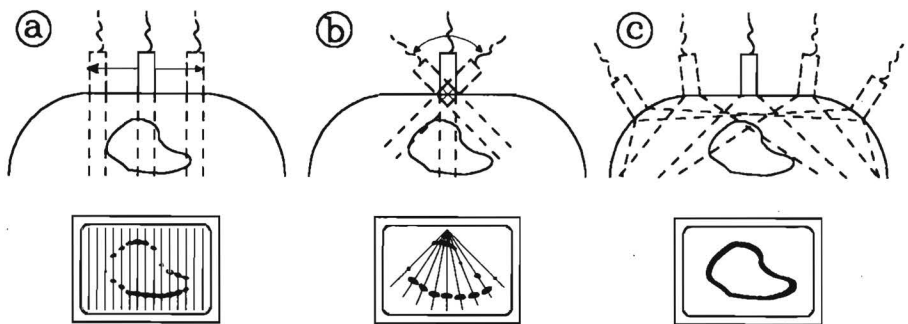
Fig.1.2) Scanning techniques for reflection imaging.
        a) Linear scan, b) sector scan, c) compound scan.

5

* The compound scan.

Major drawbacks of the linear and of the sector scan are that the resolution in the direction of the beam and the resolution in the direction normal to the beam are different so that point-shaped reflectors are imaged as small lines perpendicular to the direction of the beam. Furthermore, only surfaces normal or almost normal to the direction of the beam produce a clear echo. These problems are largely solved by the compound scan. With this technique, shown in Figure 1.2c, sector or linear scans are recorded in several directions within one plane. When these scans are shown on an integrating display or film so that the brightness of each scan is added to the previous ones, the quality of the obtained image is much better than with the single scans. A disadvantage of this method is that it is almost impossible to make real-time recordings. This is why the compound scan has not become very popular in clinical practice.

* Reflection tomography.

In this technique linear or sector scans are recorded in many directions within one plane (many more than in compound scanning), digitized and stored in a computer. By means of this computer such a set of scans can be reconstructed into an image of the scan plane (Wade, 1978, Hiller and Ermert, 1980). This technique gives very clear images with a constant resolution in all directions but it requires expensive equipment and it has no real-time imaging capabilities because of the time consuming scanning process. Only recently a fast, and very expensive, scanning system has been developed which indicates the possibility of producing real-time images (Newerla, 1987).

1.3 Transmission techniques

The first ultrasound transmission images (called ultrasonograms) were based on the assumption that, as in X-ray imaging, tissue structures could be imaged because of differences in absorption of transmitted radiation. In X-ray imaging it is possible to record the intensity distribution in a whole plane at once. This proved to be impossible with ultrasound transmission imaging. Therefore, a device was developed with a transmitting and a receiving transducer mounted on opposite sides of the object in a way that made it possible to scan a plane, normal to the

beam direction, in order to measure the absorption of the ultrasonic energy in the object between the transducers for every point in that plane, so that a shadow image could be obtained similar to an X-ray photograph. (Hueter and Bolt, 1951). This technique was meant to be used in the detection of brain tumors because it was assumed that the images depicted the geometry of the ventricles of the brain. However, soon it turned out that the contrast in the images caused by brain structures was negligible compared to the contrast caused by inhomogeneities of the skull (Ballantine et al., 1954).

Although this technique did not serve its original goal, it has been developed further because it was expected to have other biomedical applications. These developments concentrated mainly on image converters which are devices in which the intensity of the received ultrasound field is scanned electronically and converted directly into a "shadow" image on a screen. Although image converters offered the possibility of real time imaging and eliminated the need of mechanical scanning, there has never been much interest in these transmission images, probably because of the rapid developments in the pulse-echo techniques.

The latest development in transmission imaging is computed tomography (Greenleaf et al., 1974, 1975, Carson et al., 1976, 1977, Glover and Sharp, 1977, Greenleaf et al., 1979, Mol, 1981, Stapper and Sollie, 1985). The principles of this technique are not explained here because they will be discussed in detail later on in this thesis. Although investigators in this area state that transmission tomography has at least some clinical relevance, up to now this technique has not been accepted in clinical practice, probably because the systems that have been developed are all very complicated and expensive while their imaging capabilities are limited.

This thesis deals with the development of a low-cost and simple ultrasound transmission tomography system (Sollie and Stapper, 1987). In the next chapter a brief explanation of the tomographic principle will be given and the advantages and disadvantages of computed ultrasound transmission tomography will be discussed. It will be explained why this imaging system has been developed in spite of the seemingly small interest from clinical practice. In Chapter 3 the theory of reconstructing an image from the measured data is described and in Chapter 4 the

physical quantities that can be measured with the tomography system will be given together with their measurement methods. In Chapter 5 and 6 the measurement apparatus is described in increasing detail. Chapter 7 is about several types of ultrasound transducers and their possible applications in the tomography system. In Chapter 8 the effects of phase cancellation and interference will be discussed. These effects prove to be an important problem in transmission measurements as well as in reflection measurements using ultrasound. In Chapter 9 some results obtained with the described tomograph will be presented. Finally, in Chapter 10, a discussion of the project will be given together with a number of recommendations for further development of the described tomography system.

Motivation of the Study

In this chapter it is explained why ultrasound transmission tomography has been chosen to be the subject of this study, in spite of the fact that there does not seem to be much clinical interest in it at the moment.

Before discussing the advantages and disadvantages of ultrasound transmission tomography compared to other medical imaging techniques, it may be useful to give a very brief description of its principles. This description will be given in Section 2.1. Then, in Section 2.2, the advantages and disadvantages of ultrasound in general and ultrasound transmission tomography in particular will be discussed, and in Section 2.3 the aim and the motivation of the study, described in this thesis, will be given.

2.1 The principles of ultrasound transmission tomography

In ultrasound transmission tomography two transducers are used which are submerged in a water tank and mounted opposite to each other. The object is also submerged and between the two transducers (Figure 2.1). An ultrasound pulse is transmitted by one of the transducers and travels through the object and the water to the other one. From this received pulse some acoustical properties of the material along the path of the sound pulse can be derived. The method for doing this will be described later in this thesis. The transducers move simultaneously along a straight line perpendicular to the direction of the transmitted sound beam and the properties of the intervening material are determined at constant sample intervals along that line. In this way a linear scan of the cross-section of the object is obtained in one direction. Such a linear scan is called a projection. A number of these projections are measured in different directions within one plane and stored in a computer which reconstructs a cross-sectional image of the distribution of a physical quantity from this
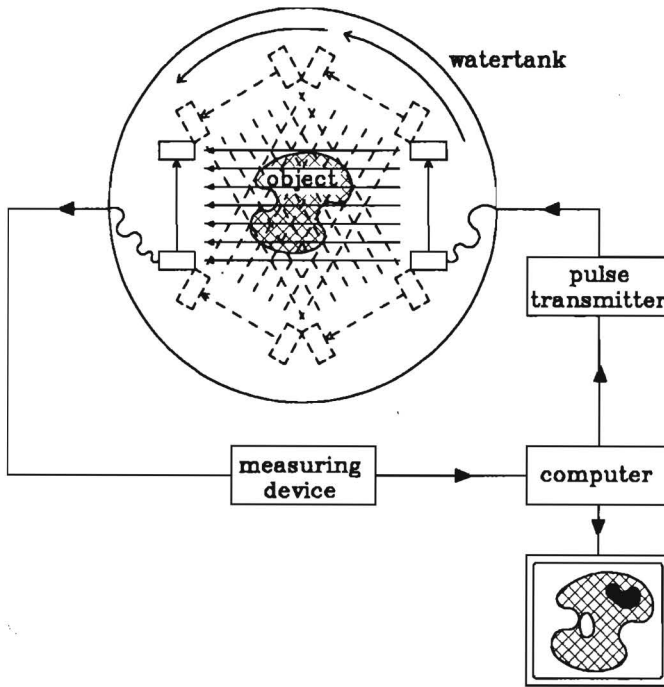
Fig.2.1) Schematic representation of the scanning process used in ultrasound transmission tomography.

set of linear scans. This process is drawn schematically in Figure 2.1.

All steps of the tomographic process will be described in detail in the next chapters.

2.2 Advantages and disadvantages

In this section ultrasound transmission tomography is compared to several other medical imaging techniques.

X-ray imaging (Macovski, 1983a): the most important advantage of ultrasound above X-rays is, that sound radiation is, at least in the intensities used in diagnostic applications, harmless where X-rays are not. Another advantage is that ultrasound has a much lower propagation velocity. In most biological tissues the ultrasound propagation velocity is

different for different tissues and ranges from about 1450 to 1600 m/s while the X-ray propagation velocity is 3×10^8 m/s and the same for all tissues. Because of the constant value of the propagation velocity, in X-ray imaging only the attenuation coefficients can be used to differentiate between tissues, where in ultrasound imaging it is possible to determine the attenuation coefficients, the sound propagation velocities and the reflection coefficients of different tissues. An additional advantage of ultrasound is that the generation of ultrasound is much easier and less expensive than the generation of X-rays.

A disadvantage of ultrasound compared to X-rays is the much lower frequency that has to be used, because for the higher frequencies the sound is attenuated too much. In spite of the lower propagation velocity, this means that the wavelength of ultrasound (about 10^{-4} m to 10^{-3} m) is much larger than the wavelength of X-rays ($<10^{-10}$ m). This difference causes the resolution in X-ray imaging to be much better than in ultrasound imaging because it is impossible to visualize structures smaller than the wavelength directly. Diffraction occurs when the size of the structures in the examined object is comparable to the wavelength, so X-ray imaging does not suffer from diffraction effects where ultrasound images can sometimes be distorted severely by diffraction.

Another important imaging technique nowadays is MRI (Magnetic Resonance Imaging), also known as NMR (Nuclear Magnetic Resonance). Up to now, this imaging technique has been considered to be harmless to the patient, so compared to MRI, ultrasound has no advantage concerning safety. In addition to that MRI can yield a higher resolution than ultrasound imaging and it has the possibility of imaging parts of the body containing bone or air, which is almost impossible with the standard ultrasound techniques.

The main disadvantage of MRI is that it is a very complicated and extremely expensive technique which makes it unlikely that MRI will become a generally applied clinical investigation.

Apart from the imaging techniques mentioned above there are other ones such as positron emission tomography (PET), digital subtraction radiography, thermography and endoscopy. Because these techniques are limited to small areas of medicine, there is no need for comparison with ultrasound tomography, so they will not be discussed here.

Most of the advantages and disadvantages of ultrasound mentioned above do not only hold for transmission tomography but also for

pulse-echo techniques. In the next paragraphs pulse-echo imaging will be compared with transmission tomography. In these paragraphs a pulse-echo imaging system will mean a linear or sector scanner. Compound scanning and reflection tomography are rarely used in clinical practice so these techniques have not been included in the comparison.

A clear advantage of transmission measurements is that, when a single pulse is transmitted, only one distinct pulse is received whereas in reflection measurements a noisy signal is received, composed of the reflections of a large number of reflecting interfaces and scatterers. The single pulse in transmission measurements eliminates the need of a TGC (Time Gain Control, Wells, 1978) and offers the possibility of using straightforward data acquisition methods as will be shown later in this thesis. Because of this, the hardware can be very simple and inexpensive.

Another advantage of transmission tomography is that, in addition to the ability of imaging the topographical anatomy, it offers the possibility of performing a certain degree of tissue characterization (Greenleaf, 1978, Miller et al., 1979, Stapper and Sollie, 1987). Using transmission tomography different acoustical properties of the object under study, such as the sound propagation velocity, the attenuation coefficient and the frequency dependence of the attenuation can be determined, whereas in reflection imaging only differences in acoustical impedance and scatterer density are detected. Sometimes a pulse-echo system can perform "attenuation" measurements, but in that case the measured values give the mean value over a certain depth range and the values become less reliable when that range gets smaller. The word "attenuation" is written between quotes because it is not the real attenuation that is being measured but the frequency dependence of the attenuation (see Chapter 4). The tissue characterizing ability of the tomograph can be improved when the transmission measurements are combined with reflection measurements. Apart from the improved tissue characterization such a combined measurement offers the possibility of using the values from a sound propagation velocity measurement to correct the reflection image. In this way the topographic accuracy of the reflection image can be improved (Kim et al., 1984). The technical possibilities of implementing such a combination will be shown to be plausible in Chapter 4 and 5.

Furthermore, transmission tomography has the advantage that the

resolution in the pictures is the same in all directions and that interfaces between different tissues give a contrast independent of their orientation. This is not the case in reflection imaging (Wells, 1966).

Of course transmission tomography does also have disadvantages. One is that the object to be imaged needs to be submerged in water. Another disadvantage is that the object has to be accessible from all directions in the plane of interest. These conditions, together with the fact that it is impossible to image gas containing structures, limit the applicability of transmission tomography to certain parts of the body such as limbs or breasts. Another, very important disadvantage of transmission tomography is that it is, at least in the simple configuration described in this thesis, impossible to obtain real-time images, in fact, none of the ultrasound tomography systems developed up to now has been capable of real-time imaging.

Because of the aforementioned differences compared with pulse-echo techniques, ultrasound transmission tomography will never be able to replace reflection imaging but it may be a very useful extension of the use of ultrasound in medical imaging.

2.3 Aim of the project

The aim of this project is not to investigate the principles or the clinical applicability of ultrasound transmission tomography but to investigate the technical possibilities of realizing a simple and low-cost medical imaging system without using dedicated or expensive electronic components or computer equipment.

Ultrasound transmission tomography was first reported by Greenleaf et al. in 1974 and it has been studied by several investigators. Up to now the technical realizations of the principle have been too complicated and expensive to have had any clinical significance. However, the results obtained with these first experimental set-ups do indicate possible clinical usefulness, especially in imaging the human breast (Carson et al., 1976, Glover, 1977, Greenleaf et al., 1978, Schreiman et al.,1984), but it also proved possible to image the human head (Dines et al., 1981) and extremities containing bone (Carson, 1977). Besides the non invasive diagnostic applications, ultrasound tomography offers possibilities for in vitro studies (Mol, 1981, Miller, 1979). These promising results provide

one of the reasons for trying to develop a new implementation of the technique.

Two other, closely related and perhaps even more important aspects of the study are simplicity and cost. The aim is not to develop an imaging system capable of producing better images than the existing ones, but a system that produces images of equal, or sometimes worse quality, but in a simpler way and at much less cost. In the following paragraph the importance of simplicity and cost will be explained.

Because of the very rapid technical developments during the last decades the technical possibilities of medical imaging have become largely extended. On the one hand this is a very positive development because medical imaging becomes applicable in more and more areas with a still increasing diagnostic value and accuracy. On the other hand this development also has clear negative effects. One of them is that the imaging systems become more and more complicated and sophisticated with all the associated problems concerning maintenance, reliability, safety and especially the operating of the equipment.

Another negative aspect is that the increasing image quality enhances the tendency of the imaging systems to replace the conventional diagnosis instead of supporting it. Medicine has always been an interaction between human beings in the first place and therefore medical diagnosis is mainly a subjective process of perception, communication, intuition and experience. If the reliability of this subjective process can be improved by using objective technical resources or if the technical resources offer the physician the opportunity to concentrate more on the mental or psychological aspects of the illness, then the application of these techniques is an enhancement of the diagnostic process. However, if the technical resources (like imaging techniques) are going to substitute a part of the subjective diagnostic process, then there is no improvement, only replacement. Moreover, this will lead to a technical instead of a human concept of the patient which might cause a degradation of the diagnostic process in particular, but also of medicine in general.

A third negative aspect of the rapid technical developments is that, linked with the increase of complexity and sophistication of medical equipment, there is also an increase in the cost involved. This means that the application of such equipment has to be limited because in medicine there is only a limited amount of money available. When we draw a graphical representation of the percentage of the population for

14

which a medical action is applicable as a function of the cost of that
action we get a curve as shown in Figure 2.2. It is obvious that the most
attractive and challenging developments for engineers and scientists are
towards the tail of the curve, for there lie the borders of knowledge and
technology. It is equally obvious, however, that the number of people
served by the developments in the tail of the curve is very small.
Because of the attractiveness of developments in the tail of the curve
much research is concentrated there, leaving a gap in developments lying
closer to the top of the curve. From the previous discussion it can be
concluded that, if a medical imaging system serving a large percentage of
the population is to be developed, it must be a simple and low-cost
system which is, as a consequence, not capable of producing an image
quality as high as the more complicated and expensive systems. It is
obvious that, after the technical realization, the usefulness of such a
system will have to be proved in clinical practice, but it is expected
that the simplicity and the low cost of the system will compensate its
limitations.
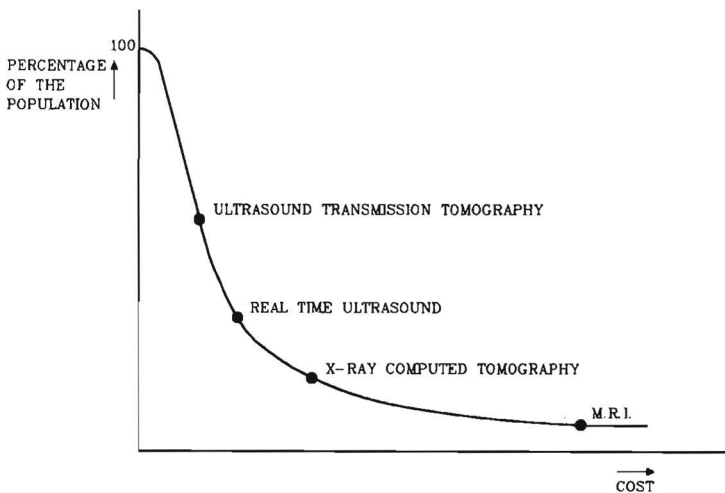
Fig.2.2) Percentage of the population for which a medical action is
applicable as a function of the cost of that action. The
estimated positions of some medical imaging systems are
indicated.

Based on the above considerations it is the opinion of the author that ultrasound transmission tomography can be a positive and useful contribution to medical diagnosis. This is the reason why a project has been started, of which this study is the first part. This project has the ultimate goal of developing a clinically useful ultrasound tomograph, using only a standard personal computer and simple, readily available electronic components. In Figure 2.2 the global positions of some imaging systems from clinical practice are given together with the estimated position of the ultrasound transmission tomography system described in this thesis.

From the goals mentioned in the previous paragraphs it may be obvious that the emphasis of this study is on the technical aspects of ultrasound transmission tomography rather than on its theoretical background.

Image Reconstruction

This chapter describes the relationship between a function and its projections. In this description the function is a two-dimensional distribution of a physical quantity and the projections are one-dimensional sets of measured data.

In this chapter it will be explained how, and under which conditions, a two-dimensional function can be represented by the collection of line integrals of that function along all lines in the plane. A set of line integrals taken along all lines in one direction is called a projection. The representation of a function by its projections is called the Radon-transform and consequently the reconstruction of a function from its projections is the inverse Radon-transform. The name of Radon has been connected to this problem because he was the first one who gave an extensive description of it (Radon, 1917), although, according to Cormack (1983), the Dutch physicist Lorentz had provided a solution for a special case of the problem several years earlier. An interesting detail is that Radon had no reason for stating and solving the problem other than that it was a very interesting mathematical problem and a challenge to solve it. It took until 1936 for the mathematical solution to be applied in a physical situation (Cormack, 1983). The first well-known application of the inverse Radon-transform was in radio-astronomy and it was presented by Bracewell in 1956. In 1973 the principle of image reconstruction from projections was introduced in medical radiology by EMI Ltd. of England (Macovski, 1983a) and it soon became a very popular medical imaging technique. Nowadays the inverse Radon-transform has a wide variety of applications in several areas of science and technology (Herman and Lewitt, 1979, Deans, 1983).

The image reconstruction from projections is mostly called computerized tomography (CT) or computer assisted tomography (CAT) because the inverse Radon-transform is almost always performed with the aid of a computer. The word tomography is derived from the greek words *tomos*, which means slice or section, and *graphein*, which means to draw.

This chapter deals with the mathematical background of computerized tomography and is subdivided in the following way. In Section 3.1 a physical derivation will be given of the filtered back-projection image reconstruction method together with a physical interpretation of the central-section theorem and the Fourier-transform reconstruction method. In Section 3.2 the Radon-transform will be discussed and the definition of a projection will be given. In Section 3.3 the definitions of the Fourier-transforms used in this chapter will be given in order to provide an easy reference to them. Then, in Section 3.4, the central-section theorem will be derived and in Section 3.5 some methods of performing the inverse Radon-transform will be presented in their analytical form. Following that, in Section 3.6, there will be some discussion as to why the filtered back-projection has been chosen to perform the image reconstruction in the ultrasound tomography system. Furthermore the discrete form of the filtered back-projection will be given together with some remarks on the consequences of discretization. Finally, in Section 3.7, the conditions will be formulated which must be satisfied when the distribution of a physical quantity is to be determined from its measured projections.

The reader who is not interested in the exact mathematics of the problem can confine himself to the reading of the Sections 3.1 and 3.7. The sections 3.2 to 3.6 do not contain information that is essential for understanding the rest of this thesis. Although Section 3.1 may be omitted if sections 3.2 to 3.6 are to be read, this section may be useful in understanding the other sections.

3.1 Physical interpretation

This section contains the physical interpretation of the image reconstruction by means of filtered back-projection. Physical interpretations of the central-section theorem and the Fourier-transform reconstruction method will also be given.

The description of the filtered back-projection will be done by means of showing the reconstruction of a single "pole" shaped object in the origin of the plane (Figure 3.1a). Since the reconstruction is a linear process, the superposition principle will hold. Thus, if a discrete, two-dimensional function is thought of as a set of these "poles" with different lengths and packed closely together, it will be obvious that the
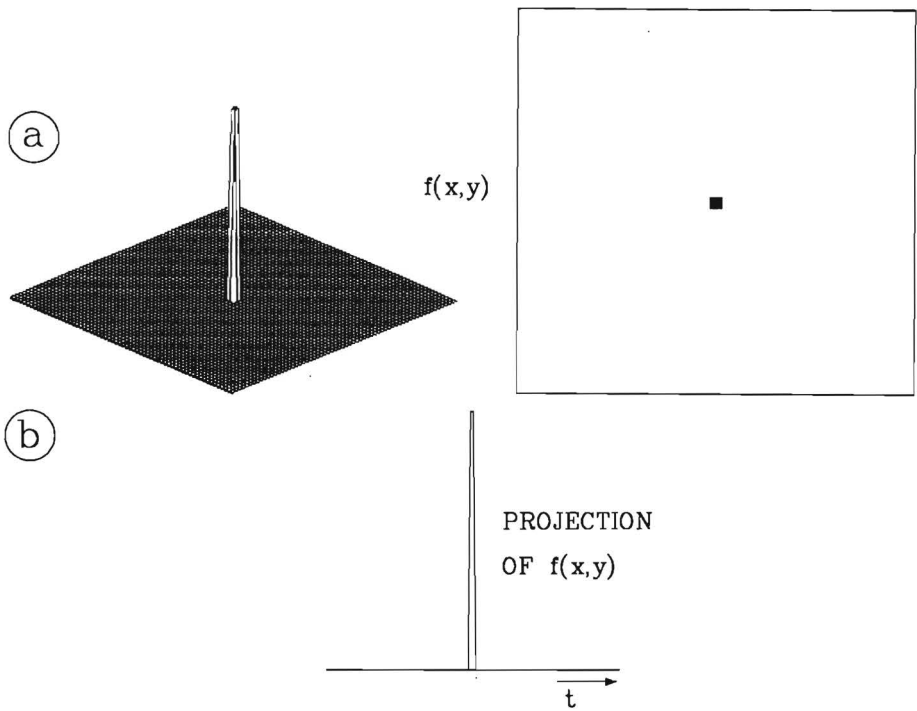
Fig.3.1) The original object used for the physical derivation of the filtered back-projection. a) Two-dimensional object, b) projection of the object.

discussion given in this section holds for any other two-dimensional function as long as its value is zero outside the measured area. In the pictures used in this section the two-dimensional functions will be shown in two ways: one way is representing the values of the function in the plane by different grey levels and the other way is giving a three-dimensional representation in which the height above a point represents the value of the function in that point.

In Section 2.1 it was explained that for each transducer position along the linear scans the measured value is related to the values of a physical quantity along the path of the ultrasound pulse. Such a path is often called a ray.

In the derivation of the filtered back-projection two assumptions will be made. The first is that the relationship between a measured value and the actual values along the corresponding ray is given by a line integral. This means that the measured value is the sum of all values along the ray. The second assumption is that the rays are straight lines between
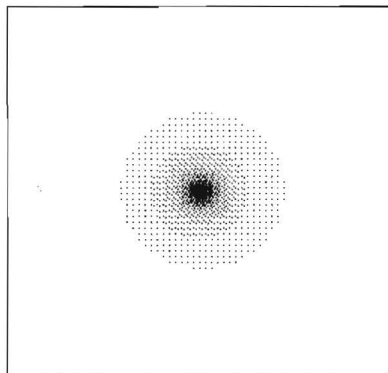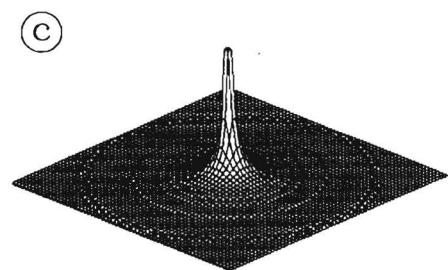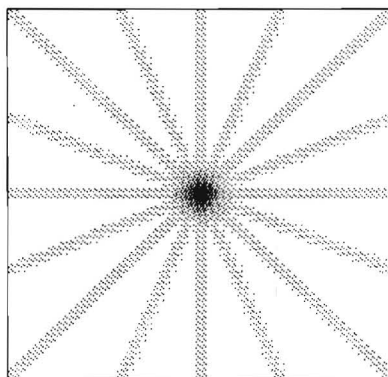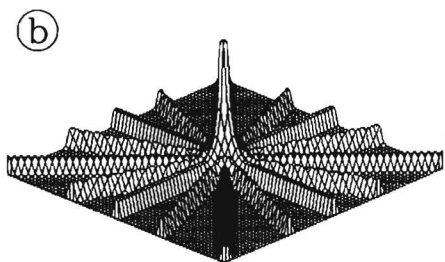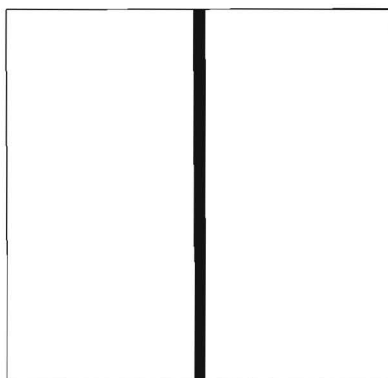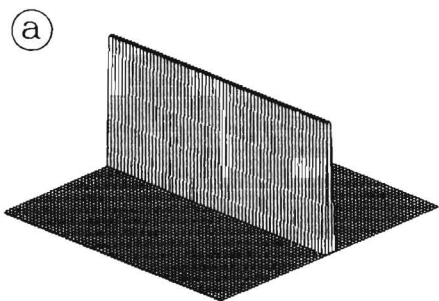
Fig.3.2) Images obtained by the back-projection of different numbers of
projections of the object in Figure 3.1.
a) 1 projection, b) 8 projections, c) 128 projections.

the transmitting and the receiving transducer. These assumptions imply that the measured values from one linear scan are a set of line integrals along lines in the same direction. As mentioned in the introduction of this chapter, such a set of line integrals is called a projection. A projection can be written as a one-dimensional function of the position of the measured ray within the scan. Keeping in mind the mentioned assumptions it is easy to see that the projections of the object from Figure 3.1a will all look like the one shown in Figure 3.1b.

First an attempt will be made to reconstruct the original function by simply projecting the projections back into the plane, all values from a projection are "smeared out" along the rays from which they have been measured. The back-projection of one projection will give an image like the one shown in Figure 3.2a. All projections are subsequently smeared out into the same plane, each one in the direction from which it has been measured. The final image is the sum of the back-projected images of all projections. In Figure 3.2b and 3.2c this result is shown for back-projection from 8 and 128 different angles. Note that the projections are always measured at a constant angular interval over a range of 180 degrees. From Figure 3.2c it is obvious that the reconstructed image gives some representation of the original one, but also that it is severely blurred by the fact that the rays have been smeared out throughout the whole plane and not only in the origin. In order to obtain a good reconstruction of the original function we will have to try to compensate for this blurring effect. To do this a two-dimensional filter has to be applied to the back-projected image. Because the back-projection only consists of adding the "smeared out" projections, the process is linear. Therefore, it is also possible to apply such a filter before the back-projection. In that case it is necessary to use a one-dimensional filter on each projection. After this filtering, the projections of the "pole" shaped object will look like the one given in Figure 3.3a. The back-projected image from 128 of these filtered projections is given in Figure 3.3b.

As we have mentioned before, a more complicated function than the one in our example can be seen as composed of a number of these "poles". When such a function is to be reconstructed from its projections, the filter to compensate the blur has to be applied to each point of all projections. This means that the projections have to be convolved with that filter. An example of the effect of filtering on a more complicated
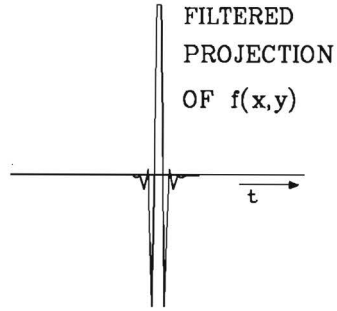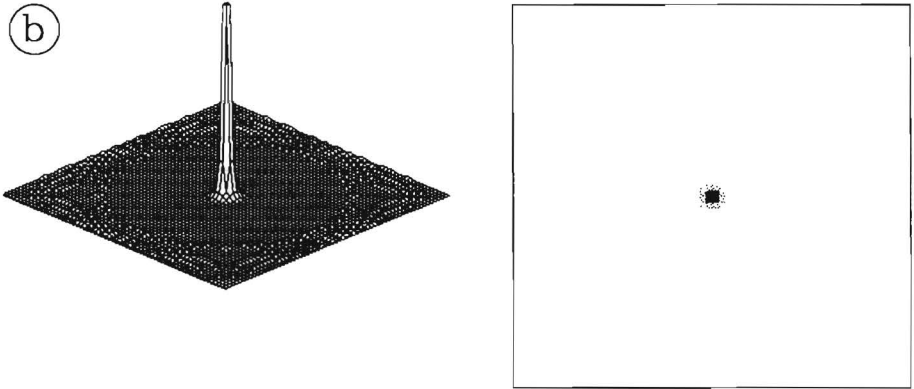
Fig.3.3) a) Filtered projection. b) Image obtained by the back-projection of 128 filtered projections.
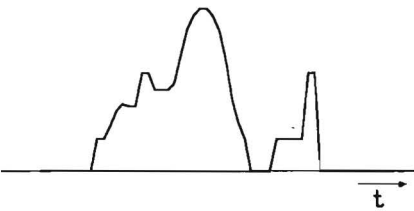
Before filtering: **After filtering:**

Fig.3.4) Unfiltered and filtered version of a more complicated projection.

projection is shown in Figure 3.4. At this point it will probably be clear why this reconstruction method is called the filtered back-projection or convolution back-projection method.

Because the central-section theorem is a very important theorem in the area of image reconstruction and a lot of reconstruction methods are based on it, this theorem will be given here, together with its physical meaning, but without going into mathematical details. If we consider the two-dimensional Fourier-transform of a function, then the central-section theorem states that the values of this transform on a line at an angle θ and going through the origin, give the one-dimensional Fourier-transform of the projection of the function taken at the same angle θ. A graphical presentation of the central-section theorem is given in Figure 3.5. The central-section theorem can be explained in the following way. The two-dimensional Fourier-transform decomposes the function into a set of infinitely wide two-dimensional sinusoids. A part of some of these sinusoids is shown in Figure 3.6. From this figure we can see that, if we take the projection of a function at some angle θ, then only the sinusoids in the direction of the projection will contribute to that projection. All other sinusoids in the plane will have a projected value of zero because
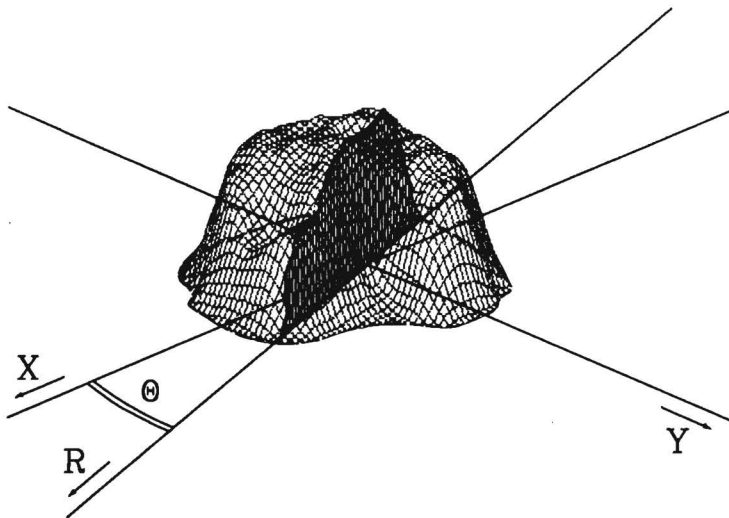
Fig.3.5) Graphical representation of the central-section theorem.
▨ Two-dimensional Fourier-transform of a function $f(x,y)$.
▥ One-dimensional Fourier-transform of the projection of $f(x,y)$ taken at the angle θ.
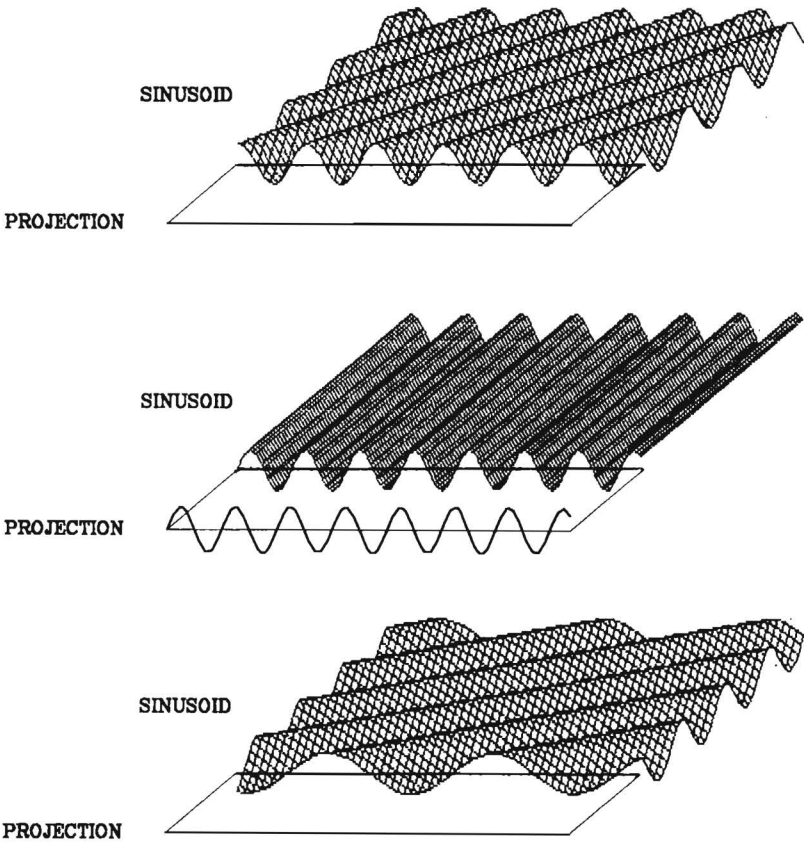
Fig.3.6) Some sinusoids in which a two-dimensional function is
decomposed by Fourier-transformation. Of each sinusoid the
projection in the same direction is shown.

the rays experience equal positive and negative contributions from them.
Thus, if the one dimensional Fourier-transform of this projection is used,
only the frequencies of the sinusoids in the direction of the projection
will be found. In the Fourier plane these frequencies lie on a line
through the origin at an angle θ (Figure 3.5).

From the central-section theorem another method of reconstructing a
function from its projections becomes quite obvious: a one-dimensional
Fourier-transform on all projections is performed and those transforms are
put together in a plane, each transform along a line through the origin
in the direction of its corresponding projection. Then a two-dimensional
inverse Fourier-transform on that plane will yield the reconstruction of

24

the measured function. This method of reconstruction is called the Fourier-transform method. Although this reconstruction method seems to be quite simple, the implementation on a computer gives rise to some problems concerning the two-dimensional interpolation that is necessary because the function to be transformed is given on a discrete polar grid whereas the computer represents an image on a rectangular grid. This is why the filtered back-projection has been chosen to be used in the ultrasound tomography system described in this thesis.

3.2 The Radon-transform

This section describes the Radon-transform. The description will be limited to the special case of the transform for a two-dimensional function which is to be represented by one-dimensional projections. After the description of the transform a definition of a projection will be given.

Let us assume a two-dimensional distribution of a physical quantity that can be denoted as the function $f(x,y)$ which is zero outside a limited region Ω of the x-y plane (Figure 3.7a). When polar coordinates are used instead of Cartesian coordinates, then the relation between the polar and the Cartesian representation of this function can be written as: $f_p(r,\phi) = f(r\cos\phi, r\sin\phi)$, where the subscript "p" indicates that the function is given in polar coordinates. We also assume a line $L_{t\theta}$ determined by two parameters: the distance t from $L_{t\theta}$ to the origin and the angle θ between $L_{t\theta}$ and the Y-axis. The distance t has to be signed to get a unique definition of $L_{t\theta}$, as can be seen from Figure 3.7. In physical terms we refer to $f(x,y)$ as "the object" and to $L_{t\theta}$ as a "ray".

Now we define a two-dimensional function $p(t,\theta)$. The value of $p(t,\theta)$ is the line-integral of $f(x,y)$ along the line $L_{t\theta}$. Note that t and θ are not the normal polar coordinates but the parameters determining $L_{t\theta}$; if $t = 0$, then $p(t,\theta)$ can have different values for different values of θ. When s is the distance along $L_{t\theta}$, for example from the point A to the point B in Figure 3.7b, then the value of $p(t,\theta)$ is:

$$p(t,\theta) = \int_{L_{t\theta}} f(t \cos\theta - s \sin\theta, \ t \sin\theta + s \cos\theta) \ ds \qquad (3.2.1)$$

The two-dimensional function defined by Eq. (3.2.1) is called the Radon-transform of the function $f(x,y)$, so when the operator $R\{.\}$ represents the Radon-transform then $R\{f(x,y)\} = p(t,\theta)$. It can be seen from the geometry of the problem that:

$$p(t,\theta) = p(-t,\theta+\pi) = p(-t,\theta-\pi) = p(t,\theta+2k\pi), \ k \text{ is an integer} \qquad (3.2.2)$$

So the Radon-transform $p(t,\theta)$ of a function $f(x,y)$ is periodic in θ with a period of 2π.

When we take all line-integrals from Eq. (3.2.1) for one value of θ as a function of t, we get a one dimensional function $p_\theta(t)$ which is called
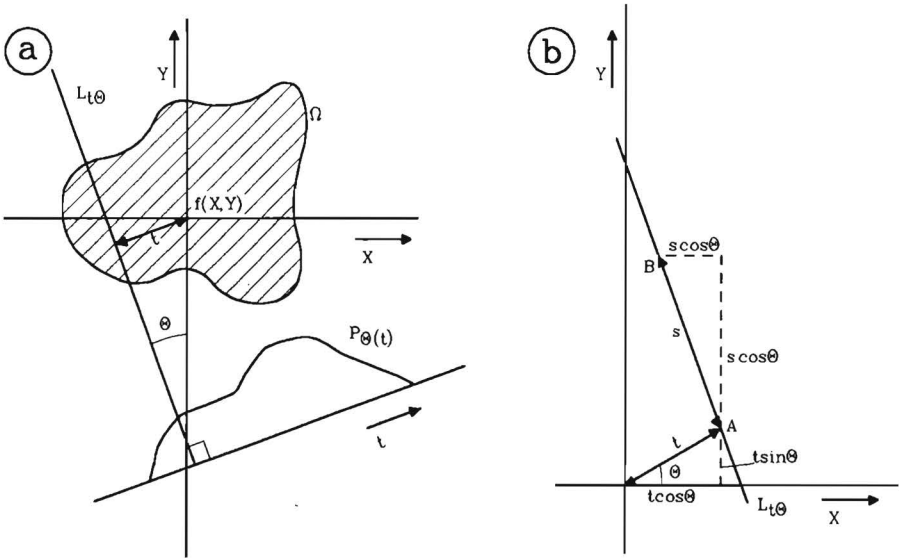
Fig. 3.7) The coordinate system used in the description of the Radon-transform. a) Coordinates in the object plane and the projection of $f(x,y)$ at the angle Θ. b) Coordinates of a point on a ray, point A is the origin for the coordinate s.

26

a projection. A projection of the function $f(x,y)$ is defined as:

$$p_\theta(t) = \int_{L_{t\theta\Omega}} f(t\cos\theta - s\sin\theta,\ t\sin\theta + s\cos\theta)\ ds \qquad (3.2.3)$$

Here is $L_{t\theta\Omega}$ the part of the line $L_{t\theta}$ within the area Ω where $f(x,y)$ is nonzero. It will be clear that $p_\theta(t) = p(t,\theta)$, where θ is a constant. In Figure 3.7a a projection of $f(x,y)$ is drawn for one arbitrary value of θ.

Based on the description of the Radon–transform and the definition of a projection, conditions can be formulated which a two–dimensional function must satisfy to be "projectable" (Radon, 1917). These conditions are:

- The function has to be limited in space, that is: there exists a finite value of q for which $f(x,y)=0$ for all values of x and y for which holds: $x^2+y^2 > q^2$ (or in polar coordinates: $f_p(r,\phi)=0$ for $r > q$).
- The function has to be bounded, that is: there exists a finite value m for which $|f(x,y)| < m$ for every x,y.

In our case the function $f(x,y)$ is the distribution of a physical quantity in a limited object and these conditions are, therefore, always satisfied.

3.3 Fourier–transforms

In this section the definitions of the Fourier–transforms and their corresponding inverse transforms in one and two dimensions will be given for reference purposes.

The one–dimensional Fourier–transform $F(X)$ of a function $f(x)$ is defined as:

$$F(X) = \int_{-\infty}^{\infty} f(x)\ e^{-2\pi i X x}\ dx \qquad (3.3.1)$$

Its inverse transform is given by:

$$f(x) = \int_{-\infty}^{\infty} F(X)\ e^{2\pi i X x}\ dX \qquad (3.3.2)$$

27

Analogously, when $F(X,Y)$ is the two-dimensional Fourier-transform of the function $f(x,y)$ then:

$$F(X,Y) = \int_{-\infty}^{\infty} \int_{-\infty}^{\infty} f(x,y)\ e^{-2\pi i(Xx+Yy)}\ dx\ dy \qquad (3.3.3)$$

With the inverse transform:

$$f(x,y) = \int_{-\infty}^{\infty} \int_{-\infty}^{\infty} F(X,Y)\ e^{2\pi i(xX+yY)}\ dX\ dY \qquad (3.3.4)$$

This can be written in polar coordinates by substituting $x = r\cos\phi$, $y = r\sin\phi$, $X = R\cos\theta$ and $Y = R\sin\theta$ in Eq. (3.3.3):

$$F_P(R,\theta) = \int_{0}^{2\pi} \int_{0}^{\infty} f_P(r,\phi)\ e^{-2\pi i Rr\cos(\theta-\phi)}\ r\ dr\ d\phi \qquad (3.3.5)$$

And the inverse transform:

$$f_P(r,\phi) = \int_{0}^{2\pi} \int_{0}^{\infty} F_P(R,\theta)\ e^{2\pi i rR\cos(\phi-\theta)}\ R\ dR\ d\theta \qquad (3.3.6)$$

When ϕ is integrated only from 0 to π these transforms can be written as:

$$F_P(R,\theta) = \int_{0}^{\pi} \int_{-\infty}^{\infty} f_P(r,\phi)\ e^{-2\pi i Rr\cos(\theta-\phi)}\ |r|\ dr\ d\phi \qquad (3.3.7)$$

And:

$$f_P(r,\phi) = \int_{0}^{\pi} \int_{-\infty}^{\infty} F_P(R,\theta)\ e^{2\pi i rR\cos(\phi-\theta)}\ |R|\ dR\ d\theta \qquad (3.3.8)$$

28

3.4 The central-section theorem

To be able to derive the inversion formula of the Radon-transform it is useful to present the so-called central-section theorem first.

When we take the one-dimensional Fourier-transform $P_\theta(R)$ (see Eq. (3.3.1)) of a projection at angle θ as defined by Eq. (3.2.3), we get:

$$P_\theta(R) = \int_{-\infty}^{\infty} p_\theta(t)\ e^{-2\pi iRt}\ dt =$$

$$= \int_{-\infty}^{\infty} \left[\int_{L_{t\theta}} f(t\cos\theta - s\sin\theta, t\sin\theta + s\cos\theta)\ e^{-2\pi iRt}\ ds \right] dt \qquad (3.4.1)$$

The combination of the two integrals represents a surface-integral on Ω because $f(x,y) = 0$ outside the region Ω. When we change the variables in Eq. (3.4.1) from polar to Cartesian, so that $t = x\cos\theta + y\sin\theta$, this expression can be rewritten as:

$$P_\theta(R) = \iint_{\Omega} f(x,y)\ e^{-2\pi i(Rx\cos\theta + Ry\sin\theta)}\ dx\ dy \qquad (3.4.2)$$

When this result is compared with the definition of the two-dimensional Fourier-transform in Eq. (3.3.3) we see that:

$$P_\theta(R) = F(R\cos\theta, R\sin\theta) \qquad (3.4.3)$$

This result is known as the central-section theorem or as the projection-slice theorem. In words the central-section theorem states that the Fourier-transform $P_\theta(R)$ of a projection $p_\theta(t)$ of $f(x,y)$ at angle θ is identical to a section through the two-dimensional Fourier-transform $F(X,Y)$ of $f(x,y)$ taken along a line going through the origin and at an angle θ with the X-axis (see Figure 3.5).

This result proves to be very important in the derivation of inverse Radon-transform methods.

29

3.5 The inverse Radon-transform

In this section the analytical descriptions will be given of four methods of performing the inverse Radon-transform. As in the previous sections, we confine ourselves to the special case of a two-dimensional function $f(x,y)$ which is to be reconstructed from its one-dimensional projections $p_\theta(t)$.

The first method of performing the inverse Radon-transform is using the inversion formula given by Radon himself (1917), which can be written as (Barrett and Swindell, 1977):

$$f_P(r,\phi) = \frac{1}{2\pi^2} \int_0^\pi d\theta \int_{-\infty}^\infty \frac{dp_\theta(t)/dt}{r\cos(\theta-\phi) - t} \, dt \qquad (3.5.1)$$

Where $f_P(r,\phi)$ is the representation in polar coordinates of $f(x,y)$.

The second method is very straightforward and based on the central-section theorem (Eq. (3.4.3)). If we take the one-dimensional Fourier-transform $P_\theta(R)$ of each projection $p_\theta(r)$ and represent these transforms in the Fourier plane (in polar coordinates) as one two-dimensional function $P_P(R,\Theta)$, then the central-section theorem implies that the two-dimensional inverse Fourier-transform of $P_P(R,\Theta)$ is $f_P(r,\phi)$. So, when $F^{-1}\{.\}$ denotes the inverse two-dimensional Fourier-transform, then the second inversion formula can be written as:

$$f_P(r,\phi) = F^{-1}\{P_P(R,\theta)\} \qquad (3.5.2)$$

This method of performing the Radon-inversion is referred to as the Fourier-transform method because the inversion is performed via the Fourier domain.

The third method for the Radon-inversion can be derived from Eq. (3.5.2) by performing the Fourier-transform and representing the function $f_P(r,\phi)$ in Cartesian coordinates. If we use the definition of the Fourier-transform given in Eq. (3.3.8) then, after applying the cosine subtraction formula, the inversion formula Eq. (3.5.2) can be written as:

$$f_P(r, \phi) = \int_0^\pi \int_{-\infty}^{\infty} P_P(R, \theta) \ e^{2\pi iR(r \cos\phi \cos\theta + r \sin\phi \sin\theta)} \ |R| \ dR \ d\theta \qquad (3.5.3)$$

If we represent $f_P(r, \phi)$ in Cartesian coordinates by substituting $x = r \cos\phi$ and $y = r \sin\phi$, then Eq. (3.5.3) becomes:

$$f(x, y) = \int_0^\pi \int_{-\infty}^{\infty} P_P(R, \theta) \ e^{2\pi iR(x \cos\theta + y \sin\theta)} \ |R| \ dR \ d\theta \qquad (3.5.4)$$

This expression can be rewritten as:

$$f(x, y) = \int_0^\pi g(x \cos\theta + y \sin\theta, \ \theta) \ d\theta, \qquad (3.5.5a)$$

$$\text{with:} \quad g(t, \theta) = \int_{-\infty}^{\infty} P_P(R, \theta) |R| \ e^{2\pi iRt} \ dR \qquad (3.5.5b)$$

So $g(t, \Theta)$ is the one-dimensional inverse Fourier-transform with respect to the first variable of $P_P(R, \Theta)|R|$. Because a product in the Fourier domain is equivalent to a convolution in the spatial domain, $g(t, \Theta)$ can also be written as:

$$g(t, \theta) = p(t, \theta) * h(t) \qquad (3.5.6)$$

Where $*$ is the convolution sign and $h(t)$ is the inverse Fourier-transform of $|R|$. So the third Radon-inversion formula can be written as:

$$f(x, y) = \int_0^\pi p(t, \theta) * h(t) \ d\theta, \quad \text{with:} \quad t = x \cos\theta + y \sin\theta \qquad (3.5.7)$$

In this case the inverse Radon-transform is performed in the spatial domain. The Radon-inversion according to Eq. (3.5.5) or Eq. (3.5.7) is called the filtered back-projection or convolution back-projection method. This

31

name comes from a physical interpretation of the inversion formula. Eq. (3.5.5a) and the integrand in Eq. (3.5.7) are the convolution of a projection $p(t,\Theta)$ with a filter function $h(t)$, which accounts for the first part of the name. For the explanation of the term back-projection we use Eq. (3.2.1), where $p(t,\Theta)$ was defined as the line-integral along the ray $L_{t\Theta}$ of the function $f(x,y)$ with $x = t\cos\Theta - s\sin\Theta$ and $y = t\sin\Theta + s\cos\Theta$. When we multiply these equations for x and y on both sides with $\cos\Theta$ and $\sin\Theta$ respectively and add the two resulting equations we get: $t = x\cos\Theta + y\sin\Theta$. So, in Eq. (3.5.5a) and Eq. (3.5.7) the value of $f(x,y)$ at the point (x,y) is obtained by adding the values from the filtered projections belonging to all rays passing through that point. In other words, the values of the filtered projections are "projected back" into the plane along the rays from which they were obtained.

The fourth method of performing the Radon-inversion is known as the algebraic reconstruction technique or ART (Glover et al., 1970). This technique is mentioned here for completeness and only a very global description will be given. A very detailed description of the method has been given by Herman et al. (1973). ART is an iterative process, performed in the following way. The starting point of the process is an estimate $f_e(x,y)$ of the function $f(x,y)$. Very often the estimated values of this function are taken zero for all values of x and y. From the function $f_e(x,y)$ the projections $p_{\Theta e}(t)$ are calculated along the same rays $L_{t\Theta}$ as used in the determination of the measured projections $p_\Theta(t)$ (see Section 3.1 and Figure 3.1). Each value $p_{\Theta e}(t)$ in the projections of the estimated function is compared with the corresponding measured one, $p_\Theta(t)$, and then, based on this comparison, the values of the estimated function on the ray $L_{t\Theta}$ are altered. This alteration of the values of $f_e(x,y)$ can be done in two ways. The first one is called additive ART. In this case the difference between the values of $p_\Theta(t)$ and $p_{\Theta e}(t)$ is spread evenly along the ray $L_{t\Theta\Omega}$, where Ω is the measured region and $L_{t\Theta\Omega}$ the part of $L_{t\Theta}$ within that region. So the new values of $f_e(x,y)$ are calculated according to:

$$f_{e\,NEW}(x,y) = f_e(x,y) + \frac{p_\Theta(t) - p_{\Theta e}(t)}{\|L_{t\Theta\Omega}\|} \tag{3.5.8}$$

In this expression $\|L_{t\Theta\Omega}\|$ indicates the length of $L_{t\Theta\Omega}$. The other method of adapting the estimated function is called multiplicative ART. In this

method, the values of $f_e(x,y)$ are altered according to the ratio of the measured and the estimated projection values, so:

$$f_{e\,NEW}(x,y) = f_e(x,y)\ \frac{p_\theta(t)}{p_{\theta e}(t)} \tag{3.5.9}$$

After adapting $f_e(x,y)$ for all rays a new estimate of $f(x,y)$ has been obtained with which the process can be repeated. This continues until the difference between the estimated and the measured projections does not decrease anymore. When this is the case, $f_e(x,y)$ is considered to be an optimal approximation of the measured function.

3.6 Filtered back-projection and quantization

In the previous section four methods to perform the inverse Radon-transform have been presented in their analytical form. In practice we will use a digital computer to perform the image reconstruction, so we will need a discrete version of the inverse Radon-transform. In this section one of the four described methods will be chosen to be implemented on a computer and the consequences of the conversion into a discrete form of that method will be discussed.

First the choice of the method. An experiment, performed by a student in our research group, indicated that the direct implementation of the inversion formula presented by Radon as given in Eq. (3.5.1) is rather complicated. Furthermore it is known that the discrete determination of a derivative tends to cause numerical instability and is very sensitive to noise. Besides the problems concerning noise and numerical instability, the denominator of the integrand in Eq. (3.5.1) has a singularity for $t = r\cos(\theta-\phi)$. Because of this the numerical approximation of the integral will need an excessive amount of computation time. These problems are probably the reason for the fact that no practical use of this inversion formula is mentioned in the literature.

In spite of the fact that the ART was originally designed as a discrete Radon-inversion, there are problems associated with this method, as indicated by the rather contradicting publications written on this subject (Gordon et al., 1970, Gilbert, 1972, Herman et al., 1973). These problems mainly concern the convergence of the algorithm, the sensitivity

to noise and the computation time. A detailed discussion of these problems is beyond the scope of this thesis. Attempts to implement an ART algorithm on a personal computer for the reconstruction of measurements showed the aforementioned problems (Muijtjens, 1985). In several cases the algorithm showed a poor convergence. Furthermore it proved to be quite difficult to determine correct projections from the estimated two-dimensional functions and it turned out that the algorithm was time consuming and sensitive to noise. Although ART was very popular in the first applications of computed tomography, it was later almost completely replaced by the so called direct reconstruction techniques (the filtered back-projection and the Fourier transform method). This was because of the previously mentioned problems, combined with the fact that ART is not guaranteed to converge to the correct image of the measured two-dimensional distribution (Gilbert, 1972).

From the previous paragraphs it may be obvious that the choice of a reconstruction technique is now restricted to the Fourier-transform method and the filtered back-projection method. The image quality of both methods will be approximately the same because both methods are based on the same Radon-inversion principle. The filtered back-projection seemed to be the most suitable one for implementation on a very small computer because no Fourier-transforms are needed. Furthermore the discrete inverse Fourier-transform that is necessary when using the Fourier-transform method, has to be calculated on a Cartesian grid, whereas the function which has to be transformed is defined on a polar grid, because of the nature of the central-section theorem. Therefore, with this method, a two-dimensional interpolation will be needed in the discrete reconstruction (Mersereau and Oppenheim, 1974). These facts are the reasons why the filtered back-projection technique has been chosen to be implemented in the ultrasound tomography system that is described in this thesis.

In the derivation of the filtered back-projection in Section 3.4 it was assumed that the projections were known for all ray positions t and for all angles Θ. In practice, however, the projections are known for only a limited number of discrete values of t and also for only a limited number of angles Θ. In the following the consequences of this quantization will be described.

For the reconstruction of an image we have at our disposal a set of N projections, measured at angles $n\Delta\Theta$ (n is an integer and $1 \leq n \leq N$). Each

of these projections consists of M equispaced samples at positions $m\Delta t$ (m is also an integer and $1 \leq m \leq M$). So, when L_P is the length of each linear scan, then $\Delta t = L_P/M$ and $\Delta\Theta = \pi/N$ because the scans are measured over a range of 180 degrees. A consequence of sampling the projections is, that their Fourier-transforms become periodic with a period of $1/\Delta t$. Because the projections are spatially limited, which means that they are equal to zero outside a finite interval, the Fourier-transforms of these projections will be unlimited. So, when such a projection is sampled, the repeated spectra will interfere with the original spectrum, making it impossible to obtain a distortion-free estimation of the real projection from the sampled one. This effect, known as aliasing, can be prevented with a low-pass pre-sampling filter with a cut-off frequency less than $1/(2\Delta t)$. Unfortunately it is impossible to filter the object itself, so the only pre-sampling filter action present is caused by the low-pass character of the measuring process. Because the cut-off frequency of this filter is hard to determine at will, the sampling frequency has to be adjusted to the measurement process. For the rest of this section it is assumed that the sampling frequency is high enough to prevent aliasing. The practical values of the sampling frequency used in the measuring apparatus will be given in Chapter 9.

Although the absence of aliasing is assumed, there is still another limitation due to the sampled nature of the projections. This limitation is that the real projections can only be estimated with a limited bandwidth of $1/(2\Delta t)$ (Nyquist theorem). From this it obvious that the reconstructed function can at best only be a band limited estimation $f_B(x,y)$ of the original function $f(x,y)$. Apart from being band limited the function $f_B(x,y)$ has to be represented in a discrete way also, so the reconstructed image $f_B(x,y)$ is a function of $k\Delta x$ and $l\Delta y$ rather than of x and y, with $1 \leq k \leq K$ and $1 \leq l \leq L$, where K and L are the respective dimensions of the reconstructed area in the X and the Y direction. To obtain the values of $f_B(k\Delta x, l\Delta y)$ by back-projection, the integral in Eq. (3.5.5a) or Eq. (3.5.7) has to be evaluated in a discrete way. The simplest way to do this is by using the trapezoidal rule, so the discrete back-projection can be written as:

$$f_B(k\Delta x, l\Delta y) \approx \Delta\theta \sum_{n=1}^{N} g(k\Delta x \cos(n\Delta\theta) + l\Delta y \sin(n\Delta\theta), n\Delta\theta) \qquad (3.6.1)$$

From this expression it can be seen that $g(t',n\Delta\Theta)$ has to be known for $t' = k\Delta x \cos(n\Delta\Theta) + l\Delta y \sin(n\Delta\Theta)$. As will be shown in the following, $g(t,n\Delta\Theta)$ is the discrete, filtered projection, so its values will only be known at the positions $n\Delta t$. These positions will, in general, not coincide with the mentioned value of t', so an interpolation will be needed to determine the value of $g(t',n\Delta\Theta)$. The interpolation used here will be a linear interpolation because it gives equally good or better results than other techniques (Rowland, 1979) and it is one of the simplest and fastest interpolation techniques for implementation on a small computer. In the Fourier domain this interpolation can be represented as a low-pass filter $I(R)$ which removes the repeated spectra introduced by the sampling and, by doing so, recovers the original signal. In the case of linear
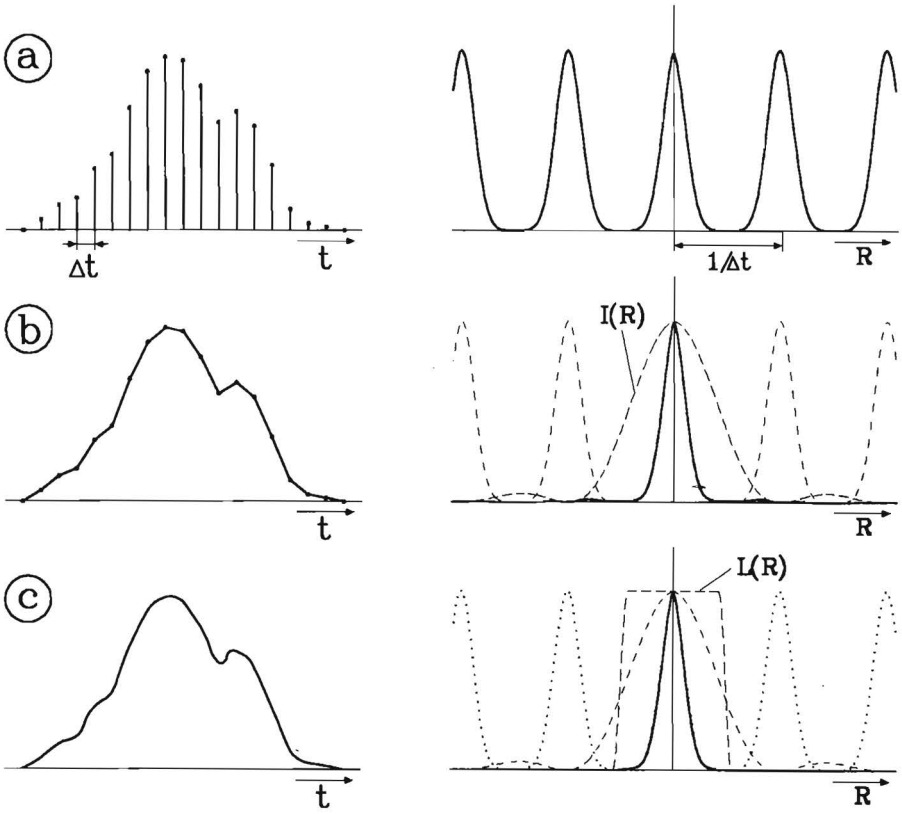
Fig.3.8) The effects of sampling, linear interpolation and low-pass filtering in the spatial domain (left) and the Fourier domain (right). a) Sampled signal, b) after linear interpolation (I(R)) without low-pass filtering and c) after linear interpolation and low-pass filtering with L(R).

36

interpolation, $I(R) = \text{sinc}^2(R)$ (Rowland, 1979), and therefore there are still some high frequency components remaining from the repeated spectra (see Figure 3.8a). This is also obvious when the spatial domain representation of the linearly interpolated function is drawn. Such a representation can have rather sharp angles at the sample points (Figure 3.8a), giving rise to high frequency components in the Fourier-transform. This effect can be reduced by applying a low-pass filter $L(R)$ before the interpolation is performed (Figure 3.8b). This low-pass filter suppresses the repeated spectra so that after the interpolation little or no unwanted high frequency components will remain. This low-pass filter can be combined with the filtering that was already necessary for performing the filtered back-projection, so the filtering given in Eq. (3.5.5b) can now be written as:

$$g(t,\theta) = \int_{-\infty}^{\infty} P_P(R,\theta) W(R) \, e^{2\pi i R t} \, dR \qquad (3.6.2)$$

In this expression $W(R) = |R| L(R)$. More details about the choice of a suitable filter function $W(R)$ will be given in Chapter 6 where the actual implementation of the discrete filtered back-projection will be discussed.

In summary, image reconstruction using the discrete filtered back-projection is performed in three steps. The first step is the discrete convolution of the sampled projections with the filter function $w(t)$, which is the inverse Fourier-transform of the function $W(R)$:

$$g(m\Delta t, n\Delta\theta) = \Delta t \sum_{i=1}^{M} p(i\Delta t, n\Delta\theta) \; w((m-i)\Delta t) \qquad (3.6.3)$$

Note that $p(l\Delta t, n\Delta\theta) = 0$ for $i < 1$ and $i > M$ so no summation from $-\infty$ to ∞ is needed. The second step is the interpolation:

$$g(t',n\Delta\theta) = g(m'\Delta t, n\Delta\theta) - \frac{t'-m'\Delta t}{\Delta t}[g((m'+1)\Delta t, n\Delta\theta) - g(m'\Delta t, n\Delta\theta)] \qquad (3.6.4)$$

Where m' is the largest value of m for which $m\Delta t \leq t'$. The third step in the reconstruction process is the discrete back-projection:

37

$$f_B(k\Delta x, l\Delta y) = \Delta\theta \sum_{n=1}^{N} g(k\Delta x \cos(n\Delta\theta) + l\Delta y \sin(n\Delta\theta), n\Delta\theta) \qquad (3.6.5)$$

In practice the last two steps are combined. The interpolation is performed at the moment that a value of $g(t', n\Delta\theta)$ is needed during the back-projection process.

The effect of the quantization of θ is quite complicated to describe analytically and there is also an interaction between the sampling of θ and the sampling of t. A rather detailed discussion of the effect of the quantization of θ is given by Lewitt (1983). Lewitt states that, in most applications, no additional errors will be introduced when the number of projections, N, and the number of rays in a projection, M, satisfy the following criterion:

$$N-1 > \frac{\pi M}{2} \qquad (3.6.6)$$

The effect of radial sampling will be evaluated in practice in Section 9.1 where some results of the reconstruction by filtered back-projection of simulated data will be shown. In Section 10.1 some remarks will be made on the influence of the discrete reconstruction process on the accuracy of the resulting image.

3.7 **Necessary conditions for application**

In this section the conditions are given which must be satisfied when the Radon-transform and its inverse are to be used in a practical application. These conditions will not be discussed here in depth because they follow directly from the previous sections or they have been discussed in detail in the literature.

1) When a function is to be reconstructed from sets of measured data these sets have to be projections. In other words: the measured values must have a one-to-one relationship with line-integrals of the two-dimensional distribution of a physical quantity in the scan plane.

2) The measured projections have to be complete, so the area where the

measured distribution is not equal to zero, must have been covered entirely by the scan plane.

3) The measured function $f(x,y)$ has to be isotropic. This means that, if $p_\theta(t)$ denotes a projection of $f(x,y)$ at an angle Θ, then for all values of Θ:

$$\int_{-\infty}^{\infty} p_\theta(t) \ dt = \iint_{\Omega} f(x,y) \ dx \ dy = C \qquad (3.7.1)$$

Where C is a constant independent of Θ. The effects of anisotropy on computed tomography have been studied extensively by Brandenburger et al. (1981).

4) The previous condition is in fact a special case of the general condition that the set of projections must be consistent, that is, all projections have to be projections of the same two-dimensional function. For example, a set of inconsistent projections will be obtained when a large measurement error occurs in only one projection. This set will be inconsistent because one projection seems to contain a projected structure which is not present in the other projections. A set of projections will also be inconsistent if there is data missing from one or more projections. It has been shown that in some cases a set of inconsistent projections can still be reconstructed into a reliable image (Choi et al., 1982).

39

Measurement Principles

This chapter discusses the physical quantities that can be measured in the ultrasound tomography system described in this thesis, together with their measurement principles.

Section 4.1 describes the measurement of the local sound propagation velocity. In the following, the sound propagation velocity will also be referred to as speed of sound or sound velocity. In Section 4.2 the "attenuation slope" measurement will be discussed. The attenuation slope is the derivative with respect to frequency of the attenuation coefficient at the center-frequency of the transmitted pulse. In the literature this attenuation slope is often, in fact incorrectly, referred to as the attenuation coefficient. In Section 4.3 the measurement of the actual attenuation coefficient will be discussed.

For each measurement it will be proved that the related physical quantity can be reconstructed from the measured values by showing that the conditions from Section 3.7 are satisfied. Because the scan plane is a rotating rectangle during the scan process (see Section 2.1), not all points of the scan plane will be projected in each projection. To be sure that the projections are complete, the second demand of Section 3.7 will be narrowed down to the demand that the measured quantity must be zero outside the object which is being measured.

At the end of this chapter, in Section 4.4, there will be a description of the possibility of performing reflection measurements with the tomography system in addition to the other three measurements. Although this measurement has not been realized yet, it is described here because there is work in progress on the implementation of the reflection measurement as an extension of the ultrasound tomography system.

4.1 The sound propagation velocity

In the tomography system the determination of the local sound propagation velocity in a cross-section of an object is performed by time-of-flight measurements. At each transducer position the time between the moment of transmission of the ultrasound pulse and the moment of arrival at the receiving transducer is measured. The technical details on this measurement will be described in Section 5.1.

It was stated in the previous chapter (Section 3.7) that, in order to reconstruct a relevant image from the measurements, it is necessary that the measured time-of-flight values represent line-integrals along the path of the sound pulse of a two-dimensional distribution. It can be seen that the time-of-flight values are indeed line-integrals. Each measured value is the total of all time-of-flight values at small parts, ds, on the path, L, of the sound pulse between the transducers. When $v(s,t)$ is the local speed of sound, where t is the coordinate giving the position along the linear scan and s the coordinate along the path of the sound pulse (Figure 4.1), it is obvious that the time-of-flight value on ds at position s is $ds/v(s,t)$. So, the total time-of-flight $T(t)$ between the two transducers at position t is:

$$T(t) = \int_L \frac{1}{v(s,t)} \, ds \qquad (4.1.1)$$

Because of this result, the sets of time-of-flight values measured along the linear scans are projections of the distribution of the local time-of-flight per unit length, $1/v(x,y)$. A set of these scans, measured in different directions can, therefore, be reconstructed into an image of $1/v(x,y)$. This image can be transformed into an image of the local sound propagation velocity $v(x,y)$ by inversion of all values in the image.

It can be seen that the condition that the time-of-flight has to be zero outside the object is not satisfied because the object is surrounded by water and water has a finite sound velocity. However, the measurements can easily be made to satisfy this condition, by subtracting the time-of-flight value measured with only water between the transducers from the other measured values. This will yield an image of the local time-of-flight per unit length values minus the value in water. This image can be converted into the image of the absolute local
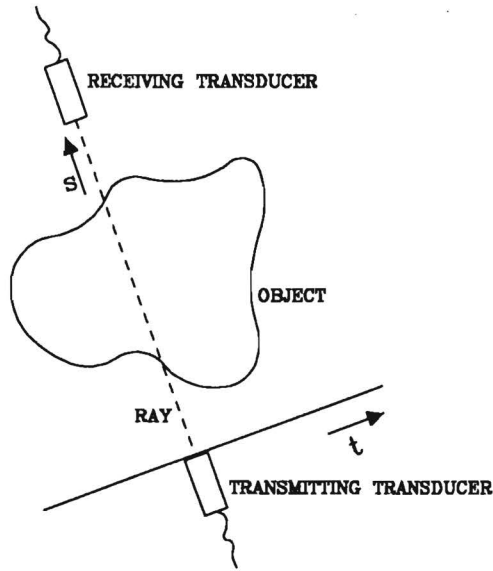
Fig.4.1) Definition of the coordinates used in the description of the measurements.

time-of-flight by adding to all values in the image the time-of-flight obtained with only water between the transducers, divided by the distance between the transducers.

From the previous paragraphs it can be concluded that the first two conditions from Section 3.7 are satisfied. The other conditions will now be examined. Although there are some biological materials that show anisotropy, biological materials will be assumed to be isotropic for the rest of this chapter. In Chapter 10 the possible effects of anisotropy will be discussed as far as they are known. If the measurements can be performed without large errors there are no other reasons for the projections to be inconsistent so all conditions from Section 3.7 are satisfied in the case of the measurement of the local sound velocity.

4.2 The attenuation slope

The physical quantity discussed in this section is generally called the attenuation coefficient. In the course of this section it will become clear why this is not entirely correct and why the name attenuation slope should be preferred.

In a homogeneous, attenuating medium the relation between the transmitted sound intensity, I_T, and the received intensity, I_R, for a plane wave is given by (Hill, 1978, Nyborg, 1978, the "Lambert–Beer law" of attenuation):

$$I_R = I_T e^{-\alpha L} \qquad (4.2.1)$$

In this expression L is the distance between the transducers and α is the attenuation coefficient of the material between the transducers. The intensity I is defined as the amount of power transferred through a unit area (Wells, 1978, Cracknell, 1980) and it is expressed in Wm^{-2} or $Js^{-1}m^{-2}$. The attenuation coefficient α is frequency dependent. In the literature (Parry and Chivers, 1979, Simonds, 1983, Janssen, 1986) it is shown that this dependence can be written in general as:

$$\alpha(\omega) = \alpha_0 + \alpha_1 (\omega/c)^n \qquad (4.2.2)$$

Here α_0, α_1 and n are material dependent constants and c is a scaling constant which serves to make the part of the expression between the brackets dimensionless. The numerical value of c is taken as equal to 1 and therefore c will be omitted in the rest of this section. The expression for $\alpha(\omega)$ given by Eq. (4.2.2) is assumed to be valid throughout the frequency range of $1-10\,MHz$, which is the range normally used in diagnostic applications of ultrasound. In the literature it is generally assumed that, in this diagnostic range, the dispersion is negligible. Therefore, although frequency dependent attenuation implies the presence of at least some dispersion (Kramers–Kronig relations), the dispersion is neglected in the derivations given in this chapter. Possible effects of neglecting the dispersion will be discussed in Section 10.6.

In the very early days of medical ultrasound it was thought that, for biological tissues, the value of n in Eq. (4.2.2) is equal to 2. This assumption was based on the classical theory for absorption of ultrasound

in liquids and gases (Cracknell, 1980). Very soon, however, it was noted that this assumption was not correct (Pohlman, 1939) and it was shown that the attenuation in tissues has an approximately linear frequency dependence (Hueter, 1948, Wells, 1975). More recently it was shown that some tissues have a nonlinear dependence on the frequency. In general, the value of n in Eq. (4.2.2) is between 1 and 2 (Hill, 1978) and sometimes even larger ($n = 4$ in the case of Rayleigh scattering).

Based on the assumption that the attenuation is proportional to the frequency, Dines and Kak (1979) showed that it is possible to determine the integrated attenuation of an ultrasound pulse passing through tissues from the difference in the center frequencies of the spectra of the transmitted and the received pulse. They showed that this method is more accurate than direct measurement of the received amplitude or intensity. The reason for this higher accuracy is the fact that amplitude or intensity measurements also measure the signal losses caused by reflection and refraction, whereas the center frequency difference is much less sensitive to those effects. The change in the center frequency of a sound pulse passing through an attenuating medium is caused by the frequency dependence of the attenuation. Because of this frequency dependence the higher frequencies are attenuated more than the lower frequencies which causes a decrease in the center frequency. In the following this decrease will be called the center frequency down shift.

The method proposed by Dines and Kak can only be used to determine an attenuation coefficient that is proportional to the frequency, that is if in Eq. (4.2.2) $\alpha_0 = 0$ and $n = 1$. These assumptions are not necessary when the decrease in the center frequency is used only to determine the derivative with respect to frequency of the attenuation coefficient and not to determine the attenuation coefficient itself. The remainder of this section deals with the determination of this attenuation slope by means of the center frequency down shift measurement.

Many investigators have indicated that a pulse, transmitted by a standard ultrasound transducer, can be considered as a cosine with a Gaussian envelope (Dines and Kak, 1979, Ophir and Jaeger, 1982, Flax et al., 1983, Simonds, 1983). The sampling and Fourier-transforming of some typical sound pulses confirmed that this is also the case for the transducers used in the tomography system described in this thesis (unpublished results), so in the following a Gaussian pulse shape will be assumed.
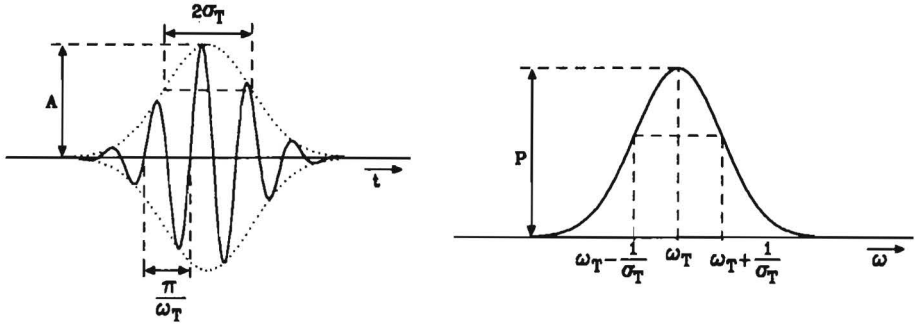
Fig.4.2) Time domain (left) and frequency domain (right)
representation of a Gaussian sound pulse.

In the time domain a transmitted sound pulse can be represented as:

$$f(t) = A \cos(\bar{\omega}_T t) \exp(-t^2/2\sigma_T^2) \tag{4.2.3}$$

In this expression $\exp(x) \equiv e^x$, $\bar{\omega}_T$ is the transmitted center frequency, σ_T is a measure for the width of the pulse and A is the amplitude of the pulse. In the frequency domain this pulse can be written as:

$$F(\omega) = P \exp\left[\frac{-(\omega - \bar{\omega}_T)^2}{2\sigma^2}\right] \tag{4.2.4}$$

In this expression $\sigma = \sigma_T^{-1}$ and P is a constant. A graphical representation of $f(t)$ and $F(\omega)$ is given in Figure 4.2. To be able to evaluate the center frequency down shift of an ultrasound pulse passing through an inhomogeneous object along a ray L, we first evaluate the center frequency down shift, $d\bar{\omega}$, on a small part ds of L. On ds the object can be considered to be homogeneous, so the attenuation coefficient is constant. Furthermore, the center frequency down shift on ds is small and therefore the curve given by Eq. (4.2.2) is approximated by a straight line for frequencies close to $\bar{\omega}_T$. The spectrum $R(\omega)$ of the pulse after passing the distance ds is then:

$$R(\omega) = P \exp\left[\frac{-(\omega - \bar{\omega}_T)^2}{2\sigma^2}\right] \exp\left[-a_0 - a_1\left[\omega - \bar{\omega}_T\right] ds\right] \tag{4.2.5}$$

46

For a Gaussian spectrum the received center frequency $\bar{\omega}_R$ of $R(\omega)$ can be determined from:

$$\left.\frac{dR(\omega)}{d\omega}\right|_{\omega=\bar{\omega}_R} = 0 \tag{4.2.6}$$

Differentiating Eq. (4.2.5), it turns out that Eq. (4.2.6) is satisfied if:

$$\frac{\bar{\omega}_T - \bar{\omega}_R}{\sigma^2} - a_1 \, ds = 0 \tag{4.2.7}$$

The center frequency down shift $d\bar{\omega}$ on the path ds is:

$$d\bar{\omega} = \bar{\omega}_T - \bar{\omega}_R = a_1 \sigma^2 ds \tag{4.2.8}$$

From this the total center frequency down shift, $\Delta\bar{\omega}$, for a pulse travelling along the ray L can be obtained. This can be written as:

$$\Delta\bar{\omega} = \int_L d\bar{\omega} = \int_L a_1 \sigma^2 \, ds \tag{4.2.9}$$

Using Eq. (4.2.2) and keeping in mind the assumption that $n=1$ for frequencies close to $\bar{\omega}_T$, this expression can also be written as:

$$\Delta\bar{\omega} = \sigma^2 \int_L \left.\frac{d\alpha}{d\omega}\right|_{\omega=\bar{\omega}_T} ds \tag{4.2.10}$$

   From Eq.(4.2.10) it can seen that the center frequency down shift of an ultrasound pulse travelling along the ray L is proportional to the line integral of the derivative of $\alpha(\omega)$. This means that if the center frequency down shift is measured at different transducer positions along a linear scan, a projection of the frequency derivative of $\alpha(\omega)$ can be obtained if σ^2 is known. In Figure 4.3 a graphical representation of the measured quantity is given. At this point it will be obvious that the name attenuation slope measurement is to be preferred above attenuation measurement.

47
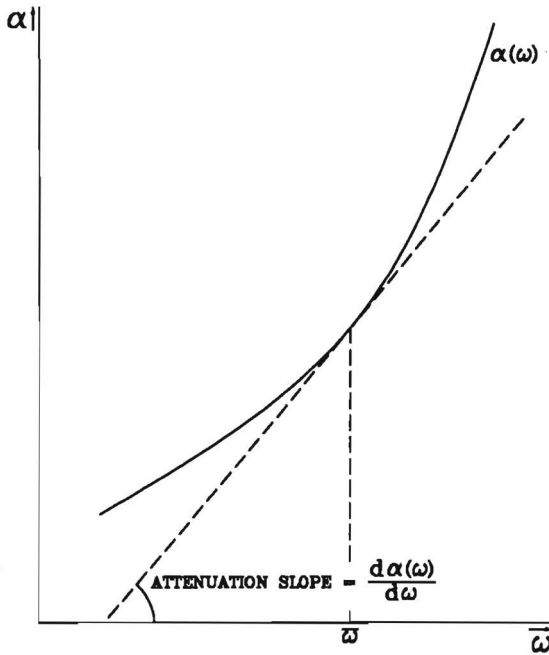
Fig.4.3) Graphical representation of the attenuation slope.

In the foregoing it was shown that the first condition from Section 3.7, which states that the measurements must yield projections, is satisfied. The other conditions will now be discussed. The attenuation slope of water is negligible compared to that of tissues (Dines and Kak, 1979), so the second condition that distribution must be space limited is satisfied. As stated in the previous section, tissues will be assumed to be isotropic which means that the condition of an isotropic distribution is also satisfied. Finally, it can be assumed that, provided that there are no large measurement errors, the projections are consistent.

Summarizing, it can be concluded that for the center frequency down shift measurement the conditions for reconstructibility are satisfied, so it is possible to obtain an image of the local attenuation slope from these measurements. The technical implementation of the center frequency down shift measurement will be described in Section 5.2.

48

4.3 The attenuation coefficient

This section describes the determination of the distribution of the attenuation coefficient by means of an amplitude measurement. Although it was stated in the previous section that this kind of attenuation measurement is, in general, less accurate than the center frequency down shift measurement, the amplitude measurement has been implemented in the tomography system. The reason for doing this is that the center frequency down shift measurement only determines the frequency derivative of the attenuation coefficient whereas the amplitude measurement yields the actual value of the attenuation (including the losses from reflection and refraction). Thus, the amplitude measurement can give additional information about the measured object.

Figure 4.4 serves to illustrate the difference between the two attenuation measurements. In this figure the values obtained from both kinds of measurements are given. This figure also shows an example of the case that two materials give the same value for the attenuation
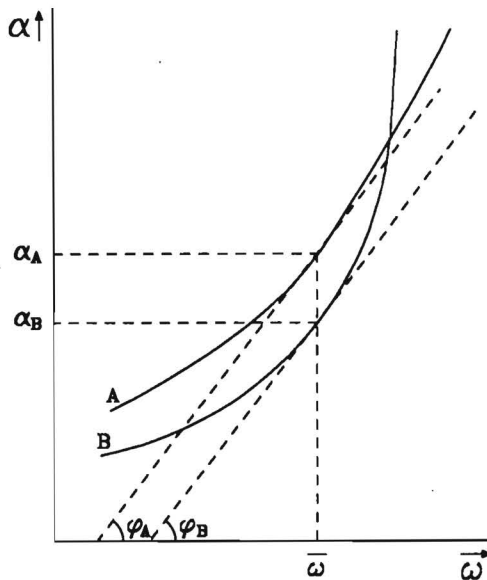
Fig.4.4) Comparison of the attenuation and the attenuation slope of two materials A and B. $\bar{\omega}$ is the transmitted center frequency, ϕ_A and ϕ_B are the attenuation slope values and α_A and α_B are the attenuation values. Note that $\phi_A = \phi_B$ and $\alpha_A \neq \alpha_B$.

slope measurement whereas the values obtained from the amplitude measurement will be different.

Another reason for performing the amplitude measurement is that the values of the amplitude may be useful in correcting the errors in the center frequency down shift measurement caused by phase cancellation or interference. A detailed description of the phase cancellation and interference errors and possible corrections of those errors will be given in Chapter 8.

The attenuation of an ultrasound pulse travelling through a medium has already been given in Eq. (4.2.1). Because the intensity of the sound is proportional to the square of the amplitude of the wave, this can be written as:

$$\ln\left(A_R/A_T\right) = -\tfrac{1}{2}\int_L a(s)\ ds \tag{4.3.1}$$

In this expression L is the path of the sound pulse (the ray), s is the coordinate along the ray and A_T and A_R are the respective amplitudes of the transmitted and the received sound pulses.

In order to determine the value of the line integral in Eq. (4.3.1) from the measured amplitude of the received signal A_R, the amplitude A_T of the transmitted signal must be known. Because the attenuation in water is negligible (Hill, 1978), it can be assumed that $A_T = A_R$ for a measurement with only water between the transducers. Thus, if the amplitude of the received pulses for all transducer positions along a linear scan are measured and the natural logarithm of the ratio of these measured values and the values measured in water are taken, a set of line integral values of the attenuation coefficient will be obtained. This means that such a set of values is a projection, so the first condition for reconstructibility from Section 3.7 is satisfied.

It will be obvious that in the water surrounding the object $A_R/A_T = 1$, so $\ln\left(A_R/A_T\right) = 0$. This means that the value of the measured quantity is equal to zero outside the object, so the second condition for reconstructibility is also satisfied.

Regarding the conditions of isotropy and consistency of the projections, the considerations from the previous sections also hold for the amplitude measurement.

From the previous it can be concluded that in the case of the

amplitude measurement the conditions for reconstructibility are satisfied.

It should be noted that the time-of-flight, the center frequency down shift and the amplitude can be measured from the same received pulse. So, after a complete scan (linear and rotational) of an object it is possible to obtain the images of the distribution of three independent physical quantities in the measured cross-section. These quantities are the local sound propagation velocity, the frequency derivative of the attenuation coefficient and the attenuation coefficient itself.

4.4 The reflectivity

This section is a preliminary one because the measurement described here has not been implemented yet. The purpose of this section is to indicate that it may be possible to perform a measurement of the reflectivity simultaneously with the three measurements described in the previous sections.

The distribution of the reflectivity in a cross-section of an object can be described as follows. The local reflectivity in a point of a cross-section is the ratio of the amplitudes of a sound pulse arriving at that point and its reflection from that point in the direction of the incident pulse.

The measurements, which have thus far been described in this chapter, use the part of the ultrasound that passes through the object. It is also possible to use the transmitting transducer as a receiver immediately after a pulse has been transmitted and thus measure the reflected signals returning from the object. It would be possible to obtain a conventional linear B-scan from these echoes at each angle of projection. The combination of all these scans from different angles would then give a compound scan. This method of reflectivity measurement will, however, need very fast analog to digital converters and a large amount of computer memory or some kind of two-dimensional analog storage. Because of the aim of simplicity and low cost it is being tried to find another way to perform the reflectivity measurement. The present idea will be explained in the following.

The method for measuring the reflectivity is based on the fact that, like in the transmission measurements, an image of the reflectivity can

be reconstructed from projections. If the measured echo-signal is integrated in time (which is easy to perform electronically), a line-integral of the reflectivity along the path of the sound pulse will be obtained. Because of this, the set of values of the integrated echo-signals taken along a linear scan will be a projection of the reflectivity distribution in the plane of interest. A problem with this is that the amplitude of the reflected signal not only depends on the reflectivity along the ray, but also on the attenuation. This causes the reflections from structures at a larger distance from the transducer to have a lower amplitude than reflections from a structure with the same reflectivity, but closer to the transducer. So, the integrated signal is not a pure line integral of the reflectivity, but a line integral of a quantity that depends on both the reflectivity and the attenuation. In order to be able to reconstruct an image of the reflectivity from these measurements, a correction for the attenuation will be necessary. This correction can be performed either during the measurement by using a time-gain-compensation (as in conventional echo scanning) or during the reconstruction. The latter will probably give better results because in that case the values of the local attenuation coefficient, obtained from the transmission measurements, can be used. Other advantages of correcting during the reconstruction is that the hardware can be much simpler and that the attenuation correction can be combined with a correction for the variation in the sound velocity. This velocity correction can be performed using the local sound velocity values obtained from the time-of-flight measurements.

To see whether the measurements of the reflectivity can be reconstructed into a relevant image, it is not sufficient to know that the measurements are projections, the other conditions from Section 3.7 will also have to be satisfied.

The condition that the function has to be space limited is satisfied because no echoes will occur when the sound beam is outside the object.

The condition concerning the isotropy of the measurement is not satisfied because the amplitude of a reflection from an interface is, among others, dependent on the angle between the interface and the sound beam. At this moment it is not easy to predict how this will affect the reconstructed image. This will have to be tested in practice.

At present there are no reasons to assume that incomplete projections will occur, so it will be assumed that the demand for the completeness of

the projections is satisfied.

From the previous it can be concluded that, although some problems may have to be overcome, it does seem to be possible to perform reflectivity measurements with the tomography system. The implementation of a reflectivity measurement is worth trying because it would probably improve the diagnostic value of the measurements performed with the ultrasound tomography system.

Measurement Techniques

This chapter describes the techniques that are used to perform the measurements which have been discussed in the previous chapter. The technical details of the implementation will be avoided as much as possible. An extensive description of these details will be given in Chapter 6.

In this chapter, and also in the following ones, the word "measurement" is used both for the determination of the characteristics of the received signal and for the complete process of scanning a cross-section of an object. In most cases it will be clear from the context which kind of measurement is referred to. In the cases where confusion may arise, the process of scanning a cross-section will be referred to as a scan or as the scanning process.

The contents of this chapter are the following: Section 5.1 will describe the time-of-flight measurement which is used to determine the local sound propagation velocity. In Section 5.2 the center frequency down shift measurement will be described. This measurement is used to determine the local frequency derivative of the attenuation which is called the local attenuation slope. Section 5.3 deals with the measurement of the amplitude of an ultrasound pulse. The amplitude measurement is used to determine the actual attenuation coefficient. Finally, in Section 5.4, some remarks will be made on the possible technique for the measurement of the reflected ultrasound. This last section will be a preliminary one similar to Section 4.4.

5.1 The time-of-flight measurement

To determine the time-of-flight of a pulse the exact moment of arrival of that pulse has to be measured. To do this accurately when only one pulse has been transmitted, a very fast analog to digital converter would be needed and a cross-correlation technique would have to be

applied (Greenleaf et al., 1975, Glover and Sharp, 1977). Because this method is expensive, another method for measuring the time-of-flight developed has been developed. This method will be described in the following paragraphs.

The time-of-flight measurement in the tomography system is performed using a reverberation technique (Baas, 1984, Stapper and Sollie, 1985). This reverberation technique is illustrated in Figure 5.1. The arrival of an ultrasound pulse at the receiving transducer triggers the high voltage pulse generator, which excites the transmitting transducer. So, each time a pulse is received a new pulse is transmitted. In this way the system reverberates with a frequency that is determined by the time-of-flight of the sound pulse between the transducers and the delay in the electronic circuitry. The latter is constant. The electronic delay does not have to be small to be negligible; it only needs to be constant because the reconstruction only uses the time-of-flight values relative to the values measured in the surrounding water (see Section 4.1). As the electronic delay is present in both the values measured in the object and the values measured in water it will not influence the reconstructed image. The detection of the arrival of a sound pulse will be discussed later in this section. The time-of-flight of the sound pulse can be determined by measuring the total duration of a number of cycles, say N, of the reverberation and dividing this duration by N. This measurement is performed by the component indicated as the time measuring device in Figure 5.1. The duration of the N cycles is measured using a counter which counts at a frequency of 1 MHz. This counter starts counting at the arrival of the first of the N pulses and stops at the arrival of the last. Note that the reverberation continues irrespective of the counter being active or not. After the N cycles, the counter is read and its value is stored by a micro-computer.

Using the reverberation technique, the accuracy of the measured time-of-flight values can, in theory, be improved at will by increasing the value of N. In practice however there are limitations to the value of N. If N is too large, then an overflow of the counter will occur. If this overflow occurs in every measured value there is no problem. In that case the error in the measured values is a constant which will be eliminated in the reconstruction process. If the overflow only occurs in some of the measurements, the error will not be eliminated, making it difficult to reconstruct a useful image from the measurements. Besides

OBJECT

AMP.

START UP OSCILLATOR → PULSE GENERATOR → TIME MEASURING DEVICE

MICRO COMPUTER

A

LEVEL DETECTOR —B→ ZERO CROSSING DETECTOR —C→ WINDOW

D
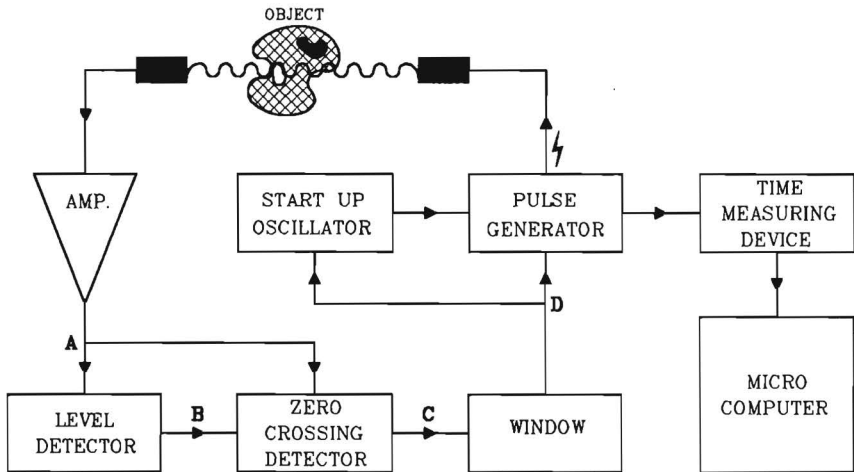
Fig.5.1) Schematic diagram of the time-of-flight measurement. The signals at the positions A to D are shown in Figure 5.2 and Figure 5.3.

the possible overflow, a large value of N will also slow down the measurement because the time needed to determine one sample will increase as N increases. In the measurements, N is chosen to be as large as possible under the condition that an overflow will not occur for the largest expected time-of-flight value. Most of the measurements are performed with $N \geq 400$.

The detection of the arrival of a pulse is performed as follows: the signal from the receiving transducer is amplified and fed into a detection circuit consisting of a level detector and a zero-crossing detector (Figure 5.1). The level detector compares the signal from the amplifier with a threshold which is just above the maximum noise level. As soon as the signal exceeds the threshold the level detector activates the zero-crossing detector which generates a pulse at the next zero-crossing of the signal (Figure 5.2). This pulse is used to indicate the moment of arrival of the sound pulse and it triggers the high voltage pulse generator. The level detector only indicates whether a pulse is received and with the zero-crossing detector the exact moment of arrival is determined. The reason for this is that the zero-crossing is independent of the amplitude of the sound pulse whereas the moment of the crossing of the threshold does depend on the amplitude. This is illustrated in Figure 5.2a.

57
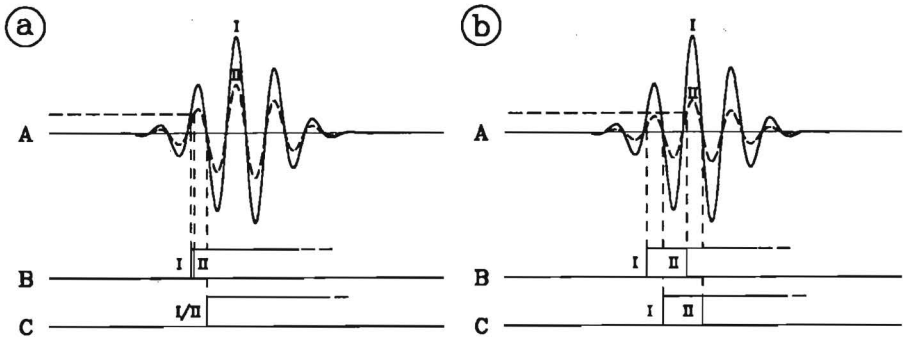
Fig.5.2) The received signal and the output signals of the level
detector and the zero-crossing detector. The signals are
indicated with the corresponding letters in Figure 5.1.
a) Shows why the zero- crossing is taken as the moment of
arrival and not the threshold crossing, b) shows why it is
necessary to use a threshold relative to the amplitude. I and
II refer respectively to the signal with the largest and the
signal with the smallest amplitude.

The dynamic range of the received signal is rather large. If a
structure containing bone is measured, the difference between the
smallest and the largest received signal can be 70 dB or even more. If the
amplifier, connected to the receiving transducer, has a fixed gain high
enough to obtain a reliable detection of the smallest signal it will
saturate for the largest signals. If this saturation occurs, the amplifier
will need some time to recover, which causes the zero-crossing to come
too late or even to disappear entirely. To prevent this the amplifier is
given an automatic gain control which reduces the gain when the
amplitude of the received signal increases.

Because the automatic gain control of the receiving amplifier is a
very simple one, the amplitude of the amplifier output signal will not be
completely constant over the full range of the gain control. If a fixed
threshold level were to be used, this could cause the zero-crossing
detector to be activated too late (Figure 5.2b). To prevent this, a better
gain control would be needed. It proved, however, to be much simpler to
use a threshold level relative to the amplitude of the signal. The latter
solution has the additional advantage that it enables, to some extent, a
reliable detection of the arrival of sound pulses with amplitudes that are
outside the control range of the automatic gain control. The determination
of the amplitude of the signal will be described in Section 5.3.

If the reverberation technique is applied as described earlier it will not function properly. There are two reasons for this. The first is obvious: the reverberation will have to start when the system is switched on or when a pulse is not detected. To be sure that the reverberation will always restart when it has been interrupted, the system has a start up oscillator which functions as a "on demand pacemaker". When, after the detection of a pulse, the next pulse is not detected within a certain preset time, which is longer than the longest expected time-of-flight, this circuit will trigger the high voltage pulse generator to generate a new pulse.

The other reason why the reverberation technique will not function is that spurious pulses can occur, for example by a vibration of the water tank or by electromagnetic interference. Each spurious pulse will also start to reverberate, causing the measured frequency to become a higher harmonic of the original reverberation frequency. This would, of course, give very large errors in the measured time-of-flight. To prevent this a time window is used. This window disables the pulse generator for some time immediately after a pulse has been transmitted, so that a spurious pulse that occurs within this window will not start a reverberation. To prevent the introduction of a higher harmonic of the reverberation frequency, the length of the window has to be at least half the cycle time of the reverberation. In that case, a spurious pulse
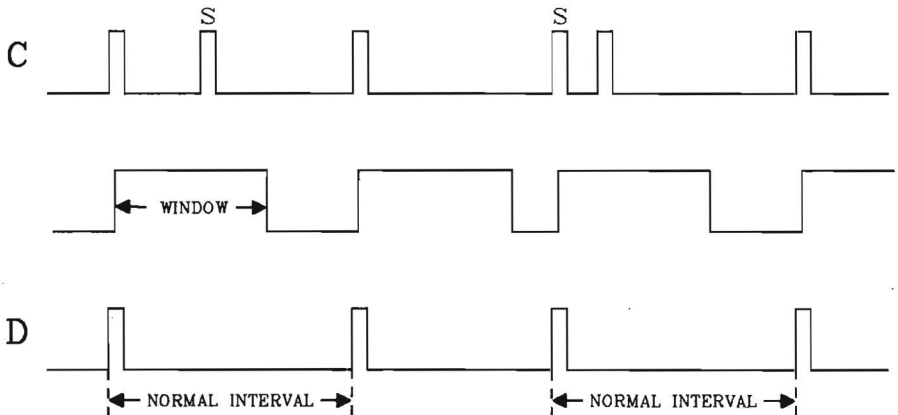

Fig.5.3) Principle of the time window. The pulses indicated with an "S" are spurious pulses, the letters to the left of the signals refer to Figure 5.1.

received after the window time will start to reverberate, but it will also activate the window again which will stop the reverberation of the original pulse (Figure 5.3). This means that a spurious pulse can cause one cycle of the reverberation to be shorter than the others, but because the measured value is the mean of 400 cycles this will not introduce a large error. It is easy to see that, if the window is set to half the cycle time, one spurious pulse can cause an error in the time-of-flight which is at worst $(0.5 / 400) \times 100 \% = 0.125 \%$. Because the sound velocity in soft tissues ranges from about 1450 m/s to 1650 m/s (Parry and Chivers, 1979), the time-of-flight in soft tissues will range from about 90 μs to 105 μs (the distance between the transducers is approximately 15 cm). If a bone of 4 cm diameter is present, the smallest value for the time-of-flight will be about 80 μs (the sound velocity in bone is about 3500 m/s). This means that the expected range of the time-of-flight values is be from about 80 to 105 μs. When the time-window is shorter than the smallest expected value (80 μs) and longer than half the largest expected value (53 μs), it will prevent all possible higher harmonics of the reverberation frequency without interfering with the measurements. To minimize the errors introduced by spurious pulses the window will be chosen to be as large as possible. For a window of 80 μs the worst possible error introduced by a spurious pulse is 0.06 % and the probability that a random spurious pulse will actually introduce an error is maximally 24 %.

To prevent errors that can be introduced by vibrations of the transducers when their scan movement is stopped for each measurement, the transducers move with a constant speed along the scan. Because of this a time-of-flight value obtained during the linear scan will be a mean of the values within a small strip instead of the value of one single ray.

The accuracy of the time-of-flight values obtained with the reverberation technique is about 25 ns, if a 1 MHz counter is used and 400 cycles of the reverberation. From this it can be calculated that a structure with a diameter of 5 mm and a sound velocity deviating 1 % (≈ 15 m/s) from its surroundings, can still be detected. Because of the fact that changes in time of flight are measured, the detectability of a structure will depend on the combination of size and sound velocity contrast. In Chapter 9 and 10 this will be evaluated further.

5.2 The center frequency down shift measurement

The measurement described in this section does not determine the center frequency down shift directly, it measures the center frequency of the received signal (Janssen, 1986). As stated in Section 4.2 the center frequency down shift in water is negligible, so the center frequency down shift of a received pulse can be determined by subtracting the center frequency of that pulse from the center frequency of a pulse measured in the water surrounding the object.

In Section 4.2 it was derived that the center frequency of a pulse, which can be described by a cosine with a Gaussian envelope, is the frequency of that cosine. This frequency can be determined by taking the inverse of the duration of one period of the received signal. So, in order to determine the center frequency of the pulse it is not necessary to sample and Fourier-transform the received signal, it is sufficient when the time between subsequent zero-crossings is measured. This time is measured using a period detector and a very high frequency counter (100 MHz). The period detector is activated by the level detector of the time-of-flight measurement. As shown in Figure 5.4, the period detector generates a pulse which has the length of half a period of the received signal. It is possible to make this pulse equal to one or one and a half period, but, as will be shown in Chapter 8, the first half period can be expected to yield the most reliable estimation of the center frequency.
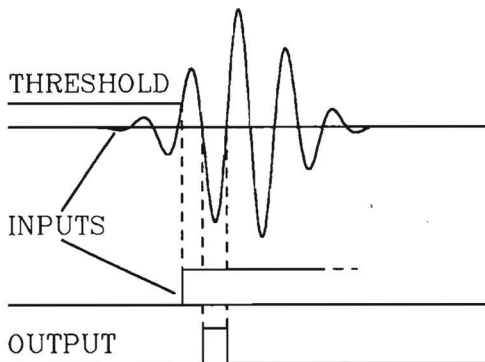

Fig.5.4) Input and output signals of the period detection circuit.

The signal from the period detector enables the high frequency counter, so this counter will only count during half a period of the received sound pulse. For a signal with a center frequency of 2 MHz this means that the counter counts during 250 ns. The length of this 250 ns will then be determined with an accuracy of 10 ns which is 4 %. It can be calculated that, to be able to recognize a structure of about 5 mm with this measurement accuracy, the structure would need to have a contrast of about 75 % with its surroundings. Because the difference in attenuation slope of tissues is often much smaller, this accuracy is insufficient.

There are two ways to improve the accuracy of the measurement. The first is to increase the clock frequency of the counter. Because 100 MHz is already the upper limit of the specifications of the available components, increasing the clock frequency will be very difficult. The other way to improve the accuracy is to perform a number of independent measurements of the same quantity and take the average of the results. As there are already N (typically ≥ 400) pulses available from the time-of-flight measurement this second method is more easily implemented. Each time the arrival of a pulse is detected by the level detector of the time-of-flight measurement, the period detection will be activated and it will subsequently connect the 100 MHz clock to the counter for the first half period immediately after the level detection. When the clock is disconnected the counter will keep its last value and it will continue counting when the clock is reconnected. After the 400 pulses the counter will be read by the micro-computer which stores the value and then clears the counter.

It will be obvious that the signal generated by the period detector can also be used to trigger the high voltage pulse generator and activate the time-window because this pulse starts exactly at the first zero-crossing after the threshold of the level detector has been crossed (see Section 5.1). This means that no separate zero-crossing detector is needed for the time-of-flight measurement. The schematic representation of the combination of the time-of-flight and the center frequency down shift measurement is shown in Figure 5.5.

The accuracy of the values obtained for the average period duration can be calculated by statistical means. In the following T_p is the length of the half period detected by the period detector and T_c is the cycle time of the high frequency clock that drives the counter. In Figure 5.6 it is shown that, if $kT_c < T_p < (k+1)T_c$, then the counter counts either k or
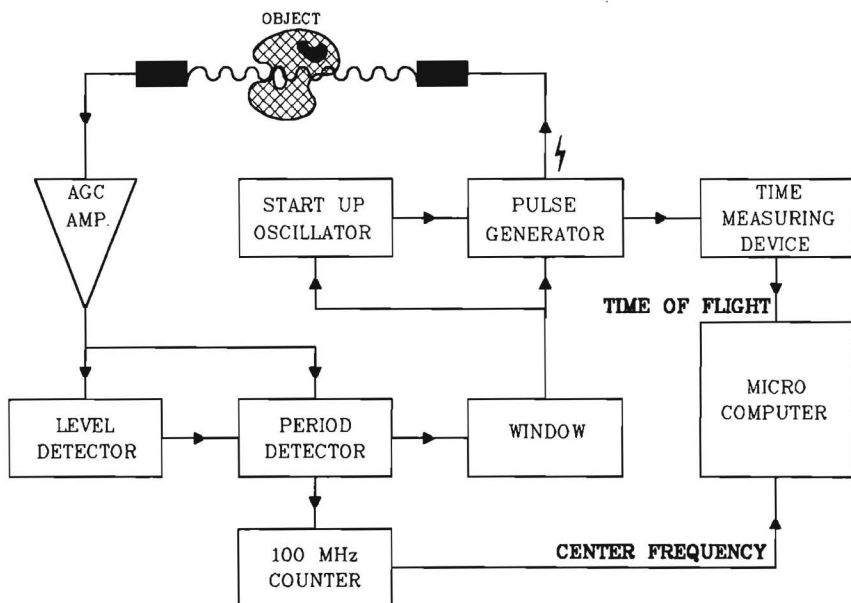
Fig.5.5) Schematic diagram of the combined time-of-flight and
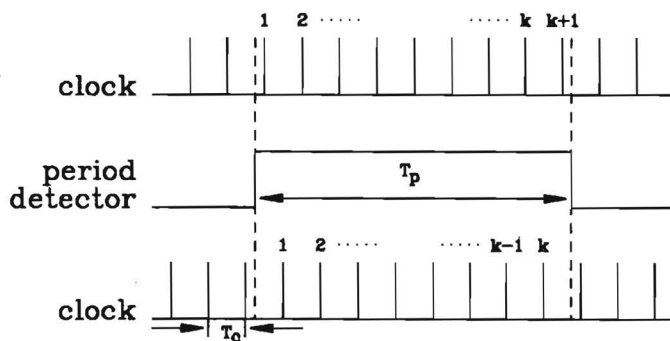center frequency measurement.

Fig.5.6) Output of the period detector with two possible phases of the
high frequency clock. With the upper clock signal $k+1$ pulses
will be counted, with the lower one k.

$k+1$ counts during T_p, dependent on the moment at which T_p starts. The high frequency clock runs independent of the activity of the period detector. Furthermore, the transducers continue to move during the N cycles of the measurement, which causes slight variations in the interval between the onsets of two subsequent observations of T_p which makes the N observations of T_p statistically independent. Let it be assumed that the probability that $k+1$ counts are counted, is equal to p. Then the probability that k counts are counted is equal to $1-p$. Now a random variable X is defined, which is equal to the number of times the counter counts $k+1$ times during T_p. It is known from the statistics that the experiment described here will give a binomial probability distribution for X (Kreyszig, 1970). This distribution will have a mean value $\mu_x = Np$ and a variance $\sigma^2_x = Np(1-p)$. Because in the experiment N is large, the binomial distribution of X can be approximated by a normal distribution with the same mean and variance. Because the measurements have a statistical character it is not possible to represent the accuracy as a single value. It can only be expressed in terms of a confidence interval. In order to have an indication of the accuracy of the measurement the confidence interval for T_p must be known when there is a total number K_T as the counter value after N measurements. In this case the estimated value $E[T_p]$ of T_p is equal to MT_c/N with $M = Np(k+1) + N(1-p)k$ This yields: $E[T_p] = (p+k)T_c$. For a confidence level of 95 % the confidence interval for T_p can be determined as:

$$\{k+p - 1.96\sqrt{[p(1-p)/N]}\}T_c < T_p < \{k+p + 1.96\sqrt{[p(1-p)/N]}\}T_c \qquad (5.2.1)$$

To give an impression of the size of this interval, $N=400$ and $k=25$ are substituted and the limits of the confidence interval are calculated for $p=\frac{1}{2}$. This value of p gives the worst case because $p(1-p)$ has its maximum value for $p=\frac{1}{2}$. The mentioned values yield the interval: $254.5 < T_p < 255.5$ (the values are given in ns). The significance of this result is that there is a probability of 95 % that the actual half period time T_p is approximated with an accuracy better that 0.4 % by the value MT_c/N.

5.3 The amplitude measurement

With this measurement the amplitude of the received pulses is determined. Because of the aim of simplicity and low cost it is not desirable to use very fast, expensive analog to digital converters. Therefore the amplitude is measured using an electronic peak detection circuit (Baars, 1987). The function of this peak detector is to generate a low-frequency voltage that is equal to the amplitude of the received pulses. This amplitude is the peak value of the double phase rectified signal from the receiving transducer. As the output of the peak detector is a low-frequency (almost D.C.) signal, a simple and cheap analog to digital converter can be used to determine the numerical value of the amplitude of the received signal.

It proved impossible to use a conventional peak detection circuit (Graeme, 1977) for this measurement because such a circuit is not capable of handling the high frequencies of the signal (2 MHz) combined with the small duty cycle (about one pulse per 100 µs). Therefore, a new type of peak detector was developed, using a principle different from the conventional peak detection circuits. This peak detector utilizes the fact that the transducers move only a very small distance between the moments of arrival of the subsequently received pulses, so the difference
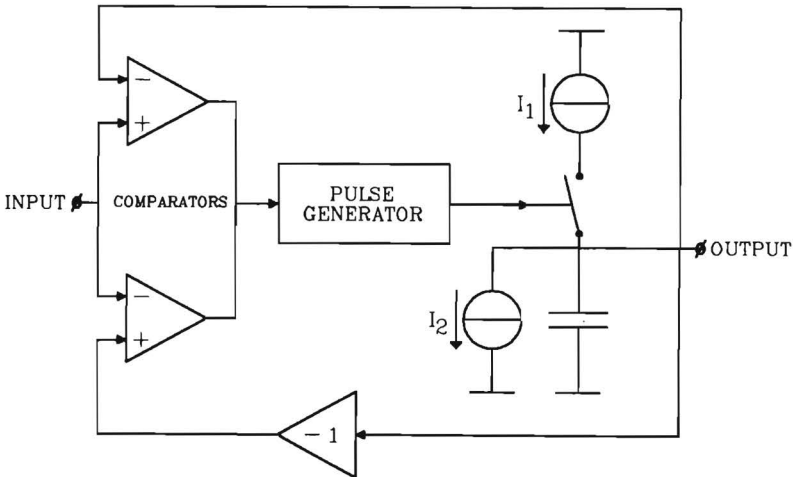
Fig.5.7) Principle of the peak detection circuit used in the amplitude measurement.

in amplitude between two successive pulses will be small (van den Keijbus, 1987). This means that the peak detector only needs to be capable of following relatively small changes in the amplitude of the signals. Figure 5.7 gives a schematic drawing of this peak detection circuit. It consists of a capacitor which is charged by a switched current I_1 and discharged by a constant current I_2. The current I_1 is switched by a pulse generator which connects the current I_1 to the capacitor for a fixed time. The pulse generator can be triggered by two comparators. These comparators compare the signal from the receiving transducer with the voltage V_c on the capacitor. When the signal from the transducer exceeds V_c or $-V_c$ one of the comparators will trigger the pulse generator. Because the current I_1 is fed into the capacitor for a fixed time, the voltage V_c will increase with a fixed amount ΔV_c each time one of the comparators is activated. The current I_2 is chosen in such a way that the decrease of the capacitor voltage in the time between the arrival of the sound pulses is about $\Delta V_c/2$. This means that the change of the output voltage of the peak detector is $\Delta V_c/2$ or $-\Delta V_c/2$ each time a pulse arrives. If the currents I_1 and I_2 are chosen in such a way that $\Delta V_c/2$ is equal to the largest expected difference between the amplitudes of two successive sound pulses, then the voltage V_c will always be within ΔV_c from the amplitude of the last received signal.

The accuracy of the amplitude measurement with the peak detector described above is ΔV_c. In the measurements this accuracy is about 12 mV while the amplitude of the received signal can range from the noise level (which is less than 500 mV) to about 10 V. Because a measured value covers typically 400 reverberation cycles the difference between two successive measurement values can not be larger than 4.8 V. This is almost half the total range of the amplitude, so this limitation is not likely to introduce errors.

Besides the ability of tracing the amplitude of a high frequency signal with a small duty cycle, the described peak detector has the advantage that it is not sensitive to sudden, large disturbances in the signal. Such a disturbance will merely cause an increase of ΔV_c in the output signal of the peak detector.

The analog to digital conversion of the output voltage of the peak detector is performed each time the stepper motors, which move the transducers along the linear scan, receive a pulse. Within one scan of a cross-section of an object, the number of motor steps taken between the

sample points is fixed and known, so within a scan all amplitude values will contain the same, known number of registrations. The converter used for the conversion of the amplitude signal has a resolution of 12 bits, so the quantization error in one conversion value is less than 2.5 mV. With the error of 12 mV of the peak detector this causes the worst case error of the amplitude measurement to be 14.5 mV.

At the end of the 400 reverberation cycles the microcomputer reads the counters of the time–of–flight measurement, the center frequency measurement and the register containing the sum of the conversion values taken within that sample, so the measurement values of these three measurements can be obtained simultaneously from the same received signals. The complete measuring system as it is at present is shown schematically in Figure 5.8.
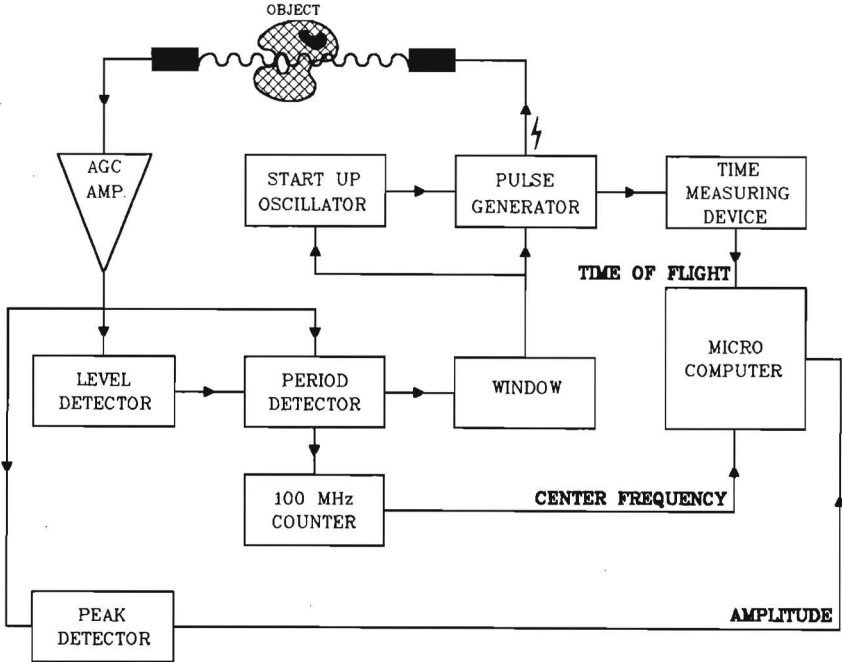

Fig.5.8) Schematic diagram of the combined time–of–flight, center frequency and amplitude measurement.

67

5.4 The reflection measurement

As stated before, the reflectivity measurement has not been implemented yet. In this section a few remarks will be made on the implementation of this measurement.

In the transmission measurements there are two transducers, one is always used as a transmitter, the other always as a receiver. In the reflectivity measurements the transmitter must also be able to function as a receiver. Therefore, the rather sensitive pre-amplifier of the receiving electronics will have to be protected from being damaged by the high voltage pulse which excites the transducer when it transmits the sound. This can for instance be done by using fast clamping diodes on the input of the receiving electronics, or by using an electronic switch which disconnects the receiving electronics during the transmission of the sound pulse.

A problem with the reflectivity measurements in the tomography system is that, because of the reverberation technique used for the transmission measurements, it is not possible to receive echoes from structures farther away from the transmitting transducer than half the distance between the transducers. Echoes from structures farther away will arrive after the next pulse has been transmitted. This means that it will be necessary to perform a scan around 360 degrees to be able to obtain a complete image of the reflectivity. Because the present scanning equipment only permits a 180 degrees scan, a solution for this problem must be found. There are three possibilities.

The first possibility is to change the scanning gear in such a way that it permits a 360 degrees scan.

The second possibility is to introduce an artificial delay which reduces the reverberation frequency to less than half its original frequency. Such a delay will enable the reception of echoes from the complete depth range and, if it is constant, it will not affect the transmission measurements (see Section 5.1).

The third possibility is to make both transducers suitable to function as a transmitter and as a receiver. In that case two 180 degrees scans can be performed, one with the first transducer as the transmitter and the other with the second transducer as the transmitter. In this way each sound path will be measured in two separate parts. This latter method may need slightly more complicated electronics, but it has the advantage

that the reflectivity measurements use a smaller depth range which reduces the probability of measurement errors due to refraction and attenuation. Another advantage of this method is that it offers the opportunity to perform the transmission measurements twice for each ray which will improve the reliability of these measurements.

At present it not possible to give any indication of the accuracy of the reflectivity measurement because experimental results are not yet available.

Implementation

In this chapter the implementation of the hardware and the software of the ultrasound transmission tomography system will be described. This experimental system has been built with low-cost, readily available electronic components and both the measuring software and the image reconstruction software have been implemented on a standard personal computer. The reader who is less interested in these technical details may omit the rest of this chapter; it does not contain information that is essential for the understanding of the next chapters.

This chapter is subdivided in the following way: Section 6.1 describes the scanning part of the tomography system. In Section 6.2 the receiving and transmitting electronics of the tomography system are described. Section 6.3 provides some additional details of the implementation of the three measurement techniques which have been described in the previous chapter. In Section 6.4 a brief, functional description of the measuring software is given and in Section 6.5 the implementation of the filtered back-projection image reconstruction technique will be discussed. This latter section will also deal with the design of the digital filters that are used for the reconstruction. In the last section of this chapter, Section 6.6, some remarks will be made about the interfacing between the measuring electronics and the personal computer.

6.1 The scanning equipment

The scanning equipment of the tomograph is mounted on a platform which can be placed over a water tank. A picture of the scanning equipment is shown in Figure 6.1. The central part of the platform can be rotated by means of a stepper motor. On this central part two sets of parallel, straight rails have been mounted which guide the carriages to which the transducers can be attached (Figure 6.1b). These transducer carriers can also be moved by means of stepper motors. When the platform
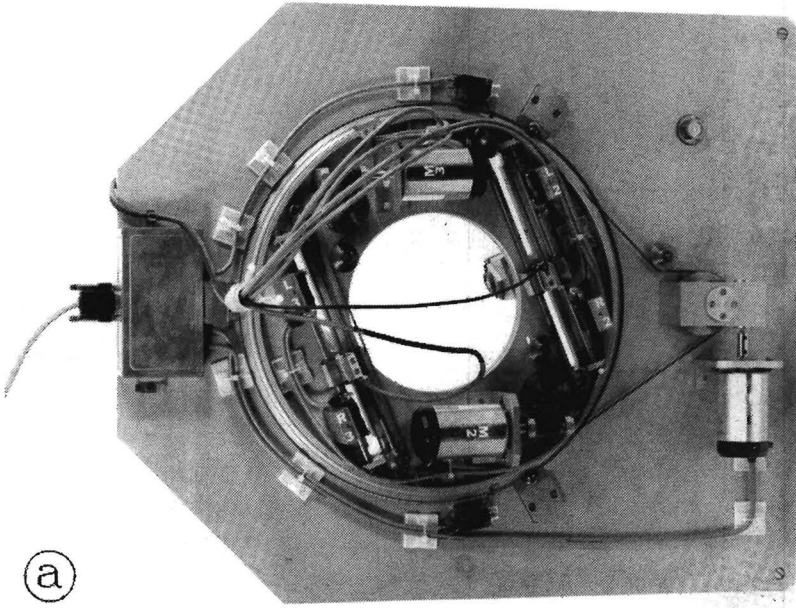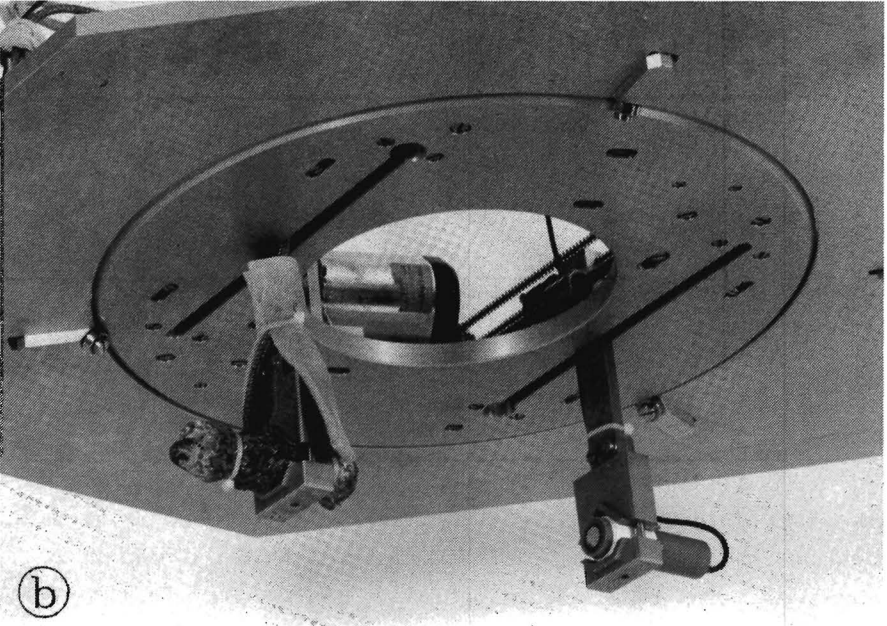
Fig.6.1) The scanning gear of the tomography system. a) Top view showing the stepper motors and the rails of the transducer carriers. b) Bottom view showing the transducers.

is placed over a water tank, part of the transducer carriers will be immersed.

The rotation of the central part of the platform is 0.10 degrees per motor step and the range of this rotation is about 190 degrees. The displacement of the transducer carriers is 0.106 mm per motor step and the maximum scan length is 15 cm. The distance between the transducer carriers of the transmitting and of the receiving transducer is also 15 cm. At each end of both the rotational and the linear scan ranges, micro switches have been mounted, that disconnect the stepper motors when the end of the scan range is reached, thus protecting the motors from being damaged when scanning beyond the maximum range is attempted. The micro switches also serve as reference points for the position of the transducer carriers and for the rotation angle of the central part of the platform.

As shown in Figure 6.2, there are two water tanks, one for large objects and one for small objects. The inner side of both tanks and the submerged parts of the transducer carriers are covered with a spongy material to reduce unwanted reflections. The conically shaped large tank has been designed in such a way that reflections from the walls that may occur in spite of the sponge, are always deflected away from the transducers in order to ensure that they will not interfere with the received signals.

6.2 The transmitting and receiving electronics

This section describes the electronics of the tomography system which is common to all three measurements. The electronics specific to each of the three measurements is described in the next section. The system components described in this section are indicated in Figure 5.8 as the pulse generator, the start up oscillator, the window and the AGC-amplifier. A schematic drawing of the electronics discussed in this section is given in Figure 6.3. To avoid possible confusion, only the components that are essential for the function of the electronics are shown in this figure.

The high voltage pulse generator which excites the transmitting transducer consists of a mono-stable multivibrator ("one-shot") connected to two fast, high voltage field effect switching transistors. The length of
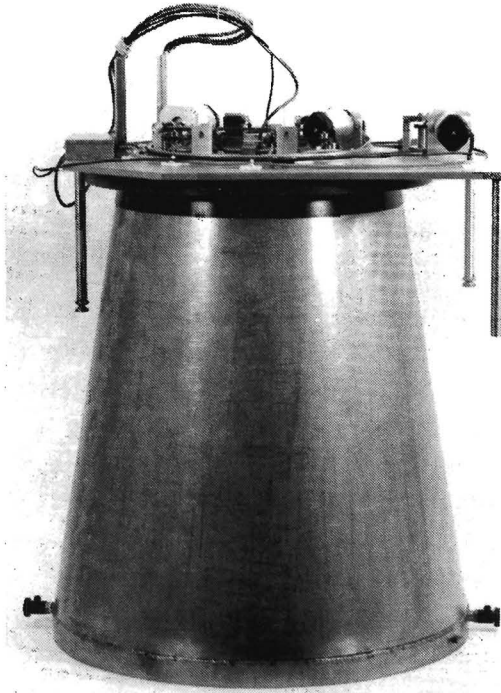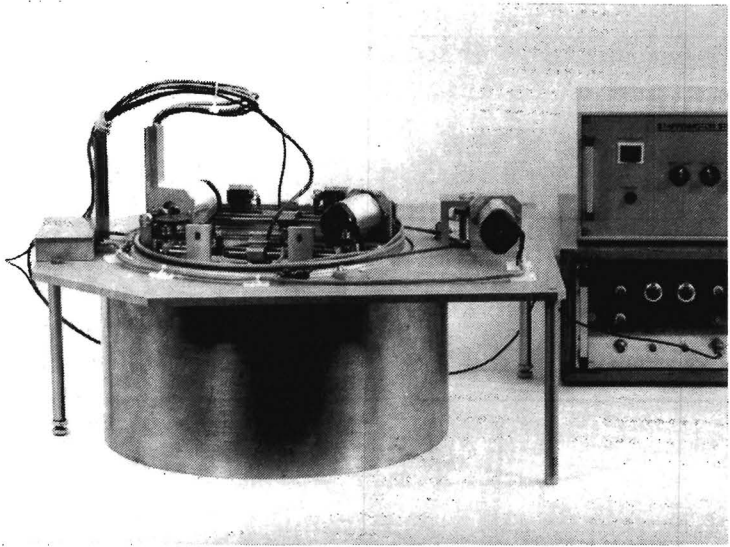
Fig.6.2) The water tanks with the scanning gear.
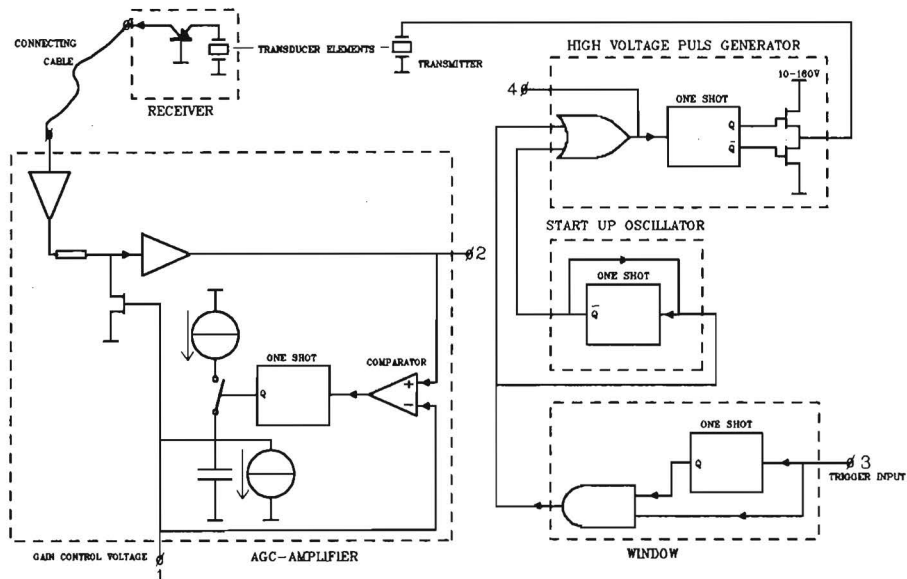
Fig.6.3) Schematic drawing of the transmitting and the receiving electronics. The numbers of the inputs and the outputs refer to Figure 6.4.

the output pulse of the one-shot can be controlled by means of a potentiometer in order to be able to adjust it to the resonance frequency of the transmitting transducer. During the pulse from the one-shot the output of the pulse generator is connected to the supply voltage which can be adjusted between 10 and 160 V.

The start up oscillator consists of a retriggerable one-shot. When it is triggered this one-shot generates a pulse of about 150 µs. If the one-shot is triggered again during this pulse, a new pulse of 150 µs will be started without a change of the output. This means that the inverting output of the one-shot will only generate a positive going edge to trigger the high voltage pulse generator, when no trigger signal is received from the time window within 150 µs after the previous trigger signal. When the one-shot triggers the pulse generator, it also triggers itself, so that it will keep generating trigger signals every 150 µs as long as no trigger signal is received from the time window.

The time window (see Section 5.1) consists of a one-shot and an AND-gate. The trigger pulses from the measuring electronics which trigger the high voltage pulse generator also trigger the one-shot of the

window which closes the AND-gate for a preset time interval. This time interval can also be adjusted to the requirements of the measurement by means of a potentiometer.

The receiving transducer has a built-in, single transistor buffer amplifier that serves to match the output impedance of the transducer element to the impedance of the connecting cable. The input impedance of the AGC-amplifier also matches the impedance of the connecting cable. The combination of the buffer in the transducer and the input stage of the AGC-amplifier has a fixed gain of 35 dB. The input stage is followed by an electronically adjustable attenuator with a maximum attenuation of 65 dB and a second amplifier stage which has a gain of 65 dB. The attenuator consists of two voltage dividers, both with a fixed resistor and an electronically adjustable resistor (field effect transistor). The total attenuation is controlled by the output of a peak detector which is connected to the output of the last amplifier stage. In this way an automatic gain control (or AGC) has been implemented, which prevents the receiving amplifier from being overloaded for the expected range of the input signal (Section 5.1). The peak detection circuit used for this AGC is a single sided version of that used for the amplitude measurement (Section 5.3).

The AGC-amplifier is broad-band in order to prevent errors in the phase of the output signal. Such errors would affect the positions of the zero crossings in the amplified signal and thus disturb the measurements of the time-of-flight and the center frequency.

6.3 The measuring electronics

The functions of the measuring electronics have already been explained in Chapter 5. This section will provide some additional details on the implementation of the described measurement techniques. A schematic diagram of a part of the circuitry described in the following paragraphs is given in Figure 6.4. The parts discussed in this section are the level detector, the period detector, the time measuring device, the 100 MHz counter and the peak detector and can be found in the schematic drawing of Figure 5.8.

The level detection circuit of the time-of-flight measurement is a comparator. The output of this comparator will be high when the input
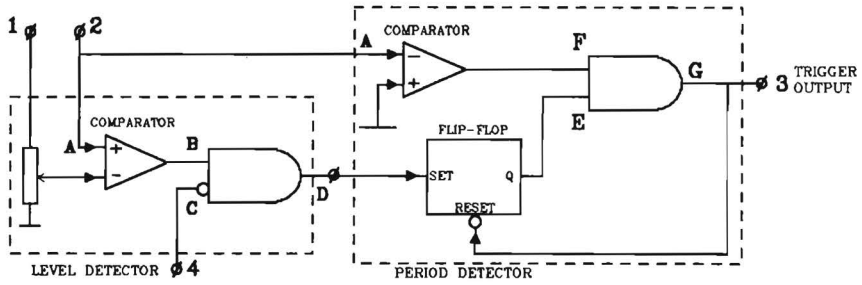
Fig.6.4) Schematic drawing of the measuring electronics. The signals at positions A to D are presented in Figure 6.5. The inputs and the outputs are connected with the outputs and the inputs with the same numbers in Figure 6.3.
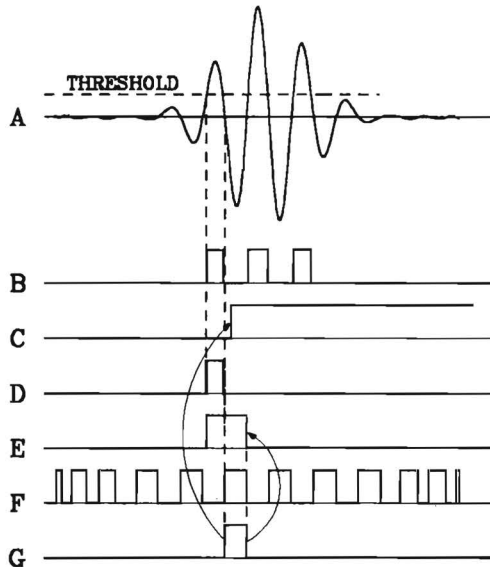
Fig.6.5) Signals from the measuring electronics. The letters to the left of the signals indicate the location of the signals in Figure 6.4. The dashed lines and the arrows indicate the important relations between the different signals.

signal is higher than the threshold voltage. This means that the comparator will generate a series of pulses each time a sound pulse is received (Figure 6.5). Because the period detector of the center frequency measurement has to be activated only once for each received sound pulse only the first pulse from the level detecting comparator will be used. The other pulses will be suppressed by the output signal of the time window. As mentioned in Section 5.1, the threshold voltage for the level detector has to be proportional to the amplitude of the received signal. This can be achieved by deriving the threshold from the gain control voltage of the receiving amplifier with a simple voltage divider. This voltage divider can be adjusted to the existing noise level. The total signal amplitude range that yields a reliable detection of the sound pulse is determined by the combination of the range of the gain control of the AGC-amplifier and the range of the variable threshold. This total range is about 80 dB.

The period detector in Figure 6.4, which is used for both the time-of-flight and the center frequency measurement (Section 5.2), also consists of a comparator but in this case the output toggles each time the input signal crosses the 0 V level. This comparator will generate pulses continuously because of the noise that is always present (Figure 6.5). The single pulse per received sound pulse that is needed for the measurements is selected using the pulse from the level detector. As shown in Figure 6.4 the pulse at the output of the level detector sets a flip-flop. The output of this flip-flop opens the AND-gate which makes the trigger output of the period detector follow the output of the zero-crossing comparator. The trailing edge of the pulse that appears at the trigger output will reset the flip-flop so that all pulses from the zero-crossing comparator are suppressed until the next pulse from the level detector sets the flip-flop again. The pulse from the trigger output also activates the time window that disables the output of the level detector to ensure that the flip-flop of the period detector will stay in its reset state until the next sound pulse arrives.

The pulse from the trigger output as described in the previous paragraph is the one needed for the time-of-flight and the mean frequency measurement because its leading edge is exactly at the first zero crossing after the detection of the arrival of a sound pulse and its length is equal to half a period of the received sound signal. For the time-of-flight measurement this pulse is fed into a programmable divider.
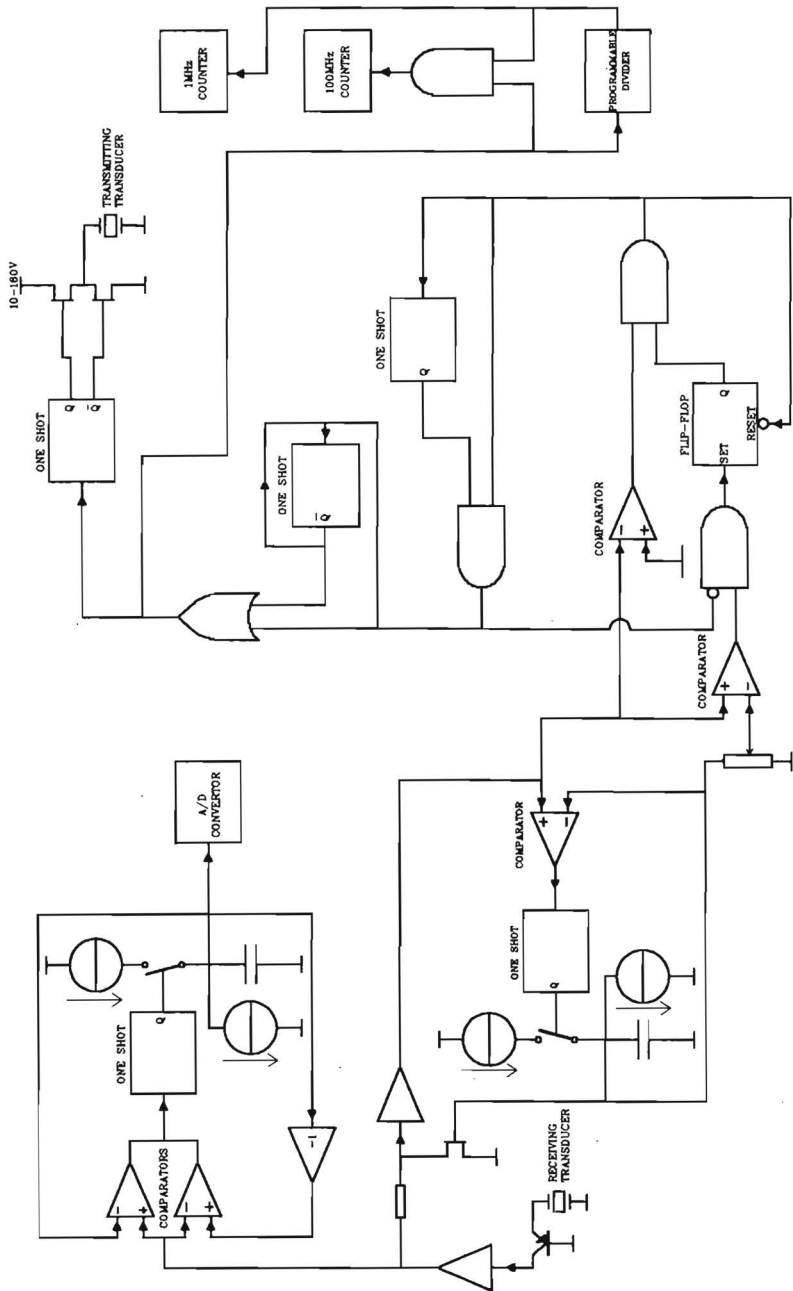
Fig.6.6) Schematic representation of the electronics of the ultrasound transmission tomography system.

The output of this divider gates the 1 MHz clock to the time−of−flight counter and the 100 MHz clock to the center frequency counter during the time that N sound pulses are detected (N can be chosen between 10 and 1650). The trailing edge of the signal from the programmable divider also indicates to the microcomputer that the values in the counters are ready to be read. After being gated by the programmable divider the 100 MHz clock is also gated by the output pulse from the period detector (trigger output). Therefore, the 100 MHz counter only counts during half a period of N received sound pulses. After the N pulses have been detected the measurement of the next value is started by clearing the counters and resetting the programmable divider.

The electronics of the amplitude measurement consist of a peak detector which has been described in Section 5.3, a simple amplifier and an analog to digital converter. The amplifier is used because the maximum output voltage of the peak detector is approximately 2.5 V and the input range of the analog to digital converter is 10 V. The timing of the conversion is controlled by the measuring software which will be described in the next section.

Figure 6.6 shows a schematic drawing of the complete electronics of the tomography system. From this figure and the previous descriptions it may be obvious that this system can be realized with simple, readily available and low−cost components.

6.4 The measuring software

In this section a functional description of the measuring software will be given. The programming details are beyond the scope of this thesis and will not be discussed here.

During a measurement the microcomputer performs a number of tasks: the controlling of the stepper motors of the scanning equipment, the reading and clearing of the time−of−flight counter and the center frequency counter, the resetting of the programmable divider at the correct moment and the controlling of the analog to digital converter for the amplitude measurement.

Because the transducers must move at a constant speed in order to prevent mechanical vibrations, the stepper motors will have to receive pulses at a constant time interval. To achieve this, the control of the

stepper motors is based on interrupts. A programmable timer repeatedly generates interrupts at a constant time interval that has been chosen before the measurement is started. Each time an interrupt from this timer occurs, an interrupt service routine is activated which sends a pulse to the previously selected stepper motors.

To explain the measuring software, the events that occur during a measurement will now be described in chronological order. A flow chart of this software is given in Figure 6.7. When the program is started it begins by asking the user to enter the measurement parameters. These parameters are the number of projections that has to be measured (equally spaced over a range of 180 degrees), the number of samples that has to be measured within one projection, the distance between two succeeding samples and the scanning speed. After checking whether the entered combination of parameters can be realized, the program will initialize the scanning equipment by moving the transducers to their starting position. During this initialization one sample is measured in order to test the measuring electronics and to check whether the time needed for the transducer carriers to move from one sample position to the next is long enough to perform the measurement of a sample. If an error occurs during this initialization the program is stopped to give the user an opportunity to correct the error.

After a successful initialization the measurement of the first projection is started. To start the measurement of each sample the hardware counters and the software register containing the result of the analog to digital conversions are cleared and the programmable divider is reset. Note that the register for the conversion values is a software register and not the output of the analog to digital converter; this will be explained in the next paragraph. As soon as this divider indicates that the measurement has been completed the counter values and the value in the register are read and these values are stored. During and after the measuring of a sample the motor steps are counted. When this counting indicates that the position of the next sample is reached the measuring of the next sample will be started.

The interrupt service routine for the timer interrupts does not only control the movement of the transducers. After sending a step pulse to the motors the routine also reads the output value from the analog to digital converter, adds it to the register for the conversion values and starts the next conversion. The analog to digital converter used in the

Fig.6.7) Flow charts of the measuring software.
a) Main program, b) interrupt service routine.

82

system has a conversion time that is smaller than the time between two motor steps, even when the motors run at maximum speed. The number of conversions within one sample is thus equal to the number of motor steps per sample but with a maximum of 16. This maximum is caused by the fact that a 16-bit data format is used (the two counters are 16 bits wide) and a 12-bit analog to digital converter. It will be obvious that, if the number of conversions taken for one sample, is less than or equal to 16, no overflow can occur in the sum of the conversion values stored in the 16 bits register. The transfer of the data during a measurement is shown schematically in Figure 6.8.

When a linear scan has been completed the three obtained projections are shown graphically on the screen of the microcomputer and, for about
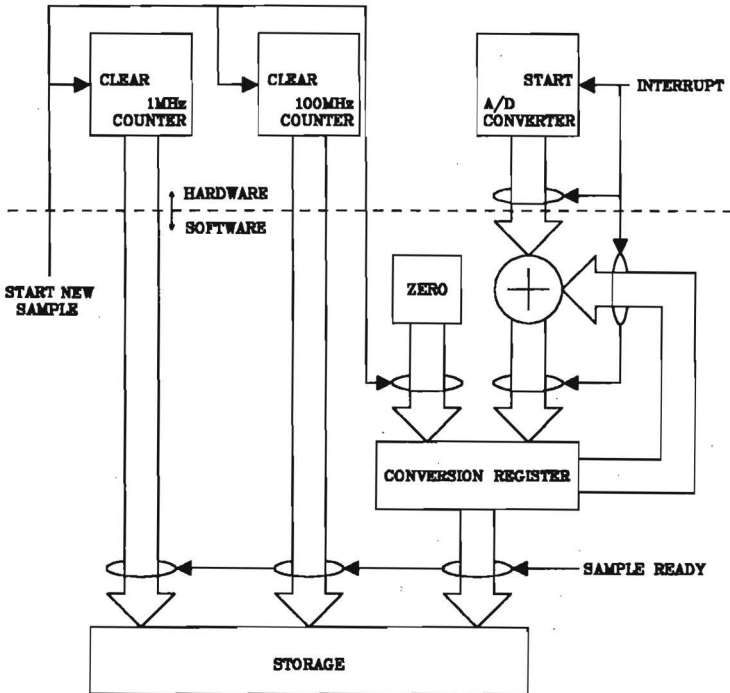
Fig.6.8) Schematic representation of the data transfer during a measurement. The broad arrows indicate the directions of the data transfer, the thin arrows indicate the moments at which the various data transfers take place.

8 seconds, the user is given the opportunity to indicate that the scan is to be repeated at the same angle. This possibility can be useful when an error occurs in one of the measured values. If the user does not indicate that the measurement is to be repeated the platform is automatically rotated to the next projection angle and the next linear scan is performed.

After the complete range of projection angles has been scanned, the user is given the opportunity to remove the object and perform a linear scan with no object between the transducers. This extra projection, called the track error, is used for the compensation of errors in the projections; its function will be explained further in Chapter 9.

After the complete measurement of an object, the user can type some comments and all the measured projections are stored on a floppy disk, together with the measurement parameters and the user's comments.

6.5 The image reconstruction software

In Chapter 3 it was stated that chosen the filtered back-projection has been chosen to be implemented for the image reconstruction in the tomography system. The discrete version of the filtered back-projection has been described in Section 3.6. If the reader has omitted Section 3.6 it may be advisable to omit this section also because it describes some details on the implementation of the filtered back-projection and Section 3.6 will referred to in some cases.

Firstly there will be some explanation of the theory behind the determination of the center of rotation for the reconstruction process and then the design of the digital filters for the filtered back-projection will be discussed. Then a description will be given of the general features of the reconstruction software. The theory described in this section is not given in a separate theoretical chapter because it describes two aspects that are directly related to the implementation of the image reconstruction algorithm and not to theory of the image reconstruction as such.

6.5.1 The center of rotation

To obtain a reliable image from the measured data, the position of the projected object within the linear scan must be correct. In other
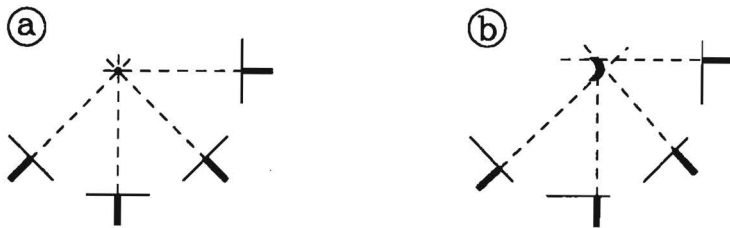
Fig.6.9) Back-projection of four projections of a delta function.
a) Correct center of rotation, b) incorrect center of rotation.

words, the back-projected rays from the projected position of the center
of rotation of the measurement will have to go through one point in the
reconstructed image. Figure 6.9 shows what happens if this is not the
case for the reconstruction of a delta function. Because of the fact that
the tomography system offers the opportunity to choose both the width of
the samples and the number of samples in a projection and because the
reference point for the linear scan is not exactly known as a
consequence of inaccuracies of the micro-switches, it is not possible to
indicate a fixed center of rotation. For each complete measurement the
center of rotation will need to be determined separately in order to be
able to reconstruct correct images. There are two methods to obtain a
correct image when the center of rotation is not known.

The first method is to use the center of gravity of the distribution
in the scan plane. The center of gravity of a two-dimensional function is
defined as follows: If (x_c, y_c) are the coordinates of the center of gravity
then:

$$
x_c = \frac{\int\limits_{-\infty}^{\infty} x\, f(x,y)\, dx}{\iint\limits_{-\infty}^{\infty} f(x,y)\, dxdy} \qquad and \qquad y_c = \frac{\int\limits_{-\infty}^{\infty} y\, f(x,y)\, dy}{\iint\limits_{-\infty}^{\infty} f(x,y)\, dxdy} \qquad (6.5.1)
$$

For the one-dimensional projection $p_\theta(t)$ of $f(x,y)$ the center of gravity t_c

85

is defined as:

$$t_c = \frac{\displaystyle\int_{-\infty}^{\infty} t\, p_\theta(t)\, dt}{\displaystyle\int_{-\infty}^{\infty} p_\theta(t)\, dt} \qquad\qquad (6.5.2)$$

In the case of a projectable function (Section 3.2) all integrals in these expressions will be defined (note that the values of the denominators in Eq. (6.5.1) and Eq. (6.5.2) are equal). Using these definitions it can be proved that the projected position of the (x_c, y_c) is equal to t_c. From this property it follows that the position of the projections is correct if the back-projected rays from the centers of gravity of all projections go through one point. In practice this holds under the condition that all calculated centers of gravity of the measured projections are correct.

The second method to perform a correct reconstruction when the center of rotation of the measurement is unknown, is based on the fact that the projection of a single, fixed point from the object describes a sine when it is taken as a function of the projection angle. Suppose that the linear scan is at a fixed position and that the object is rotating around a fixed point during the measurement. In this case each point of the object will describe a circle around the center of rotation which means that the projected position of each point will describe a sine which has the projected position of the center of rotation as its zero level and the distance from that point to the center of rotation as its amplitude (Figure 6.10). If this is applied to the center of gravity of the distribution in the cross-section of the object, it will be obvious that its projected position as a function of the projection angle will also describe a sine around the projected position of the center of rotation. Therefore, if the positions of the centers of gravity of all projections are calculated, the position of the projected center of rotation can be estimated by fitting a sine through the centers of gravity of the projections as a function of the projection angle and determining the zero level of that sine.
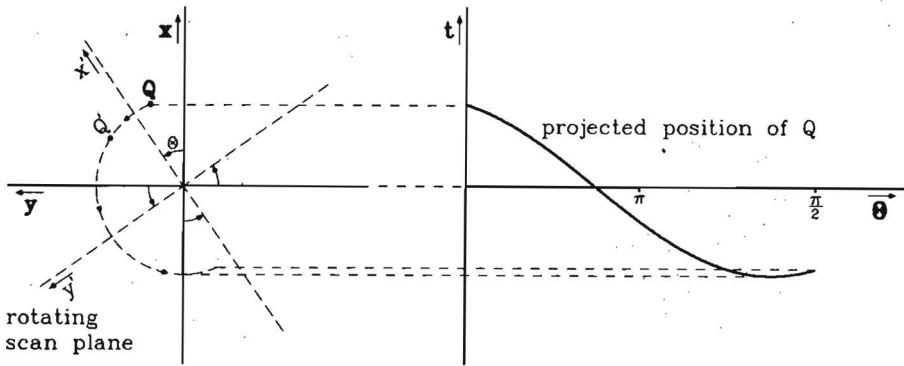
Fig.6.10) Projected position of an arbitrary point Q in the scan plane as a function of the projection angle Θ. The definition of the coordinates has been given in Figure 3.7.

The reconstruction software offers the user the possibility of choosing whether the center of rotation used for the reconstruction will be a fixed center of rotation (entered by the user), the center of gravity or the center of rotation estimated from the sine fitting. It is not possible to indicate in general which method will yield the best results; this depends on the characteristics of the measured projections. Generally it can be assumed that, if the correlation coefficient between the estimated sine and the calculated positions of the centers of gravity is low (< 0.9) then probably it would be best to use a fixed center of rotation because the low correlation indicates that the centers of gravity of the projections cannot be calculated accurately as a consequence of noise or measurement errors in the projections. If the object has been moved during the measurement it is not advisable to use a fixed center of gravity for all projections; in that case the method using the seperate centers of gravity of each projection is likely to give the best results. Often the only way to determine which method is most suitable is to try all three and compare the results. It is difficult to give criteria for this comparison if the internal structure of the object is not known; an important guideline is that errors generally lead to semi-circularly shaped distortions in the picture or to streaks outside the object. An example of the effect of an erroneous center of rotation on the reconstruction of a cylindrical object is shown in Figure 6.11.

87
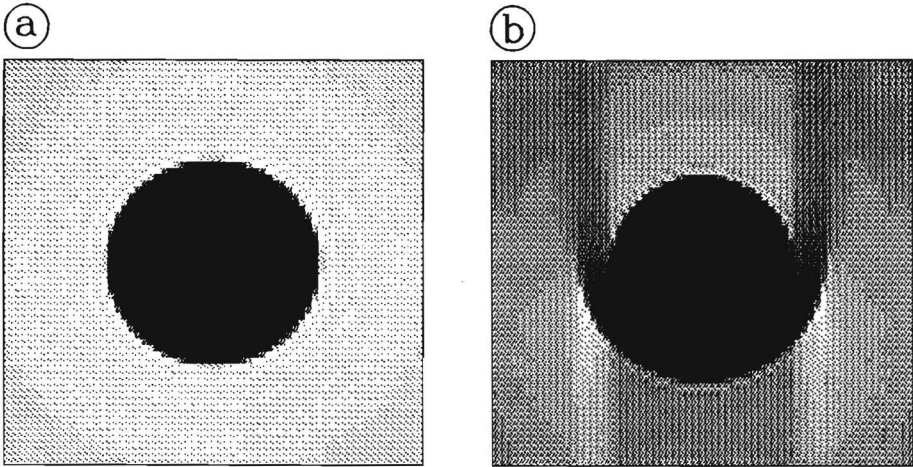
Fig.6.11) Reconstruction of a cross-section of a simulated, homogeneous, cylindrical object. a) Correct center of rotation, b) incorrect center of rotation.

6.5.2 Digital filter design

A very important aspect of the image reconstruction is the design of the digital filter with which the projections must be convolved to compensate for the blurring caused by the back-projection. One way of obtaining such a filter is to take the discrete inverse Fourier-transform of the function $W(R) = |R|L(R)$ which was derived in Section 3.6. The ideal shape of this filter function and its inverse Fourier-transform are shown in Figure 6.12a. A problem with this method is that the function is limited in the Fourier domain and therefore unlimited in the spatial domain. In the implemented digital filter this would not be a problem if the filter terms are negligible outside a relatively small area in the spatial domain. However, because of the sharp cut-off of the filter in the Fourier domain, the filter will have a very large area with non-negligible terms in the spatial domain. This means that, in order to realize the wanted filter characteristics, a very large digital filter would be needed which would lead to long computation times. In order to reduce the width of the filter a less sharp low-pass filter will need to be used, which would cause the filter function to become like the one shown, schematically, in Figure 6.12b. It will be obvious that, besides decreasing the size of the filter, the smoother low-pass character of the filter will have an increasing effect on the frequency contents of the reconstructed image. This means that a trade-off must be found between the width (in
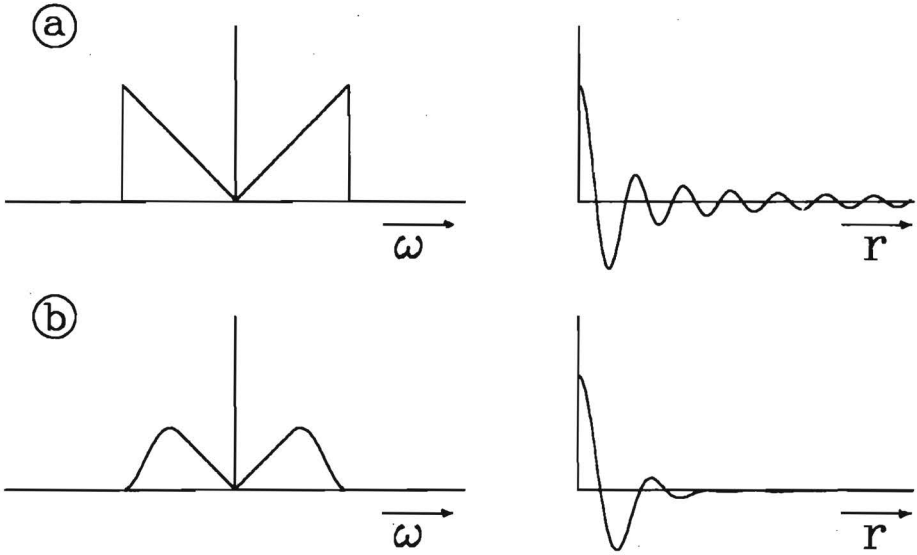
Fig.6.12) Possible filter functions for the filtered back-projection.
a) Sharp low-pass filter. b) Smooth low-pass filter.
Left: frequency domain, right: spatial domain.

the spatial domain) of the filter and the loss of high frequency components in the reconstructed image.

As it proved rather difficult to find an optimal implementation of the filter $W(R)$ and because the digitized version of this filter is not well defined (Cho, 1974), a different approach to the design of the digital filters for the software was used, which is based on the method described by Cho (1974). In the following paragraphs a brief description will be given of the principle of this method.

The design of the digital filter will be described for the case of projections of only 7 samples wide (in order to prevent the explanation from becoming rather confusing). The principle of the filter design is the same for any number of samples per projection.

Because the superposition principle holds (see Section 3.1) it is sufficient to develop a filter which yields a correct reconstruction of a delta function in the center of the image. In the following it will be assumed that the number of projections is large enough to obtain a rotationally symmetric reconstruction of the delta function. The reconstructed image of the delta function is called the point spread

function and it can be considered to be the impulse response of the reconstruction process. Because the reconstructed image is rotationally symmetric around the center of the image, the point spread function will only depend on the radial distance, r, to the center. The cross-sections through the center of the continuous and of the discrete point spread function of the unfiltered back-projection are shown in Figure 6.13. In the discrete case the point spread function can be represented by a vector $\bar{p}$ which contains the values of the point spread function on the concentric rings of which the discrete point spread function consists.

The discrete spatial domain filter function $w(t)$ will also be represented as a vector, $\bar{w}$. Because $w(t)$ is a symmetrical function with respect to $t=0$, the vector $\bar{w}$ only needs to contain one half of the discrete filter function. Note that $\bar{p}$ is the vectorial representation of a two-dimensional function and $\bar{w}$ of a one-dimensional function.

In the reconstruction process, the projections (in this case delta functions) are first convolved with the digital filter function described by $\bar{w}$ and then these convolved projections are back-projected to obtain an image (in this case the point spread function). Because the projections are delta functions, the filter function itself is being back-projected, so, the discrete back-projection gives the relation between the filter function and the point spread function. If it is possible to find the inverse of this relation any wanted, discrete point spread function (including a two-dimensional delta function without blurring) can be defined and then the digital filter that will yield that point spread function can be derived. The geometry used in the following is shown in Figure 6.14, together with the meaning of the vector $\bar{w}$.

First the influence of the elements of $\bar{w}$ on the discrete point spread function will be evaluated. If one ring of the discrete point spread function is observed, then the contribution of a filter term to the value on that ring is determined by the value of the total surface of the areas which are covered by both the concerning ring and by the back-projected "streak" from the concerning filter term, relative to the surface of the complete ring. In Figure 6.14 this area is indicated for the contribution of filter term w_1 to ring p_2 and for the contribution of w_4 to p_4. The values of the relative surfaces for all possible combinations of rings and filter terms in a matrix A are put in such a way that A_{11} is equal to the contribution of w_1 to p_1, A_{21} is the contribution of w_1 to p_2, etcetera. Now describe the relationship between the vectors $\bar{w}$ and $\bar{p}$ can

90
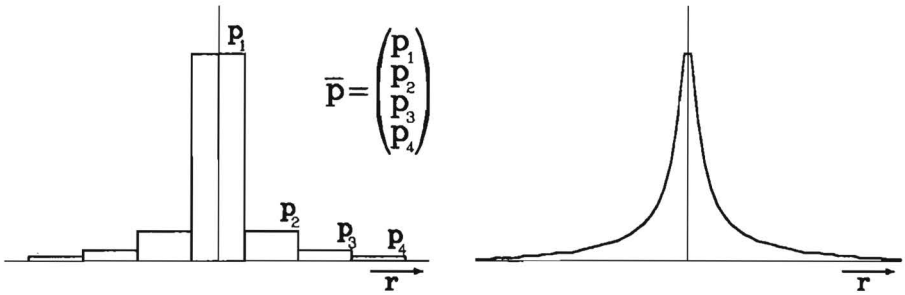
Fig.6.13) Discrete and continuous point spread function of an unfiltered back-projection with the meaning of the vectorial representation.
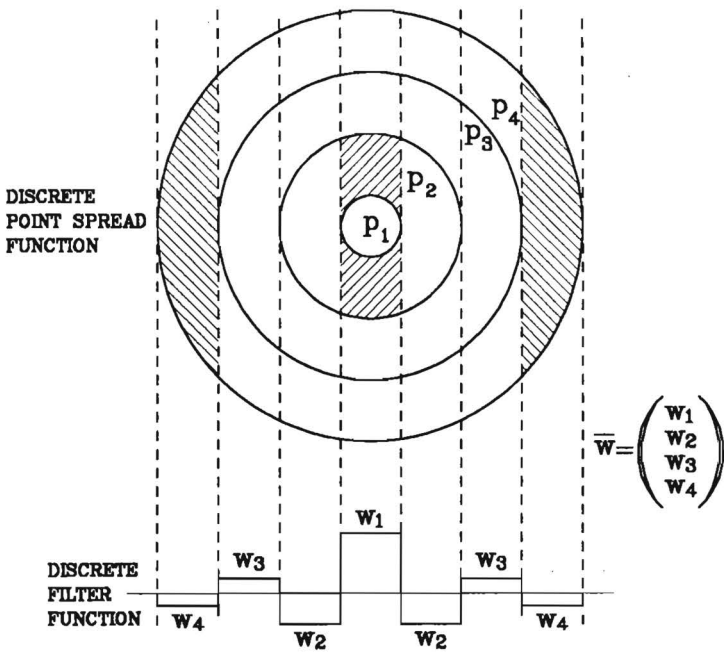
Fig.6.14) Geometry used for the derivation of the digital filter design and the meaning of the vector $\bar{w}$.

◢◢◢◢ Influence of w_1 on p_2 (= A_{21}).

◣◣◣◣ Influence of w_4 on p_4 (= A_{44}).

be described by means of the matrix equation:

$$\bar{p} = A\ \bar{w} \tag{6.5.3}$$

Because A proves to be a non-singular, square matrix its inverse matrix A^{-1} will exist, so $\bar{w}$ can always be determined from $\bar{p}$ using the following matrix equation:

$$\bar{w} = A^{-1}\ \bar{p} \tag{6.5.4}$$

This result means that the point spread function of the reconstruction process can be chosen and the digital filter that yields the chosen point spread function can be determined by a simple matrix multiplication.

6.5.3 The software

In the following a very brief description of the general features of the image reconstruction software will be given.

The implementation of the filtered back-projection is part of a software package which also contains several utilities for the handling of the measured data and the reconstructed images. The software package is capable of handling at one time, the measurement data and the reconstructed images of all three measured physical quantities. This simplifies the comparison between the images of these quantities as they have been measured simultaneously.

When the software is started, the main menu is presented to the user. This menu is concerned with manipulations of measured data and offers the following possibilities:

* Perform a reconstruction.
* Display the measured projections.
* Correct a projection manually.
* Save the corrected projections on disk.
* Display the measuring parameters with the comments.
* Reread a set of projections from the same measurement.
* Read the data of another measurement.
* Estimate the center of rotation by sine fitting.
* Go to the second menu.

The second menu concerns the handling of the reconstructed image. The items that can be chosen from the second menu are:

* Show the reconstructed image(s) in grey levels on the screen.
* Print an image in grey levels.
* Save an image on disk.
* Read a previously saved image from disk.
* Show a histogram of the grey levels within an image.
* Rescale an image.
* Apply a two dimensional moving average filter to an image.
* Present an image in a quasi three-dimensional way.
* Return to the main menu.

A further description of the options of these two menus is beyond the scope of this thesis.

The software package for the image reconstruction has mainly been written in FORTRAN 77 and it has been implemented on an IBM-compatible personal computer. It was necessary that the routines for the grey level representation of the images on the screen or the printer, were written in assembler code. Therefore these routines will have to be changed or rewritten when it is desirable to use other hardware to run the image reconstruction software.

In Figure 6.15 the three ways in which the reconstruction software can represent an image are shown. The number of grey levels displayed on the screen is 16, the number of grey levels in a printed image can be chosen by the user, with a maximum of 112 levels. These numbers of grey levels are determined by the hardware. This will not be discussed here any further.

6.6 Interfacing

This section deals with the interfacing between the personal computer and the measuring hardware.

Up to now, the measurements with the tomography system have been performed using the combination of an IBM-compatible personal computer and an ITT 2020 microcomputer (the ITT 2020 is an Apple II⁺-alike microcomputer). The ITT 2020 contains the interfaces to the measuring hardware. These interfaces have been designed in the Medical Electronics group and can only be used in Apple II compatible expansion slots. The function of the ITT 2020 is to be an intelligent interface between the measuring hardware and the personal computer. During the measurement
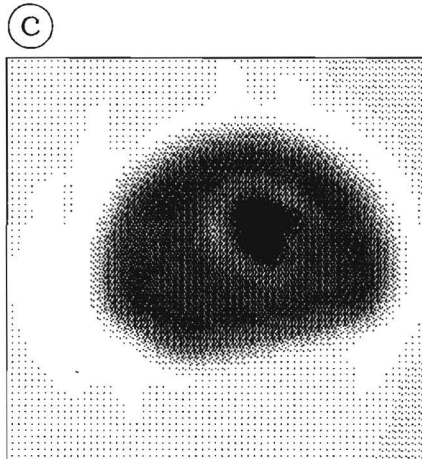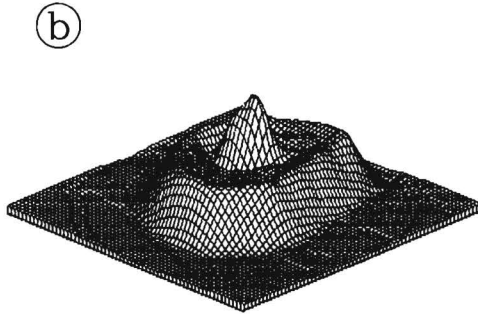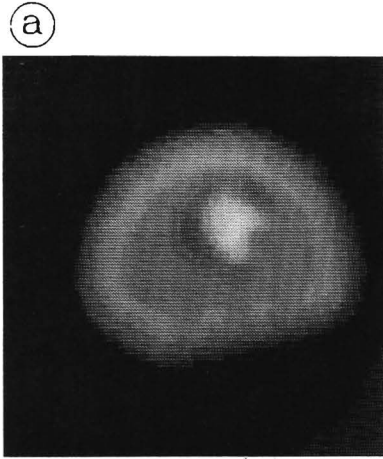
Fig.6.15) Three ways of representing a reconstructed image: a) grey levels on the screen (16 levels), b) quasi three-dimensional representation and c) grey levels on the printer (28 levels).

the ITT 2020 is controlled by the personal computer. For the communication between the two computers an RS-232 connection is used. This configuration of the measuring system is grown historically and although it functions properly, it proves to be a rather unpractical one; to begin a measurement, programs have to be started on both computers and during the measurement both computers are completely occupied.

To obtain a more practical and flexible system, it was decided to use an alternative way of interfacing the measuring hardware to the personal computer. The interface that has been chosen is the one according to the IEEE-488 (or IEC-625) standard (International Electrotechnical Commission, 1979, 1980). There are several reasons for choosing this type of interfacing. One of them is that, besides the software, the hardware also becomes transportable to other types of computers because there are IEEE-488 interfaces available for almost any type of computer. This can be an important advantage because of the rapid developments in the area of computer technology. Another advantage of the IEEE-488 interface is the transmission rate (1 Mbyte/second) which is much higher than that of the RS-232 connection (1.9 kbyte/second). Because of this, the transmission of the measured data will only use a very small percentage of the time needed for the complete measurement of a cross-section which offers the possibility to perform parts or perhaps all of the image reconstruction during the measurement. In a research environment the IEEE-488 interface has the additional advantage that several measuring instruments can be equipped with an IEEE-488 interface so that they can easily be connected to the personal computer.

All the necessary hardware for the IEEE-488 interface of the measuring hardware has already been designed, built and tested. The interface contains a single chip microprocessor which is capable of controlling the complete measurement by itself. This relieves the personal computer from the simple, but rather time consuming task of controlling the measurement. The built-in microprocessor is also capable of controlling the transmission of the measured data to the personal computer, so the only task of the personal computer during the measurement is to receive the data. The rest of the available time can be used solely for the image reconstruction. A detailed description of the hardware of the interface is given by Pijfers (1987).

The stepper motors are equipped with a separate IEEE-488 interface because in this case they can be controlled both by the interface

microprocessor of the measuring hardware and by the personal computer. This increases the flexibility of the system.

To be able to use the IEEE−488 interface optimally, a universal software package has been developed for the personal computer. This software can be used either interactively or linked to an application program. It has been written in FORTRAN 77 and it is almost completely independent of the hardware on which it runs (van den Buys, 1987).

During the writing of this thesis, the measuring software for the built−in microprocessor (written in assembler) of the tomography system was still in the phase of testing.

Transducers

Some research has been performed on the applicability of various types of transducers and transducer materials in the tomography system. Although the design of ultrasound transducers is not within the scope of this thesis, a very brief description will be given of the results of the studies that have been performed on this subject.

The following items will be discussed in this chapter: In Section 7.1 the single element ceramic transducer will be described. This is the type of transducer normally used in the measurements with the tomography system. In Section 7.2 the use of both linear and annular ceramic transducer arrays will be discussed and Section 7.3 deals with the applicability of polyvinylidene fluoride (PVDF) as an alternative transducer material.

7.1 Single element ceramic transducers

This section will describe the technical details of the construction of the single element transducers used in the tomography system. A more general and extensive discussion of the single element transducer is given, for example, by Kossoff (1978), Kikuchi (1978) or Silk (1984).

The piezoelectric elements used for the construction of the transducers are made of the material PXE-5. This is a trade name for a ceramic material based on lead zirconate titanate (PZT). The elements that are available are flat, circular disks with a diameter of 5 or 10 mm and a resonance frequency of 1 or 2 MHz. These elements are mounted in a backing material which consists of a mixture of an artificial resin and powdered tungsten. This mixture has an acoustical impedance which is very close to the acoustical impedance of the PXE-5 element and a very high attenuation coefficient. These properties cause the acoustic energy radiated from the back of the transducer element to be absorbed completely, so that, when the element is exited with a short electric
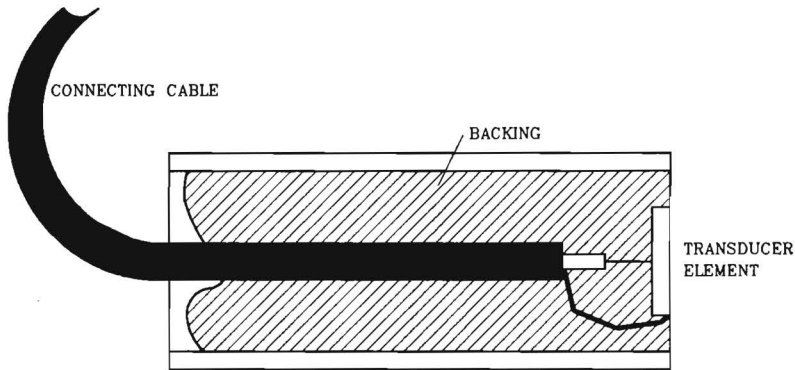
Fig.7.1) Cross-section of a single element transducer.

pulse its oscillations will be damped heavily and only a very short
ultrasound pulse will be generated. A second function of the backing is
that, by absorbing the sound from the back of the transducer element, it
prevents reflections from the back of the transducer or from the back of
the element from interfering with the ultrasound radiated from or
received at the front of the element. Figure 7.1 shows a cross-section of
a typical transmitting transducer used in the tomography system.

The construction of a receiving transducer is almost identical to that
of the transmitting transducer, the only difference is that in the case of
a receiving transducer a very small printed circuit board with a buffer
amplifier (see Section 6.2) is enclosed in the backing. This printed circuit
board is mounted far enough from the transducer element to have no
influence on the properties of the backing.

To keep the construction of the transducers simple the single element
transducers used in the tomography system are not focussed and they
have no matching layers to adapt their acoustical impedance to that of
water.

The transducers described here have a satisfying performance and
they are very simple and cheap to produce.

7.2 Transducer arrays

The mechanical scanning used in the tomography system (Section 6.1) has certain limitations concerning speed and accuracy. Although in the experimental situation these limitations are not important, they will be important in practical applications of the system. Therefore, the possibilities of replacing the moving single element transducer by a fixed, linear array which scans electronically have been studied. A linear array consists of a large number of rectangular transducer elements along a straight line (Figure 7.2a). Besides the possibility of electronic scanning, the application of an array would also offer the possibility of electronic focussing of the sound beam (Thurstone and Von Ramm, 1979, Assenza and Pappalardo, 1980).

The applicability of a linear array has been studied by computer simulation and by some experiments with a realization of a linear array which was constructed from a strip of a piezoelectric ceramic material. The simulation software used for the study of the ultrasound field generated by a linear array was based on the theory described by Freedman (1970, 1971). Using the results of these simulations an electronic circuit has been designed and built. This is capable of generating a focussed sound beam with eight elements of the experimental array. It proved that there was good agreement between the simulations and the field generated by the experimental array. A detailed description of the theory of the simulation software as well as a description of the circuit and the array used for the generation of the focussed sound beam are given by Wardenier (1985).
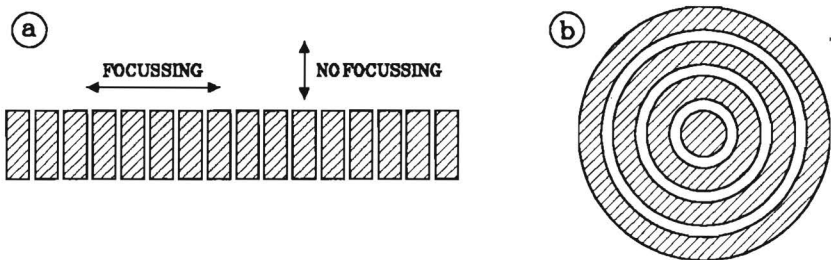
Fig.7.2) Two possible geometries of the elements of a transducer array. a) Linear array, the direction in which electronic focussing is possible is indicated. b) Annular array.

In spite of the fact that the focussing of the transmitted beam proved to be possible with relatively simple means, it turned out that the practical application of a linear array in the tomography measurements is very difficult. The reasons for this are that, although the principle of electronic scanning is quite simple, the implementation needs a large amount of additional hardware (Mathijssen, 1986). Furthermore, it also proved to be very hard to construct a reliable array and a suitable linear array for application in the tomography system is not commercially available. Because of these problems the linear array has not been implemented in the present system.

Although the electronic scanning with the linear, ceramic transducer array did not prove to be very applicable in the tomography system, the principle of electronic focussing may still be useful. With a linear array, electronic focussing can only be obtained in the direction parallel to the array (Figure 7.2a). Therefore, the possibility of using an annular array has been studied. An annular array consists of concentric, ring-shaped elements (Figure 7.2b) and it is capable of generating a sound beam which is focussed in all directions normal to the propagation direction of the sound beam (Waszczuk et al., 1983).

The applicability of an annular array has also been studied by means of computer simulation and by constructing an experimental array. Because the simulation software for the linear array is based on the fact that such an array consists of rectangular elements, a new simulation program was necessary. This program is based on the principles of calculating a pressure field as described by Lockwood and Willette (1973), Harris (1981) and Tjötta and Tjötta (1982). With the aid of this simulation program the dimensions of the implementation of an annular array have been determined and such an array has been constructed. A description of the software and construction of the array is given by Van den Keijbus (1987). A cross-section of the array is shown in Figure 7.3.

It proved that, also in the case of the annular array, there was good agreement between the simulations and the implementation and that the annular array yielded a considerable narrowing of the beam profile as compared to the single element transducer (Figure 7.4). The effect of this improved beam profile on the tomographic measurements will be discussed in Chapter 9.
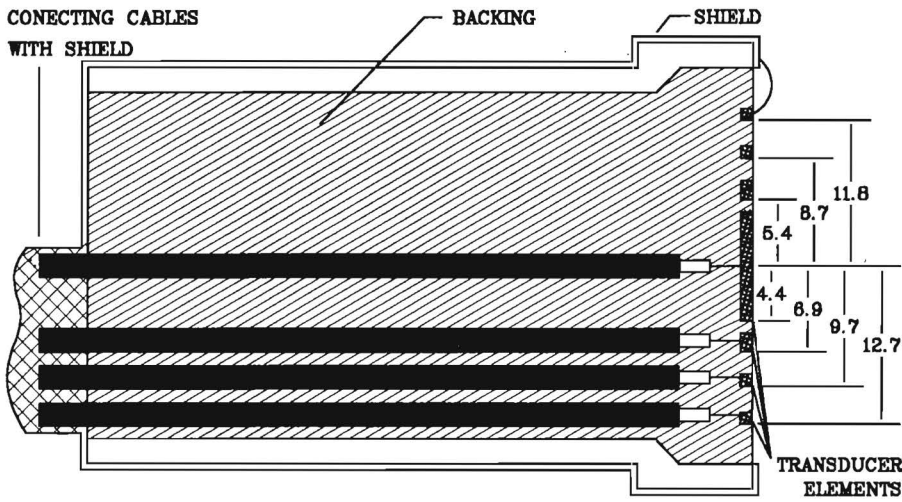
Fig.7.3) Cross-section of the implemented annular array.
The dimensions are given in mm.
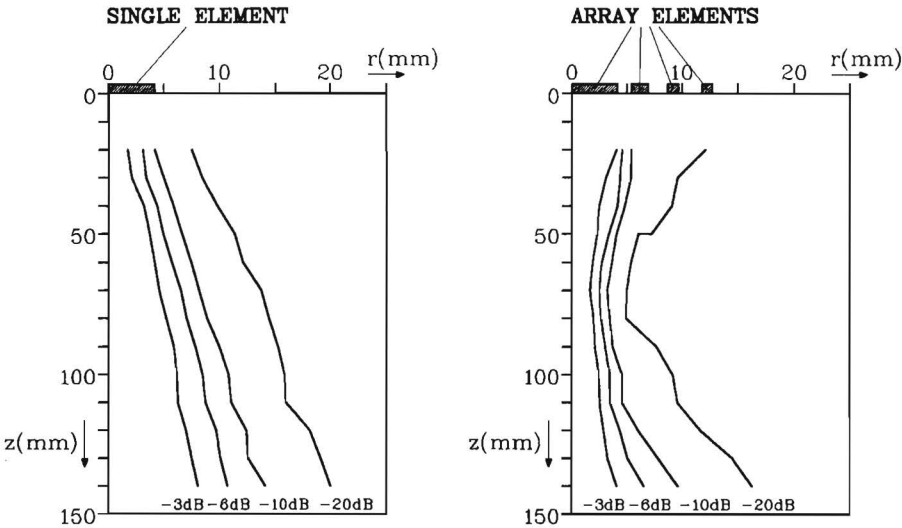
Fig.7.4) Measured beam profiles. a) Circular single element transducer,
b) annular array. The coordinate r is the radial distance to
the center of the beam, z is the distance normal to the
transducer surface. The values in the field for each distance z
indicate the pressure relative to the pressure for r=0 at the
same distance z.

101

7.3 PVDF transducers

In the previous section it was stated that it was difficult to construct a suitable ceramic transducer array for application in the tomography system. Therefore, the applicability of polyvinylidene fluoride (PVDF) for the construction of transducer arrays was studied.

PVDF is a plastic with strong piezoelectric properties (Kawai, 1969). The important advantages of PVDF are that the transducer elements are made of a flexible foil which offers almost unlimited possibilities for the shape of the transducer. Furthermore, PVDF has a high internal damping and an acoustic impedance close to the acoustic impedance of water. These properties eliminate the need for a backing or a matching layer. An important disadvantage of PVDF is that, because of the low transmitting sensitivity, it is not very suitable for the construction of transmitting transducers (Swartz and Plummer, 1980, Somer et al., 1987).

The research performed within the Medical Electronics group up to now, concentrated on the applicability of PVDF for receiving transducers in the tomography system (Van Gijsel, 1987). Some experimental single element PVDF transducers have been constructed and tested. The
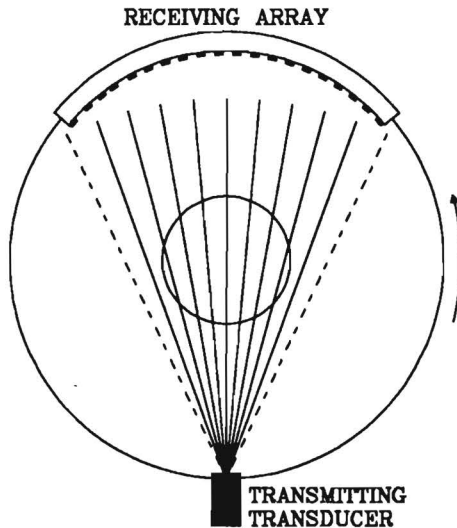
Fig.7.5) Fan-beam scanning geometry.

experiments with these transducers indicate that PVDF is a suitable material, but some practical problems concerning the mounting of the transducers and the amplification of the received signals will have to be solved.

Because of the fact that PVDF is not suitable for the construction of transmitting transducers, it is not possible to replace the linear scan movement of the single element transmitting transducer in the tomography system by a scanning linear PVDF array. A method for avoiding the mechanical linear scanning may be to use a fan-beam geometry which is very common in X-ray computed tomography. This geometry consists of a single transmitting transducer and a receiving array (Figure 7.6). The fan-beam geometry has not yet been implemented in the tomography system so it not possible to give any comments on the performance of such a geometry here.

Phase Cancellation and Interference

This chapter describes the problems caused by phase cancellation and interference. These problems have been studied by means of computer simulation. Although the aim of this study was to evaluate the effects of phase cancellation and interference on the transmission measurements as performed in the tomography system, it should be noted that the results apply as well for reflection measurements (Sollie and Stapper, 1987).

The contents of this chapter are the following: in Section 8.1 the problems and their causes will be described. Section 8.2 describes the simulation method that has been used to estimate the magnitude of the errors that may arise and Section 8.3 discusses the results of these simulations. Finally, in Section 8.4, some methods will be described that may be used for the reduction or correction of the errors caused by phase cancellation or interference.

8.1 The problem

Although phase cancellation and interference are two different phenomena, they are discussed together here because their effect on the received electrical signal is the same. Firstly phase cancellation and interference and their causes will be described (Busse and Miller, 1981).

The term phase cancellation indicates the effect that occurs when the phase of the acoustic wave arriving at the receiving transducer is not constant throughout the area of the transducer element (Figure 8.1). The electrical response of a normal piezoelectric transducer is proportional to the momentaneous average of the pressure on the element. Therefore, the electrical charge generated by the pressure at some point of the transducer surface can be enhanced or cancelled by pressures on other points of the surface.

The distortion of the arriving wave front can for example be caused by the fact that different parts of the sound beam travel through media
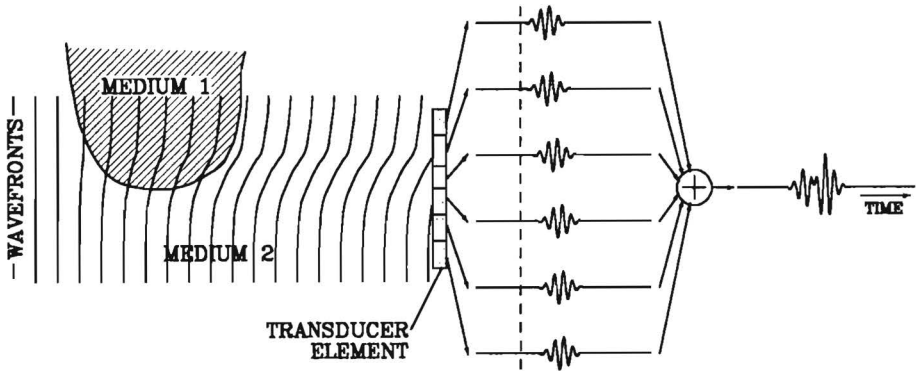
Fig.8.1) Schematic representation of phase cancellation. The sound
velocity in medium 1 is larger than in medium 2. The signals in
the middle are the locally generated electrical responses, the
signal on the right is the total response of the transducer.

with different sound velocities.

The term interference is used for the effect that occurs when sound
waves in a medium travel simultaneously in different directions. The
resulting wave will have spatial variations in the intensity and the
frequency of the sound because at each point of the sound field the
momentaneous amplitudes of the different waves are added (Figure 8.2).

Interference can be caused by refraction of a part or parts of the
sound beam or by sound waves reflected from different surfaces or
scattered by different scatterers.

It may be obvious that the electrical signal from the receiving
transducer shows the same result for waves whose momentaneous
amplitudes are added on the transducer surface as for waves added in the
medium in front of the transducer. Therefore, in the rest of this chapter
phase cancellation will only be mentioned explicitly in the cases where
there is, in some way, a difference between phase cancellation and
interference.
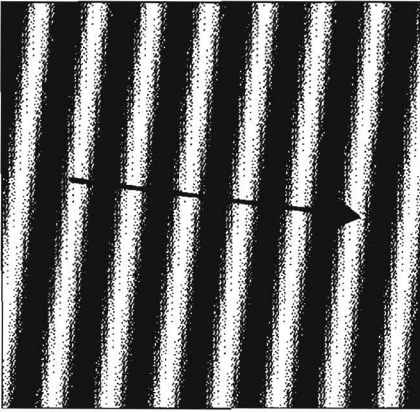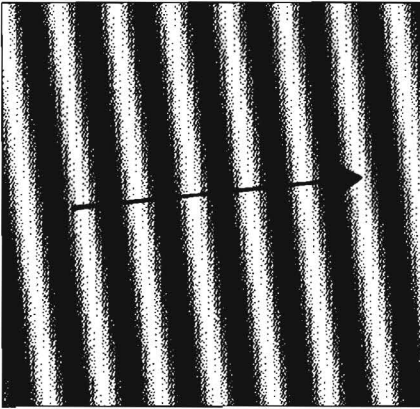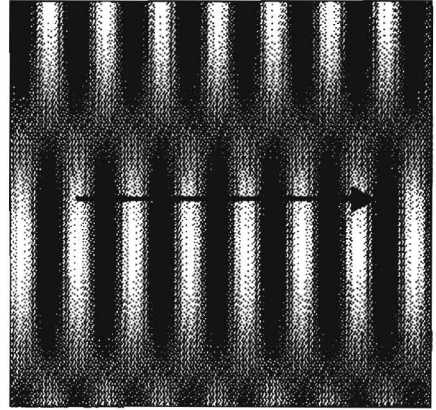
Fig.8.2) Interference of two waves. a) And b) give the two seperate waves, c) gives the resulting wave pattern of the sum of the two waves. The arrows indicate the propagation direction of the wave fronts. (The pictures a) and b) are grey scale representations of two two-dimensional sinusoids, c) is the grey scale representation of the sum of these two sinusoids.)

8.2 The simulation method

As stated before, computer simulations have been performed to evaluate the effect of interference on the measured values. The sound pulses used in these simulations are sine waves with a Gaussian envelope. To simulate the interference, two or more of these sine waves are added with a known time delay and amplitude ratio. The frequency of the sines in the basic signals from which the interference signal is equal to 2 MHz. Figure 8.3 shows the time domain and the frequency domain
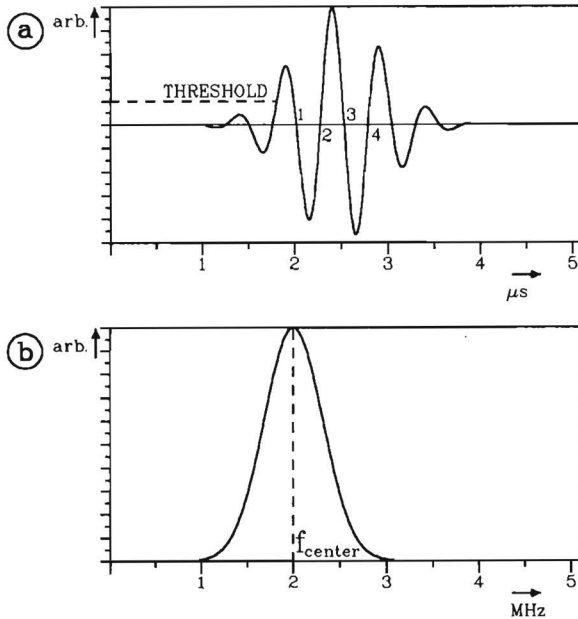
Fig.8.3) Basic pulse used in the simulations. a) Time domain. The
threshold is at 10 % of the maximum positive amplitude, the
relevant zero-crossings are numbered from 1 to 4. b) Frequency
domain. The center frequency is indicated.

representation of the basic pulse that has been used to obtain the
results shown in the next section.

During a simulation run, a series of sets of consecutive basic pulses
separated by different time delays were added in order to estimate the
interference errors as a function of the time delay. When the sets were
composed of more than two basic signals, the time delay between all
successive signals was made the same. When different amplitudes were
used, the time sequence of the basic signals is related to their
amplitude, the smallest one first as a worst case. For each time delay in
a simulation run the following values are calculated from the composed
signal:

- The position of zero-crossing 1 relative to its position in an
  undistorted wave (Figure 8.3),
- The maximum positive amplitude,
- The respective center frequencies calculated from the distances
  from zero-crossing 1 to 2, 1 to 3 and 1 to 4 (Figure 8.3).

108

- The center frequency calculated from the maximum in the spectrum of the composed signal.

The latter value is calculated in order to be able to compare the method of calculating the center frequency from the Fourier-transform with the method using the zero-crossings. The center frequency determination using the zero-crossings is performed for ½, 1 and 1½ period of the composed signal to find out which one is the least sensitive to interference.

For each simulation run the signal composed with a time delay equal to zero is taken as the reference signal. During the simulation run the relative deviations, with respect to the reference signal, in the above mentioned values are determined as a function of the time delay between the basic signals.

The error in the position of zero-crossing 1, which is the one used for the determination of the time-of-flight, is given in microseconds, the errors in the center frequency and the amplitude are given in percentages relative to the concerning values in the reference signal.

As indicated in Figure 8.3, the determination of which zero-crossing is number 1, is performed in the same way as in the hardware of the tomography system, it is the first zero-crossing after the crossing of a detection level which is related to the maximum positive amplitude of the signal. In the simulations the detection threshold is at 10% of this maximum amplitude.

8.3 Simulation results

The simulations described in the previous section have been performed for a large number of possible combinations of basic signals. Only a few typical results will be shown here. The other results will not be shown because they would not provide extra information.

For comparison, the noise levels of the measurements are given first. The noise in the time-of-flight measurement is within ± 0.015 μs. For the center frequency measurement the noise is within ± 0.5% and for the amplitude measurement it is within ± 0.4%. These values have been determined from a complete measurement, performed with no object in the water tank, so that all conditions in this measurement were identical to those in a normal measurement.
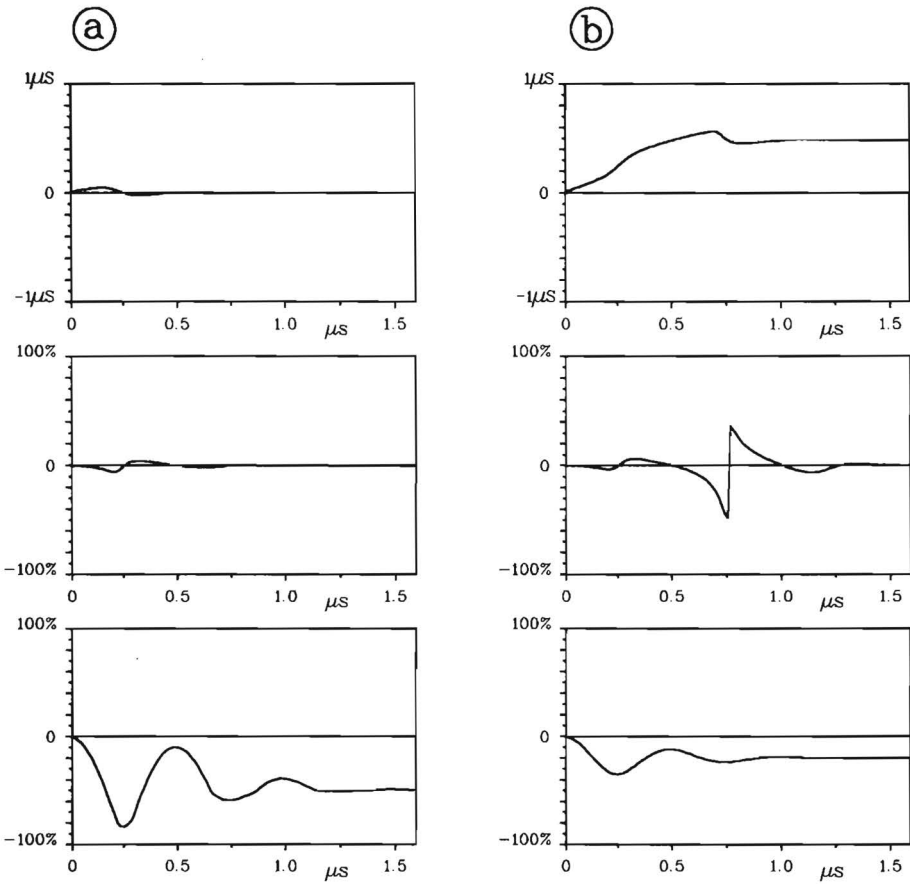
Fig.8.4) Errors caused by simulated interference as a function of the time delay. Top curves: time-of-flight error, middle curves: center frequency error, bottom curves: amplitude error.
a) Calculated using 2 basic signals with equal amplitudes.
b) Calculated using 2 basic signals with amplitude ratio 4, the smallest signal arriving first.

Figure 8.4 and Figure 8.5 each show two sets of curves. Each set consists of three curves that represent the respective errors in the time-of-flight, in the center frequency determined from the distance between zero-crossing 1 and 2 and in the amplitude values, all given as a function of the delay-time. Figure 8.4a has been calculated from a signal composed of two basic signals with equal amplitudes. Figure 8.4b is the result of composing two signals with an amplitude ratio of 4 (the smallest one first). Figure 8.5a has been calculated with eight basic signals with equal amplitudes and Figure 8.5b was also obtained with
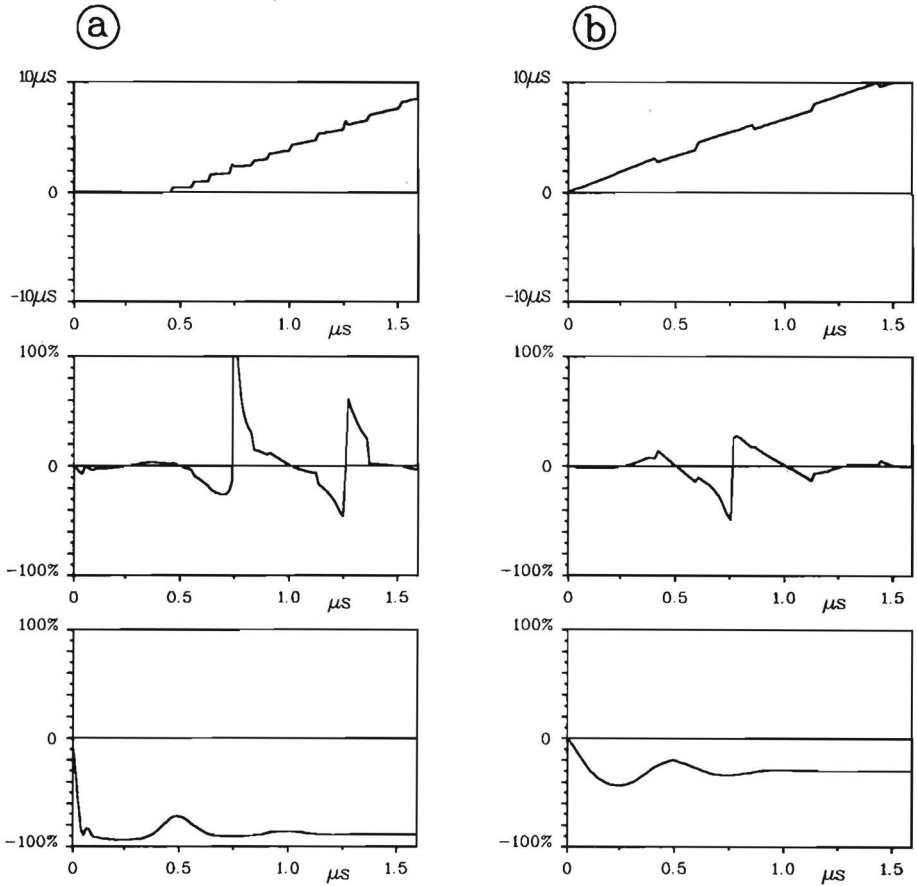
Fig.8.5) Errors caused by simulated interference as a function of the time delay. Top curves: time-of-flight error, middle curves: center frequency error, bottom curves: amplitude error.
a) Calculated using 8 basic signals with equal amplitudes.
b) Calculated using 8 basic signals with amplitude ratio 3, arriving according to increasing amplitude, the smallest one first.

eight basic signals but in this case each amplitude was 3 times the amplitude of the previous signal.

Based on the results of the simulations it can be concluded that interference can cause severe errors, especially in the amplitude and in the center frequency. Furthermore it was found that using a larger number of zero-crossings or using a Fourier-transform for the determination of the center frequency did, in general, not reduce the effects of interference. Moreover, in the majority of the simulated cases, the center frequency calculated only from the first half period of the

composed signal (between zero-crossing 1 and 2 in Figure 8.3) showed smaller errors than the center frequency calculated from a larger number of zero-crossings. Because of this result and because of the fact that in a practical situation the zero-crossings later on in the signal will be influenced by the resonance of the receiving transducer element, the center frequency in the tomography system is determined from the first half period of the received signal (Section 5.2).

Simulations using wider and narrower Gaussian envelopes of the sine functions in the basic signals showed that the width of the envelope has only a minor influence on the interference errors. For signals with a wider envelope the errors tend to be slightly smaller.

8.4 Solutions

In the previous section it was shown that interference can cause rather large errors. Therefore, it is desirable to reduce or correct the interference errors. In this section some possibilities for doing this will be discussed.

To minimize the chance of the occurrence of interference, the sound beam should be kept as narrow as possible. The narrower the beam, the smaller the chance that parts of the beam will travel through media with different sound velocities or hit different reflectors or scatterers.

The effects of phase cancellation may be reduced by using a smaller receiving transducer element. This will, however, not reduce the effect of interference of the waves in the medium in front of the transducer.

A way of reducing the interference errors in the amplitude measurement is proposed by Klepper et al. (1977) and Miller et al. (1979). They use receiving transducers that generate an electrical response which is proportional to the received acoustic energy, irrespective of the distribution of the phase of the wave on the transducer surface. Because the electrical response of such a phase insensitive transducer does not contain the zero crossings needed for the center frequency measurements, the application of such a transducer in the tomography system would only be possible in combination with a normal, phase sensitive transducer, otherwise the attenuation slope measurement would be impossible. The time of flight measurement would be possible with a phase insensitive transducer. In that case the moment of the passing the threshold would
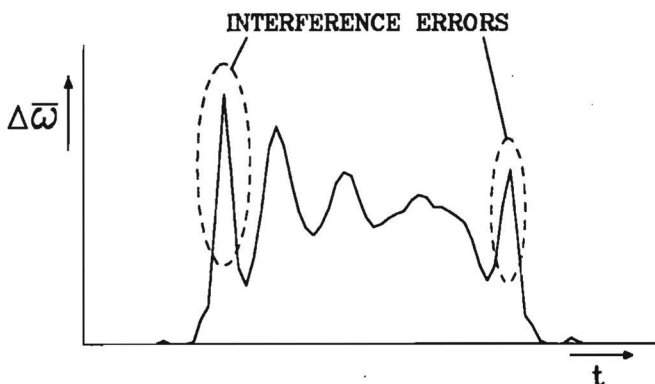
Fig.8.6) A typical case of obvious interference errors in a measured attenuation slope projection.

have to be used for the determination of the moment of arrival of the pulse and, therefore, the automatic gain control would have to be improved (Section 5.1).

Some attempts have been made to correct the interference errors in the measured projections by means of software. Many interference errors can be easily recognized as large, relatively narrow peaks in the projections (Figure 8.6). A rather rigorous way of correcting these errors is to remove such peaks and replace their values by values obtained by linear interpolation between the values on both sides of the peak (Baars, 1987). This method did give an improvement of the reconstructed images in some cases but in general the results of this correction method are not very promising; it removes only the large, obvious errors.

Another, more sophisticated correction method is described by Heddes (1987). In this method it is assumed that the transducer element consists of vertical strips with a width equal to the sample distance (this gives a geometry similar to the one shown in Figure 8.1). Furthermore it is assumed that the signal from each strip is a sine with a Gaussian envelope and a frequency equal to the resonance frequency of the transmitting transducer. Based on these assumptions, the signal from the complete transducer is derived for all transducer positions along a linear scan by adding the signals from the different strips. The time delays between these signals are equal to the differences between values of the samples in the time-of-flight projections that are covered by the aperture of the transducer (the transducer element covers 5 to 10 sample

positions, depending on the chosen sample distance). In the resulting signals, the magnitude of the errors in the center frequency and the amplitude is determined in the same way as in the described simulations. Using the values of these errors, the correct values of the center frequency and of the amplitude can be estimated from the measured values. In the calculation of the errors it has been assumed that the amplitudes of the pressures on each strip of the transducer is the same and, consequently, it was found that this correction method only yielded improvement in measurements with a very low attenuation contrast. An improvement of the method may be achieved by using the measured amplitude values together with the measured time-of-flight values in estimating the interference errors.

It can be concluded that, up to now, no satisfying solutions have been found for the problem of interference. Although it is possible to some extent to correct the interference errors in the measured projections manually, this is a very time consuming process and therefore the search is continued for a reliable way to correct the errors automatically.

Results

In this chapter some results will be presented which have been measured with the ultrasound transmission tomography system that is described in the previous chapters.

First, in Section 9.1, some remarks will be made on the spatial sampling during a measurement. Then, in Section 9.2, The so called "track error" and its correction will be discussed. Section 9.3 describes the composition and the production of the tissue mimicking phantoms that have been used in the measurements. The results of the measurements on these phantoms are presented in Section 9.4. In Section 9.5 the results are given for some measurements on biological tissues. Finally, in Section 9.6, Some remarks will be made concerning the effect on the measurements when using a focussed sound beam.

9.1 Spatial sampling

This section deals with the spatial sampling in the measurements and it links up with Section 3.6.

In Section 3.6 it was assumed that the low-pass character of the measuring process acts as a pre-sampling filter that prevents aliasing. To see whether this assumption is true, an estimation of the filter function of the measuring process will be given.

Both the wavelength of the sound (about 0.7 mm) and the fact that the transducers keep moving during the measurement of one sample will introduce some spatial low-pass filtering, but these effects will only affect structures with sizes on the order of 1 mm or less. A more important spatial low-pass filter is caused by the fact that the aperture of the transducer covers several samples. In the measurements non-focussed transducers are used with a diameter of either 5 or 10 mm. The sample distance is normally chosen in such a way that the transducer can be considered to act as a moving average filter with a width of at least

115

four sample distances. Because it is very hard to determine the exact transfer function of the transducer, a simplified model has been used here in which it is assumed that the sensitivity of the receiving transducer is uniform throughout the width of the transducer element and that the diameter of the sound beam is independent of the distance normal to the transducer surface.

If τ is the sample interval within a projection, then $\omega_s = 2\pi/\tau$ is the spatial sample frequency. The transfer function of a moving average filter with a width of 4τ has its first minimum at $\omega_s/4$. Because this value is smaller than half the sample frequency the moving average filter is a suitable pre-sampling filter for the prevention of aliasing. The transfer function of the moving average filter is shown schematically in Figure 9.1.

As mentioned before, the moving average filter is a rough approximation of the measuring process. In practice, the filter will not have a square spatial window but a window with smoother edges because the sensitivity of the transducer is not constant throughout the aperture of the transducer (Kossoff, 1978). These smoother edges will cause a faster decrease of the envelope of the transfer function of the filter
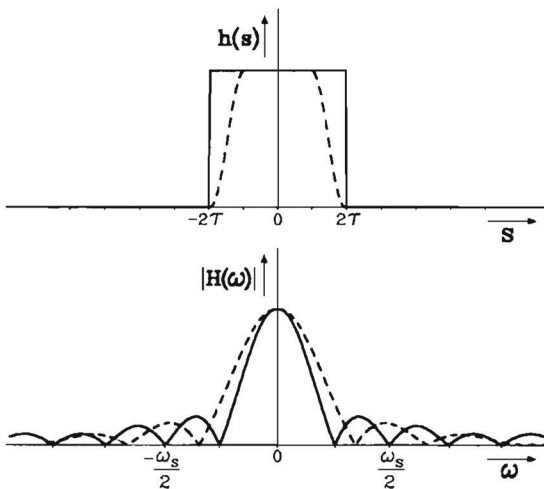
Fig.9.1) The spatial domain representation (h(s)) and frequency domain representation (H(ω)) of the approximate filter function of the measuring process; ω_s is the sample frequency, τ is sample distance. The dashed lines indicate the effect of a smoothed spatial window.

which will give a better suppression of the spatial frequency components that cause aliasing (Figure 9.1).

The sample distance has been chosen to be approximately 1 mm for the following reasons: A smaller distance is not expected to yield more information because in that case the sample distance is smaller than the wavelength. A much larger distance will cause a worse performance of the pre-sampling filter because in that case the transducer aperture covers less sample distances.

The previous paragraphs deal only with the spatial sampling within a projection. As mentioned in Section 3.6, it is very difficult to give an analytical description of the effect of the angular sampling. Therefore, the effect of the angular sampling will be evaluated by means of reconstructions using simulated projections of an object with various angular sampling frequencies. The sample width within the projections is the same for all the simulated projections. Figure 9.2 shows the results of the reconstructions of the simulated data for 10, 25, 50, 75, 100 and
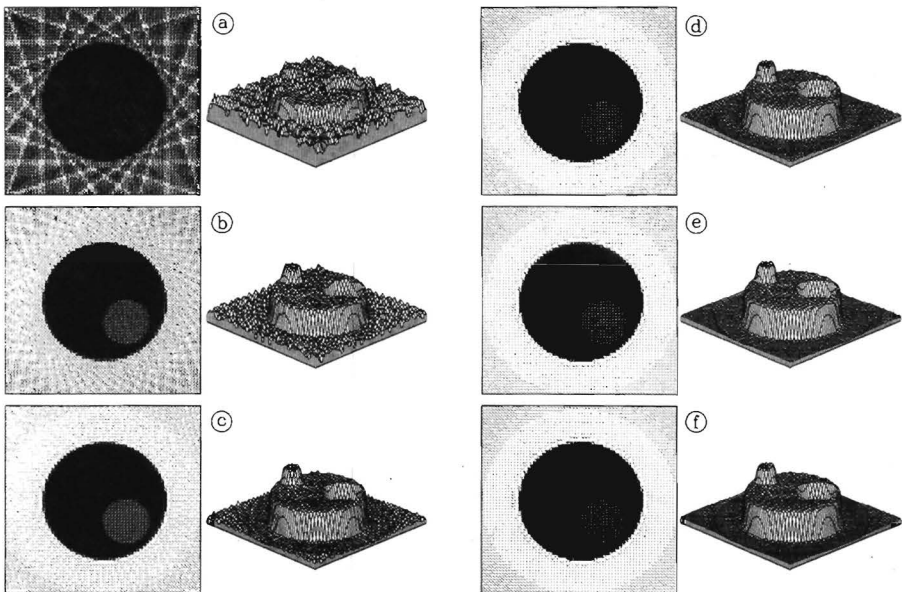
Fig.9.2) Reconstructed images, obtained from various numbers of simulated projections. The images are shown both in a grey scale representation (left) and three-dimensionally (right). The images have been reconstructed from: a) 10, b) 25, c) 50, d) 75, e) 100 and f) 125 projections.

125 projections. The reconstruction filter used to obtain these results is the same as the one used for the reconstruction of the real measurements presented in the following sections. From Figure 9.2 it can be seen that the reconstruction process introduces a considerable amount of noise when a small number of projections is used. Beyond 75 projections, increasing the number of projections only yields a marginal improvement.

In the presented case, where there were 64 samples per projection, the condition given by Eq. (3.6.6) indicates that, if the number of projections is 102 or more, the angular sampling will not influence the results of the reconstruction. The results in Figure 9.2 are in agreement with this; in fact, these results indicate that even fewer projections than given by Eq. (3.6.6) will be sufficient for the reconstruction of a reliable image.

9.2 The track error

In the description of the measuring software (Section 6.4) it was already mentioned that there exists a so-called "track error". In this section the cause of this error and the way of correcting it will be described.

The measurement of a linear scan is performed by moving the transducer carriers along two sets of parallel rails (Section 6.1). Figure 9.3 shows a drawing of such a transducer carrier. From this figure it can be seen that a small vertical deviation of one of the rails will result in both a horizontal displacement of the transducer that is about 6 times larger, and a small deviation of the direction of the sound beam. Because of inaccuracies in the rails, the distance between the transducers varies about 0.6 mm during a linear scan and the direction of the sound beam varies about 0.3 degrees. This yields a variation in the time-of-flight of about 0.4 µs, a variation in the measured center frequency of 0.7% and a variation in the amplitude of about 3%. Figure 9.4a and Figure 9.4c show how this track error occurs in the reconstructed image.

Especially in the time-of-flight measurement, the variations caused by the track error can be rather large compared to the variations caused by the object between the transducers and therefore a correction is needed. To perform this correction the projections are used that are
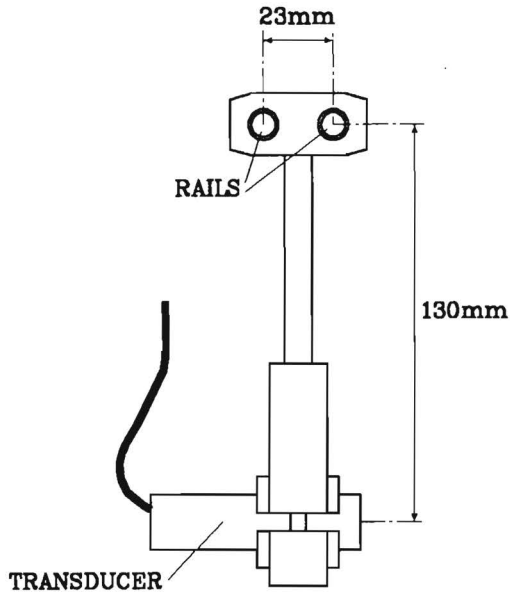
Fig.9.3) Schematic drawing of a transducer carrier (side view) with some essential dimensions.

measured at the end of each complete scan, without an object between the transducers (see Section 6.4). Before performing the reconstruction this projection is subtracted from the projections that have been measured with the object between the transducers. This subtraction combines the correction of the track error with the subtraction needed to obtain projection values that are zero for rays outside the object (Section 4.1). The Figures 9.4a and 9.4b respectively show the reconstructed images of a measurement with no object, without and with correction for the track error. In the latter image only the measuring noise remains. From these images it is obvious that the attenuation slope image obtained from the center frequency measurement, which is a statistical measurement (Section 4.2), contains more noise than the images from the other two measurements. The Figures 9.4c and 9.4d respectively show the reconstructions of the measurement of a tissue phantom, which is described in Section 9.4 (see Figure 9.11), without and with correction of the track error. From these images it can be seen that the effect of the track error is the most severe in the time-of-flight measurement.

The reason for measuring the track error after each complete scan is

that hitting a transducer carrier during the installation of an object or replacing a transducer may cause a slight bending of the rails which can cause changes in the track error. The risk of bending the rails during the removal of the object is very small.
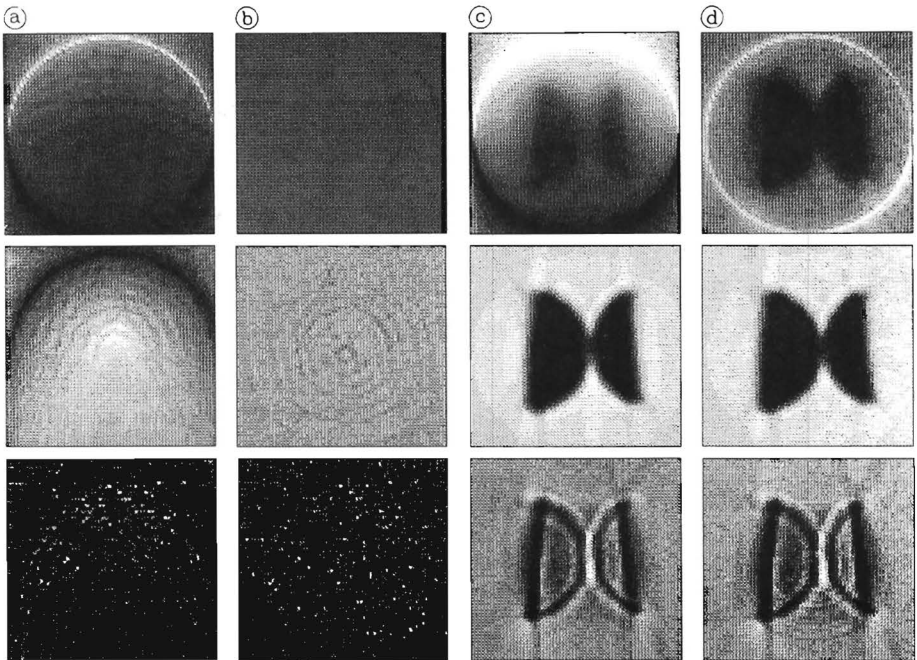
Fig.9.4) Effect of the track error on reconstructed images.
a) no object, not corrected, b) No object, corrected.
c) with object, not corrected, d) With object, corrected.
Top row: sound velocity, middle row: attenuation coefficient, bottom row: attenuation slope.

9.3 Tissue mimicking phantoms

In order to evaluate the performance of the tomography system, objects are needed with a known internal geometry and known acoustical properties. These acoustical properties should resemble the acoustical properties of biological tissues because the tomograph is meant to be used for the imaging of biological tissues. Objects that meet these requirements are called tissue mimicking phantoms. This section describes the fabrication of the phantoms that were used in testing the tomography system.

The basic material for the phantoms is agar gel. The acoustical properties of this gel are very close to those of water but, by adding other materials it can be made to exhibit a wide range of speeds of sound and attenuation coefficients (Burlew et al., 1980).

The sound velocity in the gel can be influenced by adding n-propanol, either during the fabrication or afterwards by diffusion. The sound velocity in the gel proves to have a linear relationship with the concentration of n-propanol. The range of the sound velocities that can be achieved with these phantoms is from about 1480 to 1600 m/s. This is a useful range because the sound velocity of most biological tissues is within this range (Parry and Chivers, 1979).

The attenuation properties of the phantoms can be influenced by adding various concentrations of a powder such as graphite (Burlew et al., 1980), ferri-oxide (Fe_2O_3) powder or silicon carbide grinding powder (Mesdag, 1985). By adding the powder in various concentrations the attenuation coefficient and its frequency dependence can also be varied throughout the major part of the range of the values appearing in biological tissues. These ranges are respectively from 0.6 through 4.0 dB/cm at 2 MHz and from 0.3 to 2.0 dB cm^{-1} MHz^{-1}. Because graphite powder with the desired particle size (about 7 µm) proved to be very difficult to obtain, Fe_2O_3 and silicon carbide were used. The particle size of the silicon carbide was about 20 µm. The particle size of the Fe_2O_3 was not well defined.

The phantoms were made by boiling a mixture of 3% (mass percent) dry agar, an amount of Fe_2O_3 or silicon carbide powder and water, for about a minute. During boiling the mixture was homogenized using a household blender. After boiling the mixture was poured into a cylindrical mould and placed in cold water. This cold water served to

121

speed up the congealing process in order to try, as much as possible, to prevent the sinking of the suspended powder. The phantoms that have been produced have a diameter of 5.0 cm and a height of about 7 cm.

The phantoms can be given an internal structure by cutting out small cylinders or other shapes with thin walled tubes of various dimensions. The holes that arise in this way can be filled with inserts that have been cut from phantoms with other acoustical properties. An example of a tissue mimicking phantom with such an artificial internal structure is shown in Figure 9.5.

In order to preserve the phantoms they must be kept under water. To prevent bacteriological degradation this water must be refreshed regularly (at least every week) or alternatively a chemical preservative may be used. If a chemical preservative is used, it should be noted that this preservative can influence the acoustical properties of the phantom. Because n-propanol has a rather high diffusion rate in agar gel, the phantoms containing n-propanol should be kept in a mixture of water and n-propanol with a concentration that is the same as the n-propanol concentration in the phantom. In this case the n-propanol acts as a preservative. If the phantoms are treated properly, they can be used for a very long period. Some of the older experimental phantoms proved to be usable for well over a year.
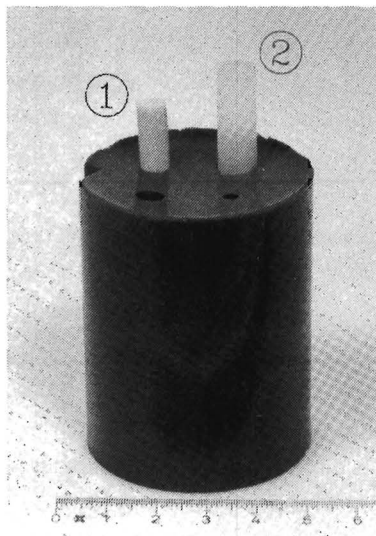
Fig.9.5) Photograph of a Fe_2O_3 phantom with several holes, an insert of agar gel with silicon carbide (1) and an insert of agar gel without a powder (2).

9.4 Measurements on the tissue phantoms

In this section the results of some measurements will be presented that have been performed on the tissue mimicking phantoms described in the previous section.

For the determination of the values of the sound velocity (Section 4.1) and of the attenuation coefficient (section 4.2) it was assumed that the sound velocity in water is 1480 m/s and from the signal received with only water between the transducers it was determined that σ_t is about 2.5 µs, so that in Eq. (4.2.14) $\sigma = 0.4$ MHz $(= 1/\sigma_t)$. All measurements presented in this section have been performed with a non-focussed single element transmitting transducer with a diameter of 10 mm and a non-focussed single element receiving transducer with a diameter of 5 mm. Each measurement was performed with 102 projections and 64 samples per projection. The reconstruction filter was the same for all measurements and equal to the one used to obtain the images from the simulated data (Figure 9.2).

Ten phantoms were available with the following compositions: Three contained Fe_2O_3 in the respective concentrations of 2.7%, 5.3% and 8.0%, three phantoms contained silicon carbide in concentrations of 2.0%, 4.0% and 6.0% and four phantoms contained no powder. Three of these four phantoms were diffused with n-propanol in the respective concentrations of 2.0%, 4.0% and 6.0%. The concentrations given here and in the rest of this section are all represented in mass percentages.

Before cutting internal structures in the phantoms, they were measured first to check the homogeneity in the reconstructed images and to determine the values of the sound velocity, the attenuation coefficient and the attenuation slope in the ten available material compositions. These values will be used as reference values for the measurements of the phantoms with an internal structure. The results of these measurements showed slight inhomogeneities in the phantoms containing powder, especially in the 5.3% Fe_2O_3 phantom and the 4.0% silicon carbide phantom. Futhermore, it showed that the addition of a powder to the agar gel caused a slight decrease of the sound velocity. This decrease was largest in the phantoms with Fe_2O_3. The thirty images resulting from these measurements will not be presented here. The mean values of the sound velocity, the attenuation coefficient and the attenuation slope in the ten homogeneous phantoms are given in

Table 9.1, together with the range of each value within the phantom in which it was measured. The mean values given in Table 9.1 have not been calculated exactly, they have been estimated from the values in the center of the phantoms and the histograms of the grey levels of the images.

From Table 9.1 it can be seen that, especially the values of the attenuation coefficient and attenuation slope show large variations From the images it can be observed that these variations occur mainly on or near to the edges of the phantom. This might be caused partially by inhomogeneities in the phantom resulting from the fact that the congealing of the phantoms always started at the edges, giving the powder in the center of the phantom more time to sink. If this is the cause of the inhomogeneities, they should also be visible in the sound velocity images because the concentration of powder also influences the local sound velocity. However, the inhomogeneities could barely be found in the velocity images, which leads to the suggestion that the inhomogeneities may not be as large as shown in the images of the attenuation coefficient and the attenuation slope. Therefore it must be assumed that the deviations along the edges of the phantoms in these images are caused for a considerable part by other effects. Based on the fact that the deviations are hardly visible in the sound velocity images

phantom material (agar +)	c in m s^{-1}			α in dB cm^{-1}			$d\alpha/d\omega$ in dB cm^{-1} MHz^{-1}		
	mean	range min.	max.	mean	range min.	max.	mean	range min.	max.
----	1486	1485	1486	0.0	-0.1	0.4	0.0	-0.1	0.3
2.7% F	1483	1482	1483	1.0	0.9	1.1	0.4	0.3	0.8
5.3% F	1479	1477	1479	1.8	1.7	2.0	0.6	0.5	1.2
8.0% F	1473	1472	1475	2.9	2.6	3.3	0.9	0.7	1.5
2.0% S	1487	1485	1487	1.1	1.0	1.6	0.2	0.1	1.1
4.0% S	1485	1484	1486	2.3	2.2	3.1	0.6	0.3	1.3
6.0% S	1483	1483	1484	3.6	3.4	4.5	0.5	0.3	1.9
2.0% P	1497	1496	1499	-0.1	-0.5	2.4	-0.1	-1.0	2.1
4.0% P	1507	1506	1511	-0.3	-1.9	6.3	-0.3	-4.0	5.4
6.0% P*	1522	1515	1522	-0.5	-1.2	5.7	-0.5	-1.0	3.2

*)These results needed correction for the interference errors.

Tab.9.1) Values of the measured physical quantities in the ten homogenous phantoms. c is the sound velocity, α is the attenuation coefficient and $d\alpha/d\omega$ is the attenuation slope.

and also that the deviations are the largest in the phantoms containing n-propanol, it can be concluded that the most important of these effects will be the interference (including phase cancellation), although, especially in the amplitude measurements, reflection and refraction effects may also have some influence. The presence of interference is sometimes indicated by "streaks" in the images (see for example Figure 9.11) or, in an earlier stage, by observing the received signal with an oscilloscope. Interference causes obvious changes in the shape of the received signal. It showed that interference (and eventually reflection and diffraction) can cause an amplitude or a center frequency that is higher than the values measured in water, which means that negative values can be observed for the attenuation and the attenuation slope (Table 9.1).

The Figures 9.6 to 9.11 show results of measurements using phantoms with various internal structures. Each result is presented in four images and a table. The four images are: the distribution of the local sound velocity, the distribution of the local attenuation coefficient, the distribution of the local attenuation slope and a drawing of the internal geometry of the phantom. All four images have the same geometrical scale which is indicated in the drawing of the geometry. In all images the grey scale is such that the smallest value of the represented quantity within the image as white and the largest value as black. Each set of four images is accompanied by a table in which the composition of the phantom and the various structures within the phantom are given, together with the reconstructed values of the three physical quantities in the center of each structure. In the majority of cases this value proved to be a local extreme. Of all cylindrical structures the diameter is also given.

In the column "material" of the tables, "agar" indicates agar gel without powder or n-propanol, "water" indicates that the concerning structure has no insert and in the other cases the material added to the agar gel is given, with its concentration. In the following, c is the sound velocity, α is the attenuation coefficient, and $d\alpha/d\omega$ is the attenuation slope. For easy reference the values of Table 9.1 are also included in the tables accompanying Figures 9.6 to 9.11.

The values of the physical quantities are only given if the structure is recognizable in the related image; unrecognizable structures are indicated with an "x" (Figure 9.10 and 9.11). In some cases the structures

were recognizable when the image was represented on the screen, whereas they are barely recognizable in the image as it is presented here. In these cases the value of the related physical quantity is given in brackets (Figure 9.6, 9.8, 9.9 and 9.11). The values of the physical quantities that are given for the bulk material are determined as far away as possible from the edges of the phantom and the internal structures. When the values in the bulk showed variations, a mean value was estimated from a small area.

The structures in the phantoms serve to evaluate the perceptibility of various insert materials in various background (or bulk) materials. When structures have an additional purpose, this will be explained in the descriptions of the phantoms.

Following the discussion of the individual results of each phantom, some general remarks will be made that apply to all the measurements on phantoms, including those that are not presented here.

Figure 9.6 shows the results of the measurement of a phantom that served to investigate whether the position of a structure within the phantom has any influence on its reproduction in the reconstructed image and to see if the sound velocities in smaller structures are reconstructed yielding correct values. From these results it can be concluded that the position of the structure has no influence on the reconstructed values as long as the structure is not very close to the edge of the phantom. The small structures with the different n-propanol concentrations show an increasing value of c with increasing concentration but the structures, especially those with the highest concentrations, show much lower values than the values given in Table 9.1. It shows that, although it is the same phantom, the value of c in the bulk differs from the value in Table 9.1. The possible causes of this difference will be discussed later in this section. The values of $d\alpha/d\omega$ in the bulk material and the insert with 8.0% Fe_2O_3 and the value of α in the bulk material show a good agreement with the reference values in Table 9.1. The deviations of the values α and $d\alpha/d\omega$ in the inserts are due to interference and will also be discussed later in this section.

The phantom of Figure 9.7 served to investigate the relation between the diameter of the structure and the reconstructed value in that structure. The phantom was given two sets of four inserts, each set consisting of the same material but with increasing diameters. The small

struct. no.	size in mm	material (agar gel +)	c in m s^{-1}	ref.	a in dB cm^{-1}	ref.	$da/d\omega$ in dB cm MHz	ref.
bulk	50	6.0%S	1492	1483	3.6	3.6	0.5	0.5
1	4	6.0%P	1501	1522	5.7	-0.5	-0.5	-0.5
2	4	4.0%P	1498	1507	4.3	-0.3	-0.3	-0.3
3	4	2.0%P	1495	1497	2.7	-0.1	0.1	-0.1
4	6	8.0%F	1487	1473	0.5	2.9	0.9	0.9
5	3	water	(1491)	1480	1.9	0.0	0.2	0.0
6	3	water	(1491)	1480	1.8	0.0	0.1	0.0
7	3	water	(1491)	1480	1.9	0.0	0.2	0.0
8	3	water	(1488)	1480	2.4	0.0	0.2	0.0

Fig.9.6) Reconstructed images of a phantom of agar gel with 6.0 % silicon carbide and geometry d). a) Sound velocity, b) attenuation coefficient and c) attenuation slope. F = Fe$_2$O$_3$, S = silicon carbide, P = n-propanol.

struct. no.	size in mm	material (agar gel +)	c in m s^{-1}	ref.	a in dB cm^{-1}	ref.	$da/d\omega$ in $\frac{dB}{cm\,MHz}$	ref.
bulk	50	agar	1487	1486	0.3	0.0	0.4	0.0
1	3	8.0%F	1483	1473	-0.7	2.9	0.9	0.9
2	4	8.0%F	1481	1473	-1.2	2.9	0.4	0.9
3	6	8.0%F	1476	1473	-0.8	2.9	1.5	0.9
4	8	8.0%F	1476	1473	-0.7	2.9	1.8	0.9
5	3	4.0%P	1490	1507	1.3	-0.3	-0.4	-0.3
6	4	4.0%P	1491	1507	1.6	-0.3	-0.6	-0.3
7	6	4.0%P	1499	1507	2.1	-0.3	-0.9	-0.3
8	8	4.0%P	1501	1507	2.1	-0.3	-1.6	-0.3

Fig.9.7) Reconstructed images of a phantom of agar gel without additional material and geometry d).
a) Sound velocity, b) attenuation coefficient and c) attenuation slope.
F = Fe$_2$O$_3$, S = silicon carbide, P = n-propanol.

notch in the edge of the phantom serves only as a reference for the geometry. It shows that for both sets of inserts the value of c is closer to the reference value in Table 9.1 for a larger diameter of the structure and closer to the value in the bulk for a smaller structure. This is in agreement with the assumption that the measuring process has the effect of a low-pass filter (the smoothing that is found in the images is much more than the smoothing caused by the reconstruction filter).

Figure 9.8 shows a phantom that contained three inserts of equal dimensions but with different Fe_2O_3 concentrations. It also contains a non-cylindrical structure. This structure was used because it was suspected that non-cylindrical structures might give problems for both the measurement and the reconstruction. The results show that this is not the case. The three inserts with Fe_2O_3 show a decreasing sound velocity and an increasing attenuation slope with increasing Fe_2O_3 concentration. This is in agreement with the results obtained with the homogeneous phantoms but because of the two dimensional low-pass character of the measuring and reconstruction process all sound velocity values are too high and all attenuation slope values are too low.

The phantoms presented up to now, all have structures cut in a direction normal to the plane of the cross-section. In practical applications of the system this will, in general, not be the case. Therefore, a phantom was measured with a cylindrical structure cut at an angle of about 40 degrees with the measuring plane (Figure 9.12a). The results of this measurement are presented in Figure 9.9. This figure shows that the shape and the value of c of the cross-section of the oblique structure are represented correctly. The values of the three physical quantities in the bulk are in reasonable agreement with the reference values of Table 9.1.

The phantom of Figure 9.10 has a notch in the edge with the same shape as the one in the phantom of Figure 9.8, but here it has been cut at an angle of about 55 degrees with the scan plane (Figure 9.12b) to investigate the effect of a non-cylindrical structure not normal to the plane of the cross-section. Furthermore one insert was given a 4.0% n-propanol concentration in addition to a 8.0% Fe_2O_3 concentration. The results show that one edge of the oblique, non-cylindrical structure is not very clear in the images of α and $d\alpha/d\omega$. This may be due to the angle between the scan plane and the structure but, because the other edge of the structure, that has the same angle with the scan plane, is

struct. no.	size in mm	material (agar gel +)	c in m s⁻¹		a in dB cm⁻¹		da/dω in dB	
				ref.		ref.	cm MHz	ref.
bulk	50	2.0%S	1494	1487	1.1	1.1	0.2	0.2
1		water	1480	1480	-0.8	0.0	-0.2	0.0
2	3	water	1489	1480	-0.6	0.0	-1.1	0.0
3	6	2.0%P	1499	1497	1.7	-0.1	-0.6	-0.1
4	6	6.0%S	1488	1483	1.2	3.1	1.5	0.5
5	6	8.0%F	1482	1473	-1.3	2.9	1.7	0.9
6	6	5.3%F	1488	1479	-0.2	1.8	1.1	0.6
7	6	2.7%F	(1495)	1483	0.1	1.0	(0.3)	0.4

Fig.9.8) Reconstructed images of a phantom of agar gel with 2.0% silicon carbide and geometry d).
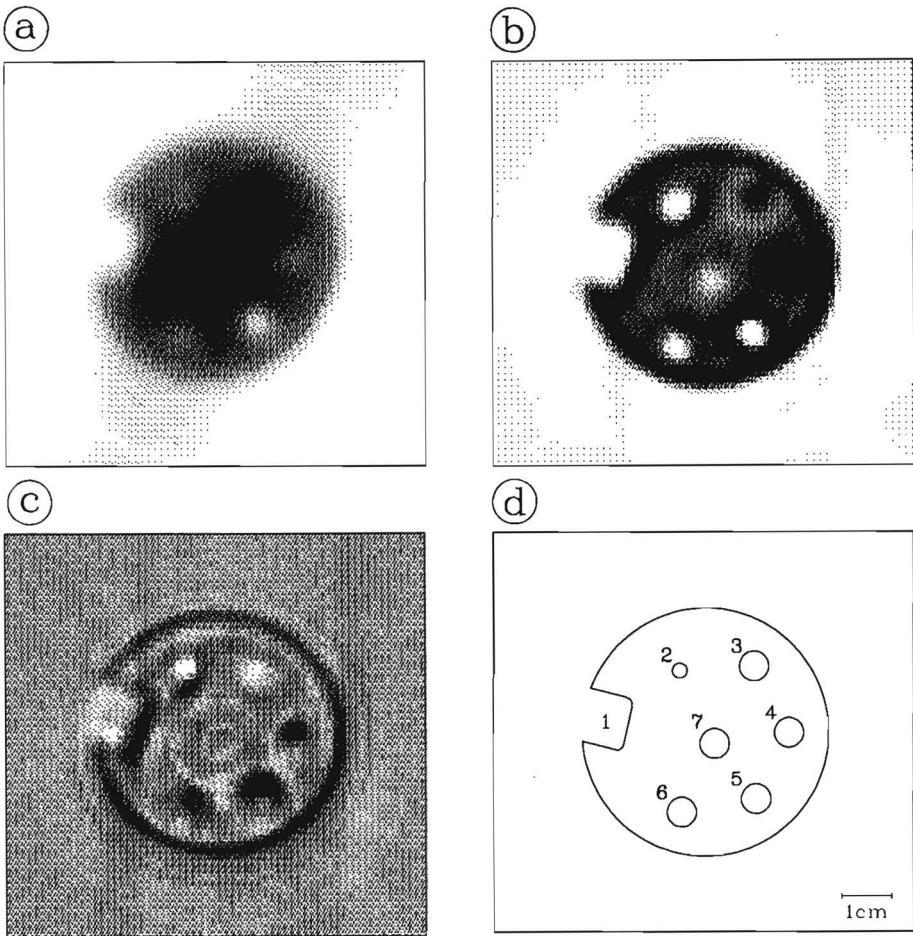a) Sound velocity, b) attenuation coefficient and c) attenuation slope.
F = Fe₂O₃, S = silicon carbide, P = n-propanol.

130

struct. no.	size in mm	material (agar gel +)	c in m s^{-1}	ref.	a in dB cm^{-1}	ref.	$da/d\omega$ in $\frac{dB}{cm\,MHz}$	ref.
bulk	50	8.0%F	1476	1473	2.8	2.9	0.9	0.9
1	8	4.0%P	1507	1507	1.2	-0.3	-2.1	-0.3
2	3	water	(1478)	1480	(3.1)	0.0	(1.2)	0.0
3	6	6.0%S	1480	1483	4.9	3.6	1.1	0.5

Fig.9.9) Reconstructed images of a phantom of agar gel with 8.0% Fe_2O_3 and geometry d).
a) Sound velocity, b) attenuation coefficient and c) attenuation slope.
F = Fe_2O_3, S = silicon carbide, P = n-propanol.

clearly visible, it is more likely that the blurring of the edge is caused by the presence of the cylindrical structure that is very close to the edge of the non-cylindrical one. According to Burlew et al. (1980) the attenuation properties in the insert with 8.0% Fe_2O_3 and 4.0% n-propanol (no.5) should be approximately the same as in the 8.0% Fe_2O_3 insert without n-propanol (no.7). Although the values of α of these two structures should be the same, they show large differences that cannot be explained merely by the difference in size of the two structures. The structure shows an increase of the local sound velocity compared to the structure containing only 8.0% Fe_2O_3, but it is not as large as expected. The values of the three physical quantities in the bulk correspond to the reference values.

Figure 9.11 shows the measurement of a phantom with large oblique interfaces. The bulk of this phantom consists of a cylindrical 4% silicon carbide phantom that has been cut diagonally in two halves. The angle between the oblique interfaces and the scan plane that is created in this way is about 45 degrees (Figure 9.12c). The images obtained from this phantom before it had been given an internal structure have already been shown in Figure 9.4, where they were used to demonstrate the effect of the track error. The values of the physical quantities in the two parts without internal structures proved to be in good agreement with the reference values. For the measurement shown in Figure 9.11 one of the parts was diffused with 4.0% n-propanol and the phantom was given an internal structure to see if the oblique interfaces have any influence on the representation of these structures. The values of c and α in the part of the bulk without n-propanol are within the ranges indicated in Table 9.1. The value of c in the part of the bulk with n-propanol is about 19 m/s higher than the value in the part without n-propanol. This corresponds to the difference in the values of c of the phantom of pure agar gel and the phantom with 4.0% n-propanol as given in Table 9.1. The values of c and $d\alpha/d\omega$ in the insert with both 8.0% Fe_2O_3 and 4.0% n-propanol prove to be very close to the values for the same insert in the measurement of Figure 9.10. In the images it can be seen that the rather long and straight velocity contrasts introduce interference errors that are visible as "streaks".

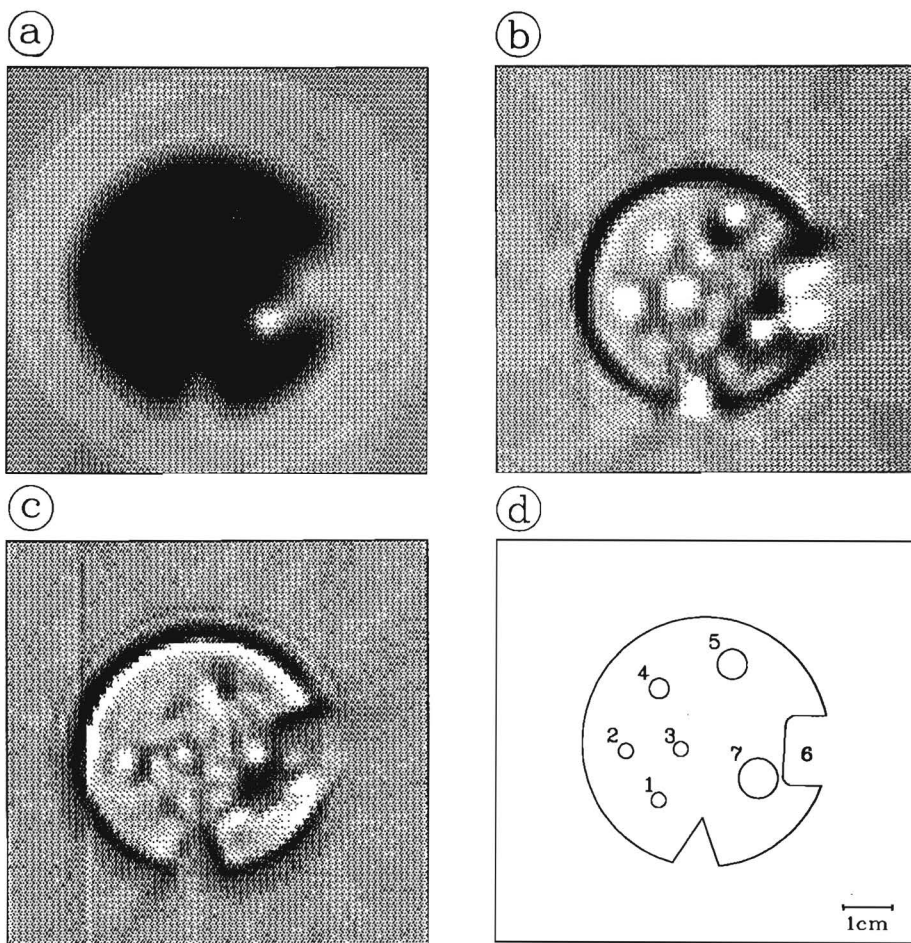| struct. no.	size in mm	material (agar gel +)	c in m s^{-1}		α in dB cm^{-1}		$d\alpha/d\omega$ in $\dfrac{dB}{cm\,MHz}$	
				ref.		ref.		ref.
bulk	50	2.0%P	1498	1497	0.0	-0.1	-0.3	-0.1
1	3	6.0%S	1495	1483	0.0	3.6	x	0.5
2	3	water	1492	1480	-0.1	0.0	-1.1	0.0
3	3	water	1492	1480	-0.1	0.0	-0.9	0.0
4	4	2.0%S	1494	1487	-0.1	1.1	x	0.2
5	6	8.0%F						
		+4.0%P	1489		1.7		1.6	
6		water	1478	1480	0.0	0.0	0.2	0.0
7	8	8.0%F	1475	1473	-0.1	2.9	1.9	0.9

Fig.9.10) Reconstructed images of a phantom of agar gel with
2.0% n-propanol and geometry d).
a) Sound velocity, b) attenuation coefficient
and c) attenuation slope.
F = Fe$_2$O$_3$, S = silicon carbide, P = n-propanol.

struct. no.	size in mm	material (agar gel +)	c in m s⁻¹		α in dB cm⁻¹		da/dω in dB cm MHz	
				ref.		ref.		ref.
bulk	50	4.0%S	1485	1485	2.8	2.3	0.0	0.6
1	3	water	1487	1480	-3.5	0.0	x	0.0
2	6	water	1497	1480	-1.3	0.0	x	0.0
3	6	8.0%F +4.0%P	(1487)		(2.0)		x	
4	6	6.0%S +4.0%P	1493		5.2		x	
5	6	4.0%P	1500	1507	4.3	-0.3	x	-0.3
6		bulk +4.0%P	1504		1.6		-0.2	

Fig.9.11) Reconstructed images of a phantom of agar gel with 4.0% silicon carbide and geometry d).
a) Sound velocity, b) attenuation coefficient and c) attenuation slope.
F = Fe₂O₃, S = silicon carbide, P = n-propanol.

134
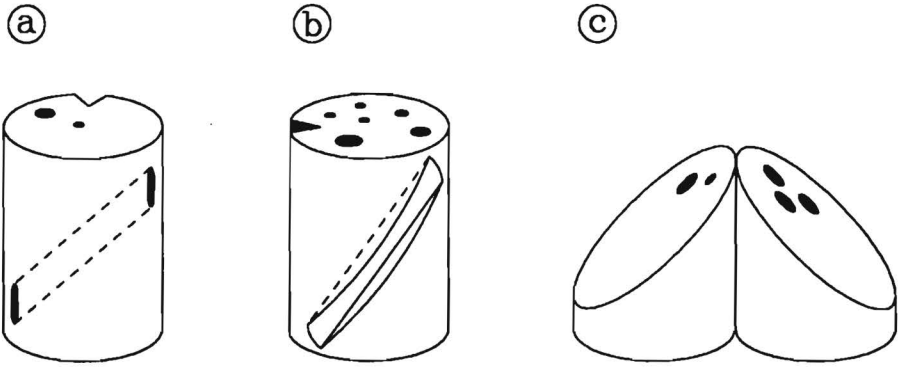
Fig.9.12) Side views of the phantoms of a) Figure 9.9, b) Figure 9.10 and c) Figure 9.11.

Concluding this section some general remarks will be made that apply to all the measurements that have been performed on phantoms, including those not discussed here. In all measurements the values of α and $d\alpha/d\omega$ show large deviations in the neighborhood of velocity contrasts. This effect, which is caused by interference, causes small structures to exhibit erroneous values of these two quantities. The fact that, in the majority of cases, the values of α and $d\alpha/d\omega$ do not show any agreement with the values of Table 9.1, indicates that, for the moment, interference can be considered to be the main problem. From the images of the homogeneous phantoms (not shown here) it could be observed that the width of the region in which the effects of interference are noticeable is generally about 1 cm. This means that a structure needs to be at least 2 cm in diameter to yield a correct value of α and $d\alpha/d\omega$ in the reconstructed images. The results of the phantom measurements indicate that reliable qualitative images of the geometry of the distributions of the physical quantities in the scan plane can be obtained but that reliable quantitative imaging is only possible for large structures (>2 cm). This implies that the possibilities of using the system for tissue characterization are limited.

Observation of the images of all measurements leads to the conclusion that there is at least a qualitative relationship between the contrast in the image of the sound velocity and the contrast in the images of the attenuation coefficient. A structure with a sound velocity that is higher than in the surroundings (darker in the velocity image)

yields a dark structure surrounded by a light halo in the images of α, whereas a structure with a lower sound velocity yields a light structure with a dark halo. Up to now it has not been possible to observe a quantitative relationship between the velocity contrast and the resulting deviation in the value of the attenuation coefficient. If such a quantitative relationship can be found, it can be used to correct the values in the image of the attenuation coefficient. For the contrast in the attenuation slope images none other than a topographical relationship has been found with the contrast in the sound velocity image. Although the measured values of the attenuation coefficient and the attenuation slope are often entirely wrong, the topographical information in these images is still correct. They generally give a clear representation of the geometry of the internal structure of the phantoms.

There is no obvious explanation for the deviations of the value of c as observed in the bulk material of the phantoms as compared to the reference values. Since the phantoms used in the measurements of the values of Table 9.1 and the ones used in the measurements of Figure 9.6 to 9.11 are the same, the values in the bulk materials were not expected to differ from the reference values. For a phantom with many inserts this may be caused by the low-pass character of the measurement and reconstruction process, but because the deviations also occur in phantoms with more space between the inserts there has to be another explanation.

It is not likely that the deviations of the sound velocity are caused by a change of the acoustical properties of the phantoms in the course of time because no relationship is found between the magnitude of the deviations and the age of the phantom.

As stated previously, the sound velocity in the water surrounding the phantoms is always assumed to be 1480 m/s and the values in the reconstructed image are values relative to the value in the surrounding water (Section 4.1). Therefore it is also possible that the deviations in the value of c are caused by a deviation of the sound velocity in the surrounding water.

There seem to be two possible explanations for the observed deviations of the value of c. The first is the fact that the water tank has no temperature regulation. Because the temperature dependence of the sound velocity in water and in agar gel are different, temperature variations may cause deviations in the measured sound velocity values.

The temperature dependence of the sound velocity in water is $2.4 \, \text{m s}^{-1} \, ^\circ\text{C}^{-1}$ (Weast, 1981), whereas in agar gel it is $1.7 \, \text{m s}^{-1} \, ^\circ\text{C}^{-1}$ (Burlew et al., 1980).

The second explanation is that the sound velocity in the water varies in time, even when the temperature is constant. The exposure of the water to open air and repeated insertion and removal of objects pollutes the water. This may affect the acoustical properties of the water. In that case the refreshing of the water will yield a change of the sound velocity in the surroundings of the measured phantoms, which affects the values in the reconstructed images.

Based on the data that is available at this time it is not possible to determine which of these effects (or perhaps both) is the most probable cause of the deviations in the sound velocity.

9.5 Measurements on biological tissues

In this section the results will be presented of the first attempts to perform in vivo measurements on biological tissues. These measurements served only to gain an impression of the applicability of the ultrasound transmission tomography system for in vivo measurements. The results presented in this section have been measured with the same measuring configuration as used in the measurements of the phantoms.

As expected, it proved that, from an ergonomical point of view, the experimental set-up as it is at present is not suitable for in vivo measurements. The persons who volunteered for the measurements of an arm or a leg had to remain in one position for half an hour or even longer without moving. Although the healthy subjects proved to be capable of this, the effort required would probably be too much for most patients.

Figure 9.13 shows the images obtained from the measurement of an arm of a 28 year old male, the leg of a 36 year old male and the breast of a 21 year old female. Especially the measurement of the breast proved to be very hard to perform with the present system. Except for the face, the subject had to be immersed in water completely and the scanning equipment had to be placed over her in such a way that the transducers could move freely around one breast. This proved to be a cumbersome procedure, both for the subject and the investigator.

The results presented in Figure 9.13 show once again that
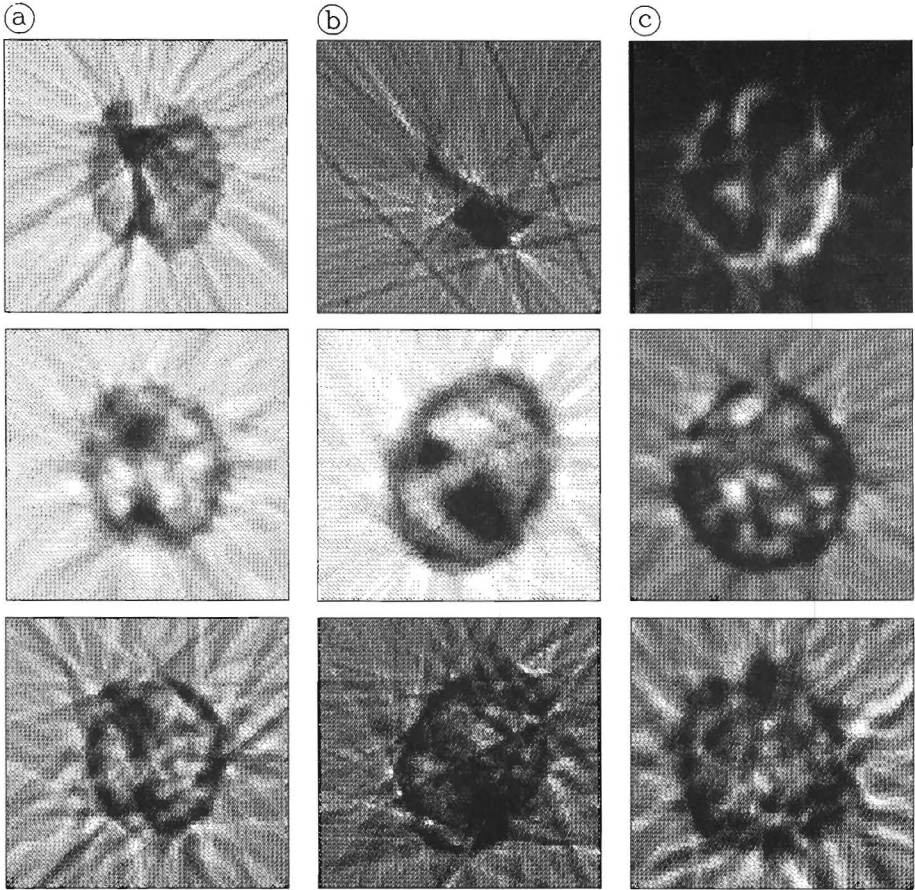
Fig.9.13) Reconstructed images of the measurements of biological materials in vivo. a) Arm of a 28 year old male, b) leg of a 36 year old male and c) breast of a 21 year old female. Top row: sound velocity, middle row: attenuation coefficient, bottom row: attenuation slope.

interference is the most important source of errors. The images are obtained after a manual correction of the obvious interference errors in the projections.

Because the measurements are very preliminary, no extensive discussion of the results will be given, only a few remarks will be made. It will be obvious that the images of the sound velocity and the attenuation slope of the arm and the leg are severely distorted and do not show much of the internal structure. The images of the attenuation

coefficient are less distorted and in those images the bones are clearly visible. In the image of the leg the triangular shape of the tibia is obvious and even the relatively small fibula is clearly visible.

The measurement of the breast showed less interference but it is still hard to recognize the internal structure in the reconstructed images. The light regions in the image of the sound velocity indicate a sound velocity that is lower than in water which suggests the presence of fat (Parry and Chivers, 1979). Because of the limited possibilities of positioning the subject and the scanning equipment, it proved impossible to measure a plane parallel to the rib cage and it was also not possible to determine the exact position of the scan plane within the breast. Because of this and because of the limited anatomical knowledge of the author no attempts will be made to give any further interpretation of the results.

With an earlier version of the tomography system, which was only capable of producing sound velocity images, some measurements have been performed on biological materials in vitro (for example an excised pig heart). It showed that these measurements yielded images that gave a good representation of the geometry of the internal structure of the objects. The results of these measurements are described by Stapper and Sollie (1985) and will not be discussed here because of the lack of quantitative information and because only one of the three possible physical quantities is represented in those images.

9.6 Effects of focussing

In this section some brief remarks will be made on the effects of using a focussed transducer in the tomography system. In Section 7.2 the design of an annular array transducer has been described. In that section it was shown that this annular array yields a sound beam that is, at least in part of the beam, much narrower than the beam of a single element transducer. To see if this narrower beam also yields a higher resolution in a tomographic measurement the annular array has been used to perform some measurements on phantoms.

The results of the measurements with the annular array indicate that focussing can, in some cases, improve the resolution. It also showed that the regions in which interference errors occur are in general smaller than

in measurements with a single element transducer, but interference seems to occur more often and the errors are much larger than in measurements with a non-focussed single element transducer. Because of this the measurements of the attenuation coefficient and the attenuation slope with the focussed transducer yield very unreliable results. The magnitude of the interference errors in these two kinds of measurements made it impossible to reconstruct useful images from the measured data.

In Figure 9.14 two images are shown, obtained using the same phantom. One of them has been measured with a non-focussed single element transducer, the other has been measured with the annular array that was focussed at approximately 75 mm from the transducer surface. From the images it can be seen that focussing does improve the resolution in the measurement of this phantom. The phantom, however, had very low velocity contrasts, which minimized the interference.

As the improvement of the resolution occurs only in some very special cases and because the measurement of the attenuation coefficient and the attenuation slope proved to be very difficult with the focussed transducer, the measurements presented in this thesis have all been measured using a non-focussed single element transducer.

The use of focussed transducers has not yet been investigated any further; this would require a separate study. A possible cause for the problems described in this section may be the fact that the length of the focal zone in the experiments was smaller than the diameter of the phantoms, so, during the measurement there is always a part of the object outside the focal zone. To investigate whether a longer focal zone yields better results, it would be necessary to use an annular array with a larger aperture and a larger distance between the transducers would be needed. This implies rather drastic changes to the tomography system.
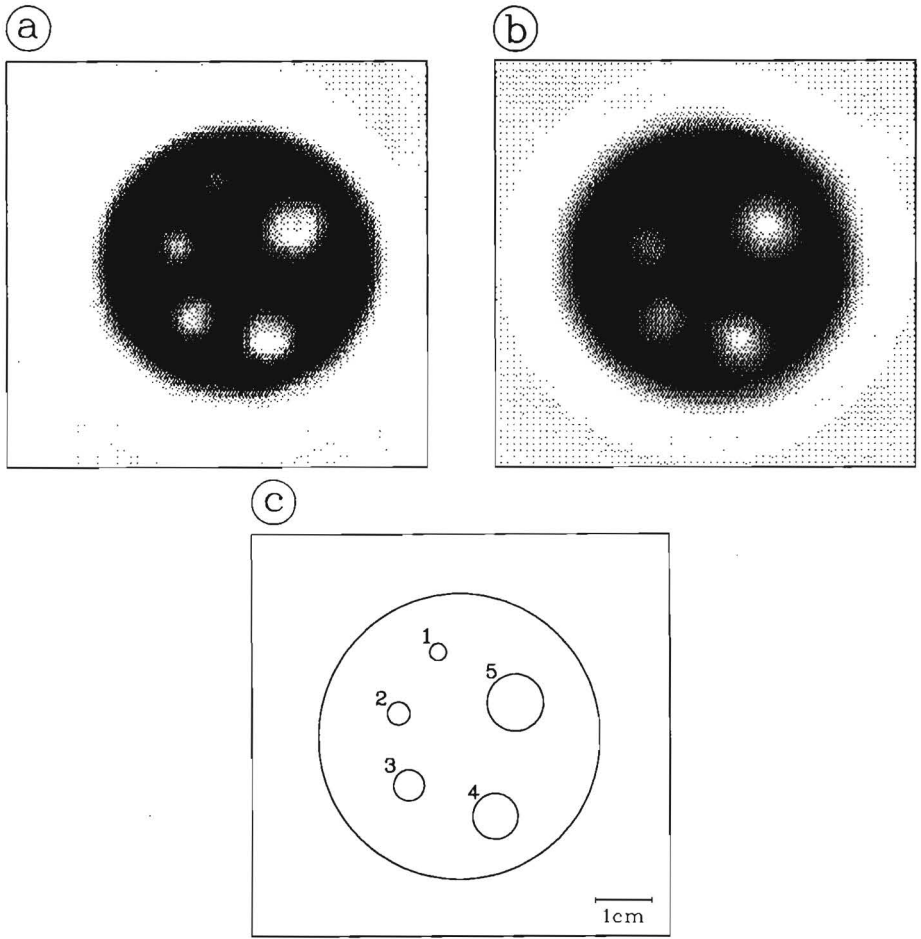
structure no.	size in mm	c in m/s with focus	c in m/s without focus
bulk	50	1496	1503
1	3	1488	1496
2	4	1484	1491
3	6	1482	1488
4	8	1481	1482
5	10	1481	1481

Fig.9.14) Images of the local sound velocity in a phantom.
a) Measured with an annular array with its focus at 75 mm,
b) measured with a non-focussed single element transducer,
c) geometry of the phantom.

Discussion

In the preceding chapters the technical realization of a low-cost ultrasound transmission tomography imaging system has been described. It was shown that it is indeed possible to build an imaging system using a standard personal computer and readily available electronic components, which is capable of producing geometrically correct images of a cross-section of an object. However, it was also shown that values of the physical quantities in the reconstructed images show rather large deviations and that the scanning equipment of the system, as it is at present, is not yet suitable for clinical use.

This final chapter gives a general discussion of the results obtained up till now and the possibilities of clinical application of the ultrasound transmission tomography system.

Firstly, in the Sections 10.1 to 10.5, a number of potential error sources will be discussed. As far as possible, the importance of each of these error sources will be evaluated and the possibilities for the prevention or correction of the related errors will be presented. Then, in Section 10.6, a number of recommendations will be given for further development of the ultrasound transmission tomography system and in Section 10.7 some remarks will be made on the clinical applicability of the system. Finally, in Section 10.8, a general conclusion will be presented.

10.1 The reconstruction process

In this section, the errors introduced by the discrete image reconstruction process will briefly be discussed.

As indicated in Chapter 3, all elements of the reconstruction process have their own influence on the accuracy of the resulting image, but they are also influenced by each other's errors and by the errors of the measuring process. Therefore, analytical approaches for estimating the

accuracy of a reconstructed image are only possible in certain trivial cases (Farrell, 1978), but, in general, it is impossible to give a quantitative expression for this accuracy. A study of the more complicated cases can be performed by means of simulation. Because the errors introduced by the reconstruction process are very small compared to some of the errors dicussed later in this chapter, no extensive study has been performed to assess the exact behaviour of these reconstruction errors.

A quantitave study of the accuracy of the discrete filtered back-projection has been performed by Farrell (1978) and by Rowland (1979). In Farrell's study, a configuration for ultrasound transmission tomography was simulated, which was similar to the configuration described in this thesis. The results presented by Farrell show that, as far as the reconstruction errors are concerned, the relative rms error in the images presented in this thesis is less than 2 %. These results also confirm the observation that fewer projections can be used than indicated by Eq. (3.6.6), without causing any significant decrease in the accuracy. In the case of 64 samples per projection, it is, in general, sufficcient to use about 60 projections.

The study presented by Rowland (1979) contains a comparison of various discrete reconstruction methods. The results of that study indicate that, of the examined methods, the filtered back-projection is the most suitable one for computer implementation. Furthermore it was shown that linear interpolation (Eq. (3.6.4)) had the most favourable performance of the examined interpolation techniques and that the trapezoidal rule yielded optimal results in the discrete evaluation of the back-projection integral (Eqs. (3.5.7) and (3.6.1)). Rowland does, however, not exclude the possibility that better techniques for performing the discrete inverse Radon-transform will be developed. For application in the tomography system described in this thesis, such a development will, as yet, only be useful when a faster and simpler method than the filtered back-projection is found.

10.2 Noise

To evaluate the noise introduced by the measuring hardware, registrations of the three measuring quantities have been made, both

with and without moving the transducers. This proved that moving the transducers introduced a considerable increase in the noise (a factor four or more), probably caused by mechanical vibrations and the stirring of the water. So, in order to reduce the noise, it would be advisable to improve the scanning equipment rather than improving the measuring electronics.

Because the actual measurements are performed with moving transducers, only the noise as it was determined with moving transducers will be given here. The noise in the projections has already been discussed in Section 8.3. In the reconstructed images this leads to a noise level of ± 0.5 m/s in the image of the sound velocity, ± 0.01 dB/cm in the image of the attenuation coefficient and ± 0.1 dB cm^{-1} MHz^{-1} in the image of the attenuation slope. Typical values of these quantities are respectively about 1500 m/s, 2 dB/cm and 1 dB cm^{-1} MHz^{-1}. It will be obvious that the relative error in the sound velocity is the smallest and the relative error in the attenuation slope is the largest.

To obtain the values given above, 102 projections were used for the reconstruction which means that the noise introduced by the reconstruction process is negligible (see Section 3.6 and Section 9.1).

The noise values given here and in Section 8.3 have been determined after the power of the measuring electronics had been switched on for more than an hour. The noise proved to be larger when it was determined shortly after switching on the system.

10.3 **Temperature influences**

Another possible error source is the temperature dependence of the sound velocity in water. When the exact distance between the transducers was well-defined and known and the delay in the measuring electronics was also known, the sound velocity in water could be determined from the time-of-flight values measured in water. However, in the tomography system this distance is not well-defined because of the track error, the very practical but not reproducible way of mounting the transducers and the fact that it is not known which planes should be taken for the exact transducer positions. To determine the sound velocity in the water, two measurements of the time-of-flight would be necessary, with two different transducer distances. When the exact difference between these

two distances is known, the sound velocity can be determined accurately from the difference in the measured time-of-flight values. By using this differential measurement the effects of the electronic delay and the uncertainty in the transducer positions can be eliminated. Because this time consuming procedure would have to be repeated with each measurement and because there seemed to be no reason for large variations to occur in the sound velocity of the water, this differential measurement has not been used and the sound velocity in the water is assumed to have the constant value of 1480 m/s (Wells, 1987). This value is added to the relative velocity values that are the result of the reconstruction (Section 4.1).

The water tank and the tissue phantoms are kept in the same room, so they can be assumed to have the same (room) temperature, except shortly after refreshing the water. Because the temperature dependencies of the sound velocity in water and in agar gel are respectively 2.4 m s^{-1} °C^{-1} and 1.7 m s^{-1} °C^{-1} (Section 9.4), the values in the measurements of phantoms will change with the temperature by -0.7 m/s per °C. The attenuation properties of water and the phantom material show a negligible dependence on the temperature (Burlew et al., 1980).

When measurements are performed on biological materials in vivo, the temperature within the measured object will be approximately constant. This means that, in this case, for an increase of the water temperature of 1 °C, the values in the reconstructed image will decrease by the full 2.4 m/s.

In order to prevent the error caused by temperature changes there are two possibilities. The first is to use a temperature regulation for the water in which the measurement is performed. The second is to change the scanning gear and the mounting of the transducers in such a way that no track error occurs and the distance between the transducers is fixed. With a fixed transducer distance it would only once be necessary to perform the differential measurement of the sound velocity in water and to determine the delay in the electronics, because the exact transducer distance can then be determined from these values and the time-of-flight measured with that transducer distance. This would eliminate the need for assuming a sound velocity in water or of repeatedly performing the differential measurement. Such a construction with a fixed transducer distance may also help to reduce the noise caused by the moving of the transducers.

146

10.4 The beam width

As mentioned in Section 9.1, the aperture of the receiving transducer is at least four times larger than the sample distance. This transducer aperture therefore acts as a spatial low-pass filter which is used as a pre-sampling filter (Section 9.1). This low-pass character of the measuring process introduces errors in the values in the reconstructed distributions especially for structures smaller in size than the width of the sound beam. Furthermore the sharp contrasts in the measured physical quantities are smoothed out. The magnitude of the errors introduced by this filtering effect depends both on the size of the structure and its contrast with the surrounding medium. The reconstruction process also has a low-pass filtering effect, but the bandwidth of this filter is much larger than the bandwidth of the pre-sampling filter, so the filter caused by the measuring process will have a much more important influence.

The low-pass character of the measuring process can be considered as a convolution of the actual projections with some filter function that describes the measuring process and which depends on the size and the shape of the transducer. If a suitable approximation of this filter function can be found, it is possible to correct the errors introduced by the low-pass effect of the measurement by a deconvolution of the measured projections with this filter function. It is, however, doubtful, whether this deconvolution will indeed yield an improvement of the image because it will compensate for the effect of the pre-sampling filter of the measuring process and will enhance the noise in the projections. Furthermore this deconvolution is expected to be rather complicated because the filter function of the measuring process will not only depend on the receiving transducer, but also on the distance to that transducer and the shape of the transmitted sound beam (Farrell, 1981).

10.5 Anisotropy

In the description of the measurement principles (Chapter 4) it was assumed that the measured structures were isotropic, so that the conditions for reconstructibility as given in Section 3.7 were satisfied. In

the case of the measurements on the phantoms this assumption is justified, the phantom material is completely isotropic. In measurements on biological materials, however, this is not always the case. For example muscles, with a structure of mainly parallel fibers, and bones, show clear anisotropic properties, both for the sound velocity and for the attenuation properties (Parry and Chivers, 1979).

Because it proved not to be possible to find a phantom material with a well-defined, known anisotropy, the effects of anisotropy could not be studied. An extensive study of the effects of anisotropy on the results of tomographic measurements is described by Brandenburger et al. (1981). From simulation and measurements on dog hearts in vitro they found that anisotropy did yield errors in the values of the reconstructed quantity but that the geometrical information was not affected. The magnitude of the errors caused by anisotropy depends on the geometry of the anisotropic structure, its degree of anisotropy and the direction of the anisotropy axes. Brandenburger et al. (1981) state that a correction of the errors is possible when the degree and the direction of the anisotropy is known. In general, however, this is not the case, which makes recognition and correction of the anisotropy errors very difficult.

10.6 Dispersion

In the description of the measurement principles in Chapter 4 the effect of dispersion was neglected. In this section it will be discussed whether this neglect was justified.

A simple, mathematical model for the propagation of ultrasound in soft tissues which includes the effects of dispersion has been described and validated by Gurumurthy and Arthur (1982). Their validation showed a good agreement between simulation results and measurement results.

To evaluate the effect of dispersion on the quantities that are measured with the tomography system, some simulations have been performed using two simple tissue models. In one model the phase velocity was logarithmically dependent on frequency (dispersion) and in the other the phase velocity was equal for all frequency components (no dispersion). The logarithmic dependence was indicated by Gurumurthy and Arthur (1982). In the simulations a Gaussian pulse was used with a center frequency of 2 MHz and a bandwidth of about 1 MHz. In the

148

simulations with the dispersive model, the difference in phase velocity between the frequency components of the pulse with the highest and the lowest frequency was about 3 m/s. This value is based on the dispersion data found in the literature (Wells, 1975, Gurumurthy and Arthur, 1982). The simulations were performed for a sound pulse travelling through 15 cm of the modelled tissue.

The results of these simulations showed that the difference in sound velocity between the dispersive and the non-dispersive model is less than 0.2 m/s. The relative difference in the peak amplitudes was less than 0.5 % and for the center frequency this difference was maximally 15 %. It is obvious that, for the measurement of the sound velocity and the amplitude, the dispersion is negligible. For the center frequency down shift measurement the errors caused by dispersion are of the same magnitude as the noise in the measurement. Therefore, it can be assumed that, at least in the present system, it is permitted to neglect the influence of dispersion.

If, in the future, the influences of the other error sources such as interference and noise, can be reduced so far that it is not allowed to neglect the dispersion anymore, it may be possible to find a correction method for the dispersion errors that is based on the one-to-one relationship between the frequency dependent attenuation and the dispersion (Kramers-Kronig relations). This will not be discussed here any further.

10.7 Beam distortions

A sound beam passing through an inhomogeneous medium can be distorted in various ways. One possible cause of such distortions is interference. This has already been discussed in Chapter 8. As stated in Section 8.1, interference can be caused by sound velocity gradients within the sound beam.

Apart from interference, sound velocity gradients can also cause refraction of the beam, especially when the size of the concerning structure is larger than the beam width. As a consequence of this the sound may not travel along the straight rays that were assumed in the theoretical foundations of the measurement principles (Chapter 4) and the image reconstruction from projections (Chapter 3).

When the sound travels along a curved ray two different errors can be introduced. The first error is that, in the reconstruction, the values that represent line integrals along a curved ray are back projected along straight rays which will be shorter that the original rays and, at least partially, cover other points in the scan plane.

The second possible error that may be introduced by curved rays is a consequence of the fact that the rays may not arrive normal to and in the center of the receiving transducer. This can cause a change in the amount of acoustical energy that reaches the transducer, which yields errors in the amplitude measurement, or, in the case of a slightly oblique incidence of the sound beam, it may cause phase cancellation, which will mainly affect both the amplitude measurement and the center frequency measurement (Section 8.3).

The errors mentioned above have been studied by several investigators (McKinnon and Bates, 1980, Farrell, 1981, Kim et al., 1984). These investigators used a correction method based on an iterative approximation of the sound path or an estimation of the sound path by solving the differential equations describing the sound path. Such an estimation of the sound path is often called "ray tracing". McKinnon and Bates (1980) and Farrell (1981) found that a correction for the first error described above yields no significant improvement of the images as long as the sound velocity in the measured structure does not deviate more than 10% from the mean value from the complete scan plane. Because this is the case in almost all biological tissues, this correction will not be necessary.

The second type of error, caused by curved rays, can have considerably greater effect than the first type. This holds mainly for the errors in the amplitude measurement caused by the variations in the amount of acoustic energy that reaches the receiving transducer. In the following this error will be called the refraction error. It may be obvious that this effect is the strongest for narrow sound beams and small receiving transducers. On the other hand, a small transducer will yield smaller phase cancellation errors. A transducer with an aperture of less than 10 mm will yield a phase cancellation error of less than 15%, provided that the phase cancellation is merely caused by an oblique incidence of the sound beam (Farrell, 1981). Because phase cancellation can affect all three measured values whereas the refraction errors will only affect the amplitude measurement, it is advisable to use a small

150

receiving transducer. The best results will probably be obtained when a combination transducer is used with a small, phase sensitive element in the center that is used for both the time-of-flight measurement and the center frequency measurement, surrounded by a large, preferably phase insensitive, element that is used for the amplitude measurement.

It has been shown by McKinnon and Bates (1980) and by Farrell (1981) that the ray tracing method mentioned above, can also be used for the estimation and the correction of the refraction errors. Because the computations involved in this correction method are said to be rather complex and time consuming, it may be better to use the technique proposed by Norton and Linzer (1982) which is claimed to have a considerable computational advantage because it only determines a first order approximation of the ray path. From the cited articles it could not be concluded if there is any significant difference between the accuracies yielded by these two correction methods.

Another kind of error, mentioned at the beginning of this section, are the interference errors (which include phase cancellation errors). These errors have already been discussed extensively in Chapter 8. It may be clear that there is no well-defined boundary between this kind of error and the errors described above. Some methods to correct the errors caused by interference or phase cancellation (caused by velocity gradients) were discussed in Section 8.4.

From the results described in Chapter 9 it can be concluded that the errors caused by phase cancellation and interference are, at the moment, the most important. This conclusion is based on the observation that the largest deviations always occur on or close to obvious sound velocity gradients. This indicates that the errors are caused by beam distortions. From the fact that these deviations occur in the center frequency measurements and, mostly to a lesser degree, in the amplitude measurements, it can be concluded that the deviations are not caused by refraction errors (refraction errors hardly affect the measured mean frequency), which leaves the interference errors as the most important error source. Thus, it will probably be of no use to try and correct the other errors mentioned in the previous sections before a satisfying solution is found for the interference problems.

10.8 Recommendations for further development

In this section some recommendations will be given for further development of the ultrasound transmission tomography system in order to make it suitable for possible clinical use.

In the first place it will be necessary to design a new scanning gear that is adapted to the clinical use in such a way that the patient or the volunteer can assume a comfortable position during the measurement. Futhermore it is advisable to design the scanning gear in such a way that the transducers have a fixed position with respect to each other, which also offers the possibility of an accurate measurement of changes in the sound velocity in the surrounding water. Such a rigid construction has the additional advantage that it will eliminate the necessity of the track error correction (Section 9.2) and that it will probably also reduce the noise (Section 10.1). Although the fan-beam geometry with the receiving PVDF array transducer, as proposed in Section 7.3, may be a very suitable one for clinical use, it is the opinion of the author that, at present it is better to alter the scanning equipment in a way that would not imply redesigning of the electronics or the reconstruction software. The reason for this will be given in the next paragraph.

As shown in the previous sections (and also in the Chapters 7 and 8) there are still many possibilities for technical improvement of the ultrasound transmission tomography system as it is at present. Although it is hard to assess the clinical usefulness of these improvements in advance, it may prove that some, or perhaps most, of these improvements yield no significant improvement for the clinical usefulness of the system. Therefore, it would probably be best to start using the system in clinical studies as soon as possible and perform technical improvements based on the results of the measurements and the experiences of one or more clinicians. As indicated in Chapter 2, the goal of this project is to develop a low cost imaging system. Therefore, in the development of the system it is important to try and avoid improvements that are not really necessary.

If, from the clinical experiments, improvements are shown to be necessary, the suggestions for correction or prevention of the possible errors as given in Sections 10.1 to 10.5 can be used. In addition to the technical improvements of the system itself, digital image processing may also prove to be a useful tool in enhancing the clinical applicability of

the system. A part of this image processing may possibly be incorporated in the reconstruction process.

Finally, there is the possibility of performing reflectivity measurements combined with the measurements of the sound velocity, the attenuation coefficient and the attenuation slope (see Section 4.4 and Section 5.4). If a low cost implementation of the reflectivity measurement can be realized, this will yield additional information which will probably improve the clinical applicability of the tomography system.

10.9 Clinical perspective

In this section some remarks will be made on the clinical possibilities of ultrasound transmission tomography. Because, up to now, no real clinical experiments have been performed with the tomography system, these remarks will be based mainly on the experiences published in the literature.

Up to now only preliminary clinical research with ultrasound transmission tomography has been reported. These investigations all concerned the imaging of the human female breast (Glover and Sharp, 1975, Greenleaf et al., 1978, Schreiman et al., 1984). The results obtained from the experimental measurement of a breast performed with the tomography system show a good similarity with the results presented by these authors. This may indicate that the imaging capability of the system is comparable to that of the much more expensive and complex systems that were used in these clinical experiments. The clinical studies that have been reported, do indicate a clinical usefulness in the detection and possibly even classification of tumors in the breast.

Apart from breast imaging, ultrasound transmission tomography is expected to have more clinical applications. Carson et al. (1977) performed an in vitro study of structures containing bone. The results of this study indicate that it is possible to obtain images of such structures. The measurements performed on an arm and a leg confirm this capability (the results presented by Carson et al. concerned only images of the attenuation coefficient). Dines et al. (1981) even report successful imaging of the brain in an intact human head (in vitro!) using ultrasound transmission tomography.

In spite of these promising results, clinical applications of ultrasound

transmission tomography have, up to now, always remained in an experimental stage. This is caused, at least partially, by the complexity and the cost of the systems yielding images of a rather poor quality. It is expected that the simplicity and the low price of the system described in this thesis can mean a considerable improvement to the clinical usefulness of ultrasound transmission tomography. This will probably be enhanced even further by the fact that the system is also capable (to a certain extent) of performing attenuation slope measurements simultaneously with the sound velocity measurements and the measurements of the attenuation coefficient. A system with these possibilities has not been found reported yet.

10.10 **General conclusion**

In Section 2.3 it was stated that the aim of this study was to investigate the technical possibilities of a simple and low-cost ultrasound medical imaging system. Therefore a prototype **transmission tomography** system has been developed and tested. With this system images can be obtained of the distributions of three independent physical quantities in a cross-section of the measured object. These three physical quantities are: the local **sound propagation velocity**, the local **attenuation coefficient** and the local **derivative with respect to frequency of the attenuation coefficient**. The images of these quantities are reconstructed from three sets of values that are measured simultaneously from one reverberating sound pulse. The measuring values, which are the time-of-flight, the amplitude and the center frequency of the pulse, are obtained from this reverberating pulse without knowing the exact rf-signal. This eliminates the need of a very expensive, high-frequency sampling device. A system using this reverberation technique has not yet been reported in the literature.

Besides its imaging capabilities, the tomography system offers the possibility of performing a limited degree of tissue characterization because of the specific combinations of the three physical quantities for different biological tissues. It is to be expected that this tissue characterizing capability will improve as a result of further development of the system.

In conclusion it can be stated that the ultrasound transmission tomography system presented in this thesis is a reliable, low-cost imaging system with a favorable clinical perspective.

References

Assenza, D., Pappalardo, M., Echographic Imaging with Dynamically Focussed Insonification, Ultrasonics 18, pp.38-42, 1980.

Baars, A.P.M., Periodetijd- en amplitude metingen aan ultrageluidspulsen bij ultrasone tomografie, MSc Thesis, Dept.El.Engng, Eindhoven University of Technology, Eindhoven, 1987 (In Dutch).

Baas, W.J.J., De analyse en verbetering van een meetmethode voor ultrasone looptijd-tomografie, MSc Thesis, Dept.El.Engng, Eindhoven University of Technology, Eindhoven, 1984 (In Dutch).

Baker, D.W., Forster, F.K., Daigle, R.E., Doppler Principles and Techniques, in: Fry, F.J. (ed.), *Ultrasound: Its Applications in Medicine and Biology*, pp.161-287, Elsevier Scientific Publishing Company, Amsterdam, 1978.

Ballantine, H.T., Hueter, T.F., Bolt, R.H., On the Use of Ultrasound for Tumor Detection, J. Acoust. Soc. Am. 26, p.581, 1954.

Barrett, H.H., Swindell, W., Analog Reconstruction Methods for Transaxial Tomography, Proc. IEEE 65, pp.89-107, 1977.

Bom, N., Lancee, C.T., Honkoop, J., Hugenholtz, P.G., Ultrasonic Viewer for Cross-Sectional Analysis of Moving Cardiac Structures, Biomed. Eng. 6, pp.500-503,508, 1971.

Bracewell, R.N., Strip Integration in Radioastronomy, Aust. J. Phys. 9, pp.198-217, 1956.

Brandenburger, G.H., Klepper, J.R., Miller, J.B., Synder, D.L., Effects of Anisotropy in the Attenuation of Tissue on Computed Tomography, Ultrasonic Imaging 3, pp.113-143, 1981.

Burlew, M.M., Madsen, E.L., Zagzebski, J.A., Banjavic, R.A., Sum, S.W., A New Ultrasound Tissue-Equivalent Material, Radiology 134, pp.517-520, 1980.

Busse, L.J., Miller, J.G., Detection of Nonuniform Ultrasonic Radiation with Phase Sensitive (Piezoelectric) and Phase Insensitive (Acoustoelectric) Receivers, J. Acoust. Soc. Am. 70, pp.1377-1386, 1981.

Buys, J.J.M. van den, Een sotware-pakket voor de besturing van een IEEE-488 standaard interface, MSc Thesis, Dept.El.Engng, Eindhoven University of Technology, Eindhoven, 1987 (In Dutch).

Carson, P.L., Oughton, T.V., Hendee, W.R., Ultrasonic Transaxial Tomography by Reconstruction, in: White, D., Barns, R. (eds.), Ultrasound in Medicine 2, pp.341-350, Plenum Press, New York, 1976.

Carson, P.L., Oughton, T.V., Hendee, W.R., Ahuja, A.S., Imaging Soft Tissue through Bone with Ultrasound Transmission Tomography by Reconstruction, Med. Phys. 4, No.4, pp.302-309, 1977.

Choi, J.S., Ogawa, K., Nakajima, M., Yuta, S., A Reconstruction Algorithm of Body Sections with Opaque Obstructions, IEEE Trans. Sonics and Ultrasonics SU-29, pp.143-150, 1982.

Cho, Z.H., General Views on 3-D Image Reconstruction and Computerized Transverse Axial Tomography, IEEE Trans. Nuclear Science NS-21, pp.44-71, 1974.

Cormack, A.M., Computed Tomography: Some History and Recent Developments, in: Shepp, L.A. (ed.), Computed Tomography, Proceedings of Symposia on Applied Mathematics 27, pp.35-42, The American Mathematical Society, 1983.

Cracknell, A.P., *Ultrasonics*, Wykeham Publications, London-Basingstoke, 1980.

Deans, S.R., *The Radon Transform and Some of Its Applications*, Wiley and Sons, New York, 1983.

Dines, K.A., Kak, A.C., Ultrasonic Attenuation Tomography of Soft Tissues, Ultrasonic Imaging 1, pp.16-33, 1979.

Dines, K.A., Fry, F.J., Patrick, J.T., Gilmor, R.L., Computerized Ultrasound Tomography of the Human Head: Experimental Results, Ultrasonic Imaging 3, pp.342-351, 1981.

Dussik, K.T., Dussik, F., Wyt, L., Auf dem Wege zur Hyperphonographie des Gehirnes, Wien. Med. Wochenschr. 97, p.425, 1947.

Farrell, E.J., Processing Limitations of Ultrasound Image Reconstruction, Pattern Recognition and Image Processing: Proc. 2nd IEEE Comp. Soc. Conf., pp.8-15, Chicago, 1978.

Farrell, E.J., Tomographic Imaging of Attenuation with Simulation Correction for Refraction, Ultrasonic Imaging 3, pp.144-163, 1981.

Flax, S.W., Pelc, N.J., Glover, G.H., Gutmann, F.D., McLachlan, M., Spectral Characterization and Attenuation Measurements in Ultrasound, Ultrasonic Imaging 5, pp.95-116, 1983.

Freedman, A., Sound Field of Plane or Gently Curved Pulsed Radiators, J. Acoust. Soc. Am. 48, pp.221-227, 1970.

Freedman, A., Farfield of Pulsed Rectangular Acoustic Radiator, J. Acoust. Soc. Am. 49, pp.738-748, 1971.

French, L.A., Wild, J.J., Neal, D., Detection of Cerebral Tumors by Ultrasonic Pulses, Cancer 3, p.705, 1950.

Gilbert, P., Iterative Methods for the Three-dimensional Reconstruction of an Object from Projections, J. theor. Biol. 36, pp.105-117, 1972.

Glover, G.H., Sharp, J.C., Reconstruction of Ultrasound Propagation Speed Distributions in Soft Tissue: Time-of-Flight Tomography, IEEE Trans. on Sonics and Ultrasonics 24, No.4, pp.229-234, 1977.

Gordon, R., Bender, R., Herman, G.T., Algebraic Reconstruction Techniques (ART) for Three-dimensional Electron Microscopy and X-ray Photography, J. theor. Biol. 29, pp.471-481, 1973.

Greame, J.G., *Designing with Operational Amplifiers: Application Alternatives*, McGraw-Hill Book Company, New York, 1977.

Greenleaf, J.F., Johnson, S.A., Lee, S.L., Herman, G.T., Wood, E.H., Algebraic Reconstruction of Acoustic Absorbtion within Tissue from Their Two-dimensional Acoustic Projections, Acoustical Holography 5, pp.591-603, Plenum Press, New York, 1974.

Greenleaf, J.F., Johnson, S.A., Samayoa, W.F., Duck, F.A., Algebraic Reconstruction of Spatial Distributions of Acoustic Velocities in Tissue from Their Time-of-Flight Profiles, Acoustical Holography 6, pp.71-90, Plenum Press, New York, 1975.

Greenleaf, J.F., Johnson, S.A., Lent, A.H., Measurement of Spatial Distribution of Refractive Index in Tissues by Ultrasonic Computer Assisted Tomography, Ultrasound in Medicine and Biology 3, pp.327-339, Pergamon Press, 1978.

Greenleaf, J.F., Johnson, S.A., Bahn, R.C., Rajagopalan, B., Kenue, S., Introduction to Computed Ultrasound Tomography, in: Raviv, J., Greenleaf, J.F., Herman, G.T. (eds.), *Computer Aided Tomography and Ultrasonics in Medicine*, pp.125-136, North-Holland Publishing Company, Amsterdam-New York-Oxford, 1979.

Gurumurthy, K.V., Arthur, R.M., A Dispersive Model for the Propagation of Ultrasound in Soft Tissues, Ultrasonic Imaging 4, pp.355-377, 1982.

Gijsel, A.J.M. van, Onderzoek naar het gebruik van PVDF als basismateriaal voor ultrasone transducers, MSc Thesis, Dept.El.Engng, Eindhoven University of Technology, Eindhoven, 1987 (In Dutch).

Harris, G.R., Transient Field of a Baffled Planar Piston having an Arbitrary Vibration Amplitude Distribution, J. Acoust. Soc. Am. 70, pp.186-204, 1981.

Herman , G.T., Lent, A., Rowland, S.W., ART: Mathematics and Applications; A Report on the Mathematical Foundations and on the Applicability to Real Data of the Algebraic Reconstruction Techniques, J. theor. Biol. 42, pp.1-32, 1973.

Herman, G.T., Lewitt, R.M., Overview of Image Reconstruction from Projections, in: Herman, G.T. (ed.), *Topics in Applied Physics 32: Image Reconstruction from Projections*, pp.1-8, Springer-Verlag, Berlin-Heidelberg, 1979.

Heddes, M., Uitbreiding en verbetering van een ultrasone dempingsmeter gebaseerd op de verschuiving van de gemiddelde frequentie, MSc Thesis, Dept.El.Engng, Eindhoven University of Technology, Eindhoven, 1987 (In Dutch).

Hill, C.R., Ultrasonic Attenuation and Scattering by Tissues, in: de Vlieger, M., Holmes, J.H., Kratochwil, A., Kazner, E., Kraus, R., Kossoff, G., Poujol, J., Strandness, D.E. (eds.), *Handbook of Clinical Ultrasound*, pp.3-23, Wiley and Sons, New York, 1978.

Hiller, D., Ermert, H., Tomographic Reconstruction of B-scan Images, Acoustical Imaging 10, pp.347-464, 1980.

Hoeks A.P.G., *On the Development of a Multi-Gate Pulsed Doppler System With Serial Data-Processing*, University of Limburg, Maastricht, The Netherlands, 1982.

Howry, D.H., Bliss, W.R., Ultrasonic Visualization of Soft Tissue Structures of the Body, J. Lab. Clin. Med. 40, p.579, 1952.

Hueter, T.F., Messung der Ultraschallabsorption in tierischen Geweben und ihre Abhängigkeit von der Frequenz, Naturwiss. 35, No.9, pp.285-287, 1948.

Hueter, T.F., Bolt, R.H., An Ultrasonic Method for Outlining the Cerebral Ventricles, J. Acoust. Soc. Am. 23, No.2, pp.160-167, 1951.

International Electrotechnical Commission, *An Interface System for Programmable Measuring Instruments 1*, IEC, Genève, 1979

International Electrotechnical Commission, *An Interface System for Programmable Measuring Instruments 2*, IEC, Genève, 1980

Janssen, J.A., Ontwerp en bouw van een dempingsmeter gebaseerd op de verschuiving van de gemiddelde frequentie, MSc Thesis, Dept.El.Engng, Eindhoven University of Technology, Eindhoven, 1986 (In Dutch).

Kawai, H., The Piezoelectricity of Poly(vinylidene Fluoride), Japanese Journal of Applied Physics 8, pp.975-976, 1969.

Kim, J.H., Park, S.B., Johnson, S.A., Tomographic Imaging of Ultrasonic Reflectivity with Correction for Acoustic Speed Variations, Ultrasonic Imaging 6, pp.304-312, 1984.

Keijbus, C.P.H. van den, De realisatie van een ultrasoon ringvormig array, MSc Thesis, Dept.El.Engng, Eindhoven University of Technology, Eindhoven, 1987 (In Dutch).

Kikuchi, Y., Transducers for Ultrasonic Systems, in: Fry, F.J. (ed.), *Ultrasound: Its Applications in Medicine and Biology*, pp.289-342, Elsevier Scientific publishing company, Amsterdam, 1987.

Klepper, J.R., Brandenburger, G.H, Busse, L.J., Miller, J.G., Phase Cancellation, Reflection, and Refraction Effects in Quantitative Ultrasonic Attenuation Tomography, Proc. IEEE Ultrasonics Symposium 1977, pp.182-188, 1977.

Kossoff, G., Technical Procedures and Imaging, in: Donald, I., Levi, S. (eds.), *Present and Future of Diagnostic Ultrasound*, pp.1-11, Wiley and Sons, New York, 1976

Kossoff, G., The Transducer, in: de Vlieger, M., Holmes, J.H., Kratochwil, A., Kazner, E., Kraus, R., Kossoff, G., Poujol, J., Strandness, D.E. (eds.), *Handbook of Clinical Ultrasound*, pp.3-23, Wiley and Sons, New York, 1978.

Kreyszig, E., *Introductory Mathematical Statistics*, Wiley and Sons, New York, 1970.

Lewitt, R.M., Reconstruction Algorithms: Transform Methods, Proceedings of the IEEE 71, No.3, pp.514-532, 1983.

Lockwood, J.C., Willette, J.G., High-speed Method for Computing the Exact Solution for the Pressure Variations in the Nearfield of a Baffled Piston, J. Acoust. Soc. Am. 53, pp.735-741, 1973.

Ludwig, G.D., Struthers, F.W., Detecting Gall-Stones with Ultrasonics, Electronics 23, No.2, p.172, 1950.

Macovski, A., *Medical Imaging Systems*, Prentice-Hall, New Jersey, 1983a.

Macovski, A., Physical Problems of Computerized Tomography, Proceedings of the IEEE 71, No.3, pp.373-378, 1983b.

Mathijssen, R.W.M., Aansturing van lineaire akoestische array's voor ultrasone transmissie tomografie, MSc Thesis, Dept.El.Engng, Eindhoven University of Technology, Eindhoven, 1986 (In Dutch).

McKinnon, G.C., Bates, R.H.T., A Limitation on Ultrasound Transmission Tomography, Ultrasonic Imaging 2, pp.48-54, 1980.

Mersereau, R.M., Oppenheim, A.V., Digital Reconstruction of Multidimensional Signals from Their Projections, Proc. IEEE 62, No.10, pp.1319-1338, 1974.

Mesdag, P.R., Report on Experts Meeting on the Fabrication of Tissue Phantoms, in: Thijssen, J.M., Mazzeo, V. (eds.), Proceedings of the fifth European Communities Workshop on Ultrasonic Tissue Characterization and Echographic Imaging, pp.237-242, Nijmegen, 1985.

Miller, J.G., Klepper, J.R., Brandenburger, G.H., Busse, L.J., O'Donnell, M., Mimbs, J.W., Reconstructive Tomography Based on Ultrasonic Attenuation, in: Raviv, J., Greenleaf, J.F., Herman, G.T. (eds.), *Computer Aided Tomography and Ultrasonics in Medicine*, pp.151-164, North-Holland Publishing Company, Amsterdam-New York-Oxford, 1979.

Mol C.R., *Ultrasound Velocity Tomography and Dynamic Cardiac Geometry*, Elinkwijk, Utrecht, 1981.

Muijtjens, P.C.E.M., Convolutie terugprojectie en algebraïsche rekonstruktie- techniek in ultrasone looptijd-tomografie, Graduation report, Dept.El.Engng, Eindhoven University of Technology, Eindhoven, 1985 (In Dutch).

Narayana, P.A., Ophir, J., A Closed Form Method for the Measurement of Attenuation in Nonlinearly Dispersive Media, Ultrasonic Imaging 5, pp.17-21, 1983.

Newerla, K., Ultrasound Reflection Tomography Using Six Modern Linear Transducer Arrays, Proceedings of Euroson '87, p.297, 1987.

Norton, S.J., Linzer, M., Correcting for Ray Refraction in Velocity and Attenuation Tomography: A Perturbation Approach, Ultrasonic Imaging 4, pp.201-233, 1982.

Nyborg, W.L., Physical Principles of Ultrasound, in: Fry, F.J. (ed.), *Ultrasound: Its Applications in Medicine and Biology*, pp.289-342, Elsevier Scientific publishing company, Amsterdam, 1987.

Ophir, J., Jaeger, P., Spectral Shifts of Ultrasonic Propagation through Media with Nonlinear Dispersive Attenuation, Ultrasonic Imaging 4, pp.282-289, 1982.

Parry, R.J., Chivers, R.C., Data of the Velocity and Attenuation of Ultrasound in Mammalian Tissues - A Survey, in: Linzer, M. (ed.), *Ultrasonic Tissue Characterization*, National Bureau of Standards, Spec. Publ. 525, U.S. Government Printing Office, Washington D.C., pp.343-360, 1979.

Pijfers, R., Aanpassing van een automatische meetopstelling voor ultrasone tomografie aan de IEEE-488 bus, MSc Thesis, Dept.El.Engng, Eindhoven University of Technology, Eindhoven, 1987 (In Dutch).

Pohlman, R., Über die Absorption des Ultraschalls im Menschlichen Gewebe und ihre abhängigkeit von der Frequenz, Physik Z. 40, No.5, pp.159-161, 1939

Reid, J.M., Principles of Doppler Ultrasound, in: de Vlieger, M., Holmes, J.H., Kratochwil, A., Kazner, E., Kraus, R., Kossoff, G., Poujol, J., Strandness, D.E. (eds.), *Handbook of Clinical Ultrasound*, pp.81-90, Wiley and Sons, New York, 1978.

Reneman, R.S., Hoeks, A.P.G., *Doppler Ultrasound in the Diagnosis of Cerebrovascular Disease*, Research Studies Press, Chichister-New York- Brisbane-Toronto-Singapore, 1982.

Rowland, S.W., Computer Implementation of Reconstruction Formulas, in: Herman, G.T. (ed.), *Topics in Applied Physics 32: Image Reconstruction from Projections*, pp.9-79, Springer-Verlag, Berlin-Heidelberg, 1979.

Schreiman, J.S., Gisvold, J.J., Greenleaf, J.F., Bahn, R.C., Ultrasound Transmission Computed Tomography of the Breast, Radiology 150, pp.523-530, 1984.

Silk, M.G., *Ultrasonic Transducers for Nondestructive Testing*, Adam Hilger Ltd., 1984.

Simonds, R.M., Propagation of Broadband Ultrasound in Attenuating Media, Ultrasonic Imaging 5, pp.148-160, 1983.

Sollie, G., Stapper, M., Interference Problems in "Attenuation" Measurements, Proceedings of the seventh European Communities Workshop on Ultrasonic Tissue Characterization and Echographic Imaging, Nijmegen, 1987 (in press).

Sollie,G., Stapper, M., A Simple Low-cost Ultrasound Transmission Tomograph Using a Personal Computer, Proceedings of Euroson '87, p.294, 1987.

Somer, J.C., Electronic Sector Scanning for Ultrasonic Diagnosis, Ultrasonics 6, pp.153-159, 1968.

Somer, J.C., Transducer Arrays, in: de Vlieger, M., Holmes, J.H., Kratochwil, A., Kazner, E., Kraus, R., Kossoff, G., Poujol, J., Strandness, D.E. (eds.), *Handbook of Clinical Ultrasound*, pp.67-74, Wiley and Sons, New York, 1978.

Somer, J., Corsel, J., van der Voort, H., Development of a Computer-model for Multilayer PVDF-transducers, Proceedings of Euroson '87, p.297, 1987.

Stapper, M., Sollie, G., Ultrasound Transmission Tomography by means of a Personal Computer, Proceedings of Ultrasonics International 85, pp.935-940, Butterworth, London, 1985.

Stapper, M., Sollie, G., Characterization of Biological Tissues by means of Ultrasound Transmission Tomography Using a Personal Computer, Proceedings of Ultrasonics International 87, pp.321-326, Butterworth, London, 1987.

Swartz, R.G., Plummer, J.D., On the Generation of High-Frequency Acoustic Energy with Polyvinylidene Fluoride, IEEE Trans. Sonics and Ultrasonics SU-27, pp.295-303, 1980.

Thurstone, F.L., Von Ramm, O.T., Electronic Beam Scanning for Ultrasonic Imaging, in: de Vlieger, M., White, D.N., McCready, V.R. (eds.), *Ultrasound in Medicine*, pp.43-48, Excerpta Medica, Amsterdam, 1974.

Tjötta, J.N., Tjötta, S., Nearfield and Farfield of Pulsed Acoustic Radiators, J. Acoust. Soc. Am. 71, pp.824-834, 1982.

Wade, G., Elliot, S., Khogeer, I., Flesher, G., Eisler, J., Mensa, D., Ramesh, N.S., Heidbreder, G., Acoustic Echo Computer Tomography, Acoustical Imaging 8, pp.565-576, Plenum Press, New York, 1980.

Wardenier, P.H., Analyse, ontwerp en bouw van een lineair akoestisch array t.b.v. een experimentele opstelling voor ultrasone tomografie, MSc Thesis, Dept.El.Engng, Eindhoven University of Technology, Eindhoven, 1985 (In Dutch).

Waszczuk, T., Kujawska, T., Somer, J.C., Focussing of an Ultrasonic Beam by means of a Piezoelectric Annular Array, Archives of Acoustics 3, pp.185-204, 1983.

Weast, R.C. (ed.), *CRC Handbook of Chemistry and Physics (60th edition)*, Chemical Rubber Publishing Company, U.S.A., 1981.

Wells, P.N.T., Some Physical Limitations in Ultrasonic Diagnosis, Bio-Med. Engng. 1. pp.390-394, 1966.

Wells, P.N.T., *Physical Principles of Ultrasonic Diagnosis*, Academic Press, London, 1969.

Wells, P.N.T., Absorption and Dispersion of Ultrasound in Biological Tissue (Review), Ultrasound in Medicine and Biology 1, pp.369-376, Pergamon Press, 1975.

Wells, P.N.T., History, Basic Physics, Pulse-echo Techniques, in: de Vlieger, M., Holmes, J.H., Kratochwil, A., Kazner, E., Kraus, R., Kossoff, G., Poujol, J., Strandness, D.E. (eds.), *Handbook of Clinical Ultrasound*, pp.3-23,31-37, Wiley and Sons, New York, 1978.

Samenvatting

Dit proefschrift beschrijft een prototype van een systeem voor ultrasone transmissie tomografie. Het beschreven onderzoek is onderdeel van een project wat tot doel heeft om een klinisch bruikbare ultrasone tomograaf te ontwikkelen waarbij het van belang is dat het systeem zo goedkoop mogelijk is.

In Hoofdstuk 1 wordt een beknopt historisch overzicht gegeven van de medische afbeeldingstechnieken die gebruik maken van ultrageluid.

In Hoofdstuk 2 wordt eerst kort het principe van ultrasone transmissie tomografie beschreven. Vervolgens wordt een aantal van de voor- en nadelen van ultrageluid in het algemeen en van transmissie tomografie in het bijzonder genoemd. De belangrijkste voordelen van ultrageluid zijn dat het ongevaarlijk is (althans bij de in de diagnostiek gebruikelijke intensiteiten) en dat het bijzonder eenvoudig op te wekken en te detekteren is. Een voordeel van transmissie-metingen ten opzichte van reflectie-metingen is niet alleen dat de ontvangen signalen een grotere informatieinhoud hebben maar vooral dat die informatie er gemakkelijker uit af te leiden is vanwege het deterministische karakter van de signalen. Verder wordt in Hoofdstuk 2 aangegeven waarom de eenvoud en de lage prijs van een medisch afbeeldingsysteem zo belangrijk geacht worden. Daarbij is een van de belangrijkste argumenten dat een goedkoop systeem nuttig kan zijn voor een veel groter percentage van de bevolking dan een duur systeem.

Hoofdstuk 3 geeft een beschrijving van de theorie van de beeld-reconstructie (de inverse Radon-transformatie). Er worden een aantal technieken aangegeven met behulp waarvan de verdeling van een grootheid in een vlak kan worden afgeleid uit groepen lijnintegralen (projecties) die onder verschillende hoeken bepaald zijn. Eén van deze technieken, de convolutie- of gefilterde terugprojectie, is geïmplementeerd in het beschreven systeem. Van deze techniek en van de consequenties bij diskrete implementatie daarvan, wordt een gedetailleerde beschrijving gegeven. Aan het eind van het hoofdstuk wordt aangegeven waaraan voldaan moet worden om beeldreconstructie vanuit projecties mogelijk te maken.

In Hoofdstuk 4 worden de meetprincipes besproken. Er worden drie

fysische grootheden bepaald die in principe onafhankelijk zijn. Deze drie
grootheden zijn: de geluidssnelheid, de dempingscoëfficient en afgeleide
naar de frekwentie van de dempingscoëfficient. Om beeldreconstructie
mogelijk te maken zullen de gemeten waarden lijnintegralen van deze
grootheden moeten zijn. De lijnintegraal van de geluidssnelheid wordt
bepaald uit de looptijd van het geluid tussen de transducers, de integraal
van de demping wordt bepaald uit de amplitude afname van het
ontvangen geluid en de integraal van de afgeleide naar de frekwentie
van de dempingscoëfficient wordt bepaald uit de afname van de centrale
frekwentie van de ontvangen geluidspuls. Deze drie meetprincipes blijken
in eerste benadering te voldoen aan de voorwaarden die gesteld zijn om
beeldreconstructie mogelijk te maken. Aan het slot van Hoofdstuk 4 wordt
beschreven hoe het in de toekomst mogelijk zou kunnen zijn om tegelijk
met de beschreven transmissie-metingen ook reflectie-metingen uit te
voeren.

Hoofdstuk 5 beschrijft de technieken die gebruikt zijn om de
meetprincipes van Hoofdstuk 4 te realiseren. De looptijd van een puls
wordt gemeten met behulp van het "rondzingprincipe" wat een nauw-
keurige meting met eenvoudige middelen mogelijk maakt. De amplitude
wordt bepaald met een speciaal daarvoor ontwikkelde piekdetector en de
centrale frekwentie wordt bepaald door de tijd tussen twee nuldoorgangen
in het ontvangen signaal te meten.

In Hoofdstuk 6 wordt de implementatie van zowel de hard- als de
software van de tomograaf beschreven. Bij de hardware worden het
scanmechanisme en de geïmplementeerde meetelektronica beschreven. Een
belangrijk aspect van deze hardware implementatie is dat de drie
genoemde meetwaarden tegelijkertijd uit één rondzingende geluidspuls
bepaald worden. Bij de software wordt eerst de meetsoftware beschreven.
Bij de reconstructie-software wordt eerst aangegeven hoe het draaipunt
voor de beeldreconstructie bepaald kan worden uit de zwaartepunten van
de projecties, dan wordt het ontwerp van het benodigde digitale
reconstructiefilter beschreven en tot slot wordt een overzicht gegeven
van het complete beeldreconstructie pakket zoals dat geïmplementeerd is
op de personal computer. Aan het eind van dit hoofdstuk worden nog
enige opmerkingen gemaakt over de koppeling tussen de hardware van de
meetopstelling en de personal computer die gebruikt wordt voor de
beeldreconstructie.

Hoofdstuk 7 behandelt de transducers. Eerst wordt een beschrijving

166

gegeven van de in de opstelling gebruikte keramische single element transducers. Verder wordt er in dit hoofdstuk aandacht besteed aan het ontwerp van array transducers (zowel lineair als ringvormig) en wordt een onderzoek beschreven naar de mogelijkheden van het gebruik van PVDF (polyvinylidene fluoride) als piëzoelektrisch materiaal bij de constructie van ontvangsttransducers.

Hoofdstuk 8 beschrijft de problemen die ontstaan als er interferentie tussen twee of meer geluidsgolven optreedt. Dit verschijnsel is bestudeerd met behulp van computersimulaties. Het blijkt dat interferentie zeer grote fouten kan veroorzaken. Er worden enkele mogelijkheden geopperd om interferentie te voorkomen of te corrigeren.

In Hoofdstuk 9 worden de meetresultaten van de geïmplementeerde proefopstelling behandeld. Eerst wordt er een beschrijving gegeven van de invloed van ruimtelijke bemonstering op de resultaten, daarna worden de zogenaamde baanfout en zijn correctie behandeld en vervolgens wordt een beschrijving gegeven van de weefselfantomen die bij de metingen gebruikt zijn. Een weefselfantoom is een object met een bekende geometrie en bekende akoestische eigenschappen die overeenkomen met de eigenschappen in biologische weefsels. Er wordt een aantal meetresultaten van metingen aan weefselfantomen beschreven. Uit deze resultaten kunnen een aantal conclusies getrokken worden omtrent de mogelijkheden en beperkingen van de meetopstelling. De belangrijkste hiervan zijn dat er, ook voor kleine structuren ($\pm 3\,$mm), een zeer goede weergave van de inwendige geometrie wordt verkregen, maar dat een betrouwbare kwantitatieve meting van de akoestische materiaaleigenschappen alleen mogelijk is bij grotere structuren ($\pm\ 2\,$cm). Tot besluit van Hoofdstuk 9 worden enige resultaten getoond van metingen aan biologische weefsels (in vivo) en er worden enige opmerkingen gemaakt over het gebruik van een gefocusseerde geluidsbundel.

Hoofdstuk 10 bevat de discussie van de resultaten van het beschreven onderzoek. Eerst worden er een aantal foutbronnen besproken. Deze foutbronnen zijn: het reconstructieproces, ruis, temperatuurinvloeden, de bundelbreedte, anisotropie, dispersie en vervormingen van de geluidsbundel. Er wordt geconcludeerd dat interferentie (zie ook Hoofdstuk 8) de belangrijkste oorzaak van fouten is. Na de bespreking van de foutbronnen worden er enkele aanbevelingen gedaan voor een eventuele voortzetting van het onderzoek. Vervolgens wordt het klinisch perspectief van ultrasone transmissie tomografie besproken. In de

literatuur worden diverse mogelijkheden voor het klinisch gebruik van ultrasone transmissie tomografie aangegeven, de belangrijkste daarvan is het gebruik voor mammografie (borstonderzoek). Het feit dat het tot nu toe nooit tot een daadwerkelijke klinische toepassing is gekomen is waarschijnlijk voor een groot deel te wijten aan de hoge kosten. Het is de verwachting dat het in dit proefschrif beschreven goedkope systeem een positieve bijdrage kan leveren aan de toepasbaarheid van ultrasone transmissie tomografie.

Tot besluit wordt een algemene conclusie gegeven waarin gesteld wordt dat het mogelijk is gebleken om een eenvoudig en goedkoop systeem voor ultrasone transmissie tomografie te onwikkelen, wat een gunstig klinisch perspectief heeft. Het unieke van dit systeem is, dat de lokale geluidssnelheid, de lokale dempingscoëfficient en de lokale afgeleide naar de frekwentie van de dempingscoëfficient tegelijkertijd bepaald worden, zonder dat het nodig is om het ontvangen hoogfrekwent signaal te bemonsteren.

Curriculum Vitae

De schrijver dezes werd geboren op 22 september 1958 te Kampen en is sinds 4 oktober 1985 gehuwd met Marlene van der Lugt. Het VWO werd gevolgd in Zwolle (Carolus Clusius College) en Harderwijk (Christelijk College Nassau Veluwe) waar hij in 1976 het Atheneum diploma verkreeg.

De studie Elektrotechniek werd in 1976 begonnen aan de Technische Universiteit Delft en werd na de propaedeuse (september 1978) voortgezet aan de Universiteit Twente, waar het kandidaats diploma behaald werd in juni 1980. De kandidaats-opdracht was het realiseren en testen van een Iridium/Iridiumoxide pH-elektrode. Het ingenieursdiploma met biomedische aantekening werd verkregen in januari 1984. Het afstudeeronderzoek betrof het ontwikkelen van een niet-invasieve methode voor het meten van spiervezel-geleidingsnelheden. Dit onderzoek werd uitgevoerd in het revalidatie centrum "Het Roessingh" te Enschede.

Een fors deel van de studietijd werd besteed aan het oprichten (november 1979 - april 1980) en voorzitter zijn (april 1980 - oktober 1981) van de Christelijke Studenten Vereniging "ALPHA" te Enschede.

De periode februari 1984 tot september 1984 heeft de schrijver gewerkt bij "Het Roessingh" waar een publicatie over het afstudeeronderzoek werd afgerond en gewerkt werd aan een microcomputergestuurde opstelling voor het meten en verwerken van oppervlakte EMG signalen.

Het in dit proefschrift beschreven promotie onderzoek betrof het ontwerp en de realisatie van een eenvoudig en goedkoop systeem voor ultrasone transmissie tomografie en het werd uitgevoerd in de periode september 1984 tot september 1988 bij de vakgroep Medische Elektrotechniek van de faculteit Elektrotechniek van de Technische Universiteit Eindhoven.

Stellingen

1. Gebruik makend van het principe van ultrasone transmissie tomografie is het mogelijk om met eenvoudige en goedkope middelen een medisch afbeeldingssysteem te maken (dit proefschrift).

2. De analyse en verwerking van radio-frequente signalen ten behoeve van ultrasone transmissie tomografie is goed mogelijk zonder gebruik te maken van snelle signaalbemonstering (dit proefschrift).

3. Bij weefseltypering met behulp van ultrageluid verdienen transmissie-metingen de voorkeur boven reflectiemetingen (dit proefschrift).

4. Zowel bij transmissie- als bij reflectiemetingen vormen interferentie-verschijnselen een hardnekkig probleem (dit proefschrift).

5. Kosten-baten beschouwingen van wetenschappelijk onderzoek bemoeilijken het doen van fundamenteel onderzoek en daardoor op den duur ook de technische vooruitgang. (H.B.G. Casimir, Natuurwetenschap, techniek en maatschappij, in: Leven met de wetenschap, Oosthoek, 1968)

6. Het is onjuist om aan te nemen dat geschiedschrijving een consistent beeld van het verleden of van een deel daarvan zou kunnen opleveren. (G. Harmsen, Inleiding tot de geschiedenis, Ambo, 1968)

7. De gebruikswaarde van een technisch ontwerp wordt niet bepaald door de gebruiksmogelijkheden, maar door de gebruikte mogelijkheden ervan. (C.L.J. Schoenmakers, Samenleving en techniek, De Nederlandsche Boekhandel, 1973)

8. Een zin-rijke toekomstverwachting is alleen mogelijk indien God als oorsprong van alle zin wordt aangenomen en afgezien wordt van zowel het uitgangspunt van algehele autonomie van de mens als van verabsolutering van de techniek. (E. Schuurman, Techniek en toekomst, Van Gorcum, 1972)

9. Het is goed mogelijk om met behulp van oppervlakte-elektromyografie de gemiddelde geleidingssnelheid van de spiervezels in de menselijke musculus biceps brachii te bepalen, mits bij de meting aan de juiste randvoorwaarden wordt voldaan. (Sollie et al., Electromyogr. clin Neurophysiol. 25, 1985, pp.45-56 en pp.193-204)

10. Het huwelijk is als een stuk landbouwgrond, een beperkte periode van verwaarlozing kan heel verrijkend werken.